rptu.de

Attila Gonda

Determination of rolling bearing electrical capacitances with experimental and numerical investigation methods

Maschinenelemente und Getriebetechnik Berichte
Band 48 | 2023
Herausgeber: Prof. Dr.-Ing. Bernd Sauer
Prof. Dr.-Ing. Oliver Koch

RPTU

Research for Sustainability

MEGT

Lehrstuhl für
Maschinen**e**lemente,
Getriebe und **T**ribologie

rptu.de

Attila Gonda

Determination of rolling bearing electrical capacitances with experimental and numerical investigation methods

Maschinenelemente und Getriebetechnik Berichte
Band 48 | 2023
Herausgeber: Prof. Dr.-Ing. Bernd Sauer
Prof. Dr.-Ing. Oliver Koch

Research for Sustainability

Lehrstuhl für
Maschinen**e**lemente,
Getriebe und **T**ribologie

Bibliografische Information der Deutschen Nationalbibliothek
Die Deutsche Nationalbibliothek verzeichnet diese Publikation in der Deutschen Nationalbibliografie; detaillierte bibliografische Daten sind im Internet über **http://dnb.d-nb.de** abrufbar.

Maschinenelemente und Getriebetechnik Berichte

Wissenschaftliche Schriftenreihe des
Lehrstuhls für Maschinenelemente, Getriebe und Tribologie
der Rheinland-Pfälzischen Technischen Universität Kaiserslautern-Landau

Herausgeber: Lehrstuhl für Maschinenelemente, Getriebe und Tribologie
Prof. Dr.-Ing. Bernd Sauer
Prof. Dr.-Ing. Oliver Koch
Postfach 3049
Rheinland-Pfälzische Technische Universität Kaiserslautern-Landau
67653 Kaiserslautern

Verlag: Rheinland-Pfälzische Technische Universität Kaiserslautern-Landau

Druck: Rheinland-Pfälzische Technische Universität Kaiserslautern-Landau
Dezernat 5 Technik
Abteilung 5.6 Foto-Repro-Druck

D-386

Rheinland-Pfälzische Technische Universität Kaiserslautern-Landau
Erwin-Schrödinger-Straße
67663 Kaiserslautern

Als Manuskript gedruckt. Printed in Germany.

ISBN 978-3-95974-216-0
ISSN 1860-8035

Determination of Rolling Bearing Electrical Capacitances with Experimental and Numerical Investigation Methods

Vom Fachbereich Maschinenbau und Verfahrenstechnik
der Rheinland-Pfälzischen Technischen Universität Kaiserslautern-Landau
zur Verleihung des akademischen Grades

Doktor-Ingenieur (Dr.-Ing.)
genehmigte
Dissertation

von
Herrn Attila Gonda, M. Sc.
aus Békéscsaba, Ungarn

Tag der Einreichung: 05.06.2023
Tag der mündlichen Prüfung: 20.11.2023

Dekan: Prof. Dr. rer. nat. Roland Ulber
Vorsitzender: Prof. Dr.-Ing. Oliver Koch
Berichterstatter: Prof. Dr.-Ing. Bernd Sauer
Prof. Dr.-Ing. Stefan Götz

D 386

Acknowledgement

The present work originated during my time as a research assistant at the Institute of Machine Elements, Gears and Transmission (MEGT) of the Technical University Kaiserslautern, under the supervision of Prof. Dr.-Ing. Bernd Sauer.

I express my sincere gratitude to my doctoral supervisor, Prof. Dr.-Ing. Bernd Sauer, for his support and for promoting my scientific work. I am grateful for his mentorship and the trust he placed in me.

I extend my sincere thanks to Prof. Dr.-Ing. Stefan Götz, the Head of the Institute of Mechatronics and Electrical Drives (MEAS) at the Technical University of Kaiserslautern, for the helpful discussions and supervision of my work. Additionally, I am thankful to Prof. Dr.-Ing. Oliver Koch, the Head of the Institute of Machine Elements, Gears and Tribology (MEGT) at the Technical University of Kaiserslautern, for chairing the examination board for my defence.

I would also like to express my appreciation to my (former) colleagues for their constant support. In particular, I am grateful to Prof. Dr.-Ing. Balázs Magyar for his valuable guidance, as well as the numerous inspiring discussions about the research projects and my dissertation. Special thanks also to Dr.-Ing. Dani Bechev, Dr.-Ing. Christoph Burkhart, M.Sc. Resat Capan, Dr.-Ing. Seiedardeshir Sebteini, M.Sc. Lionel Simo Kamga and Dipl. Ing. Lukas Rüth for the collegial and friendly discussions, the support of my work, and for contributing to a pleasant atmosphere at the MEGT.

Lastly, I want to express my heartfelt thanks to my girlfriend, Monika, and my family for their unwavering support and for keeping me motivated not only throughout my academic career but also in every aspect of my life.

Friedrichshafen, November 2023

Abstract

With the expansion of the electromobility and wind energy, the number of frequency inverter-controlled electric motors and generators is increasing. In parallel, the number of the rolling bearing failures caused by inverter-induced parasitic currents also shows an increasing trend. In order to determine the electrical state of the rolling bearing, to develop preventive measures against damages caused by parasitic currents and to support system-level calculations, electrical rolling bearing models have been developed. The models are based on the electrical insulating ability of the lubricant film that develops in the rolling contacts. For the capacitance calculation of the rolling contacts, different correction factors were developed to simplify the complex tribological and electrical interactions of this region. The state-of-the-art correction factors vary widely, and their validity range also differ significantly, which leads to uncertainty in their general application and to the demand for further investigations of this field. In the present work, a combined simulation method is developed that can determine the rolling bearing capacitance of axially loaded rolling bearings. The simulation consists of an electrically extended EHL simulation for calculating the capacitance of the rolling contact, and an electrical FEM simulation for the capacitance calculation of the non-contact regions. With the combination of the resulted capacitance values of the two simulation methods, the total rolling bearing capacitance can be determined with high accuracy and without using correction factors. In addition, due to experimental investigations, the different capacitance sources of the rolling bearing are identified. After the validation of the combined simulation method, it can be applied for the investigation of the different capacitance sources, i.e., to determine their significance compared to the total rolling bearing capacitance. The developed simulation method allows a detailed analysis of the rolling bearing capacitances, taking into account influencing factors that could not be considered before (e.g., oil quantity in the environment of the rolling bearing). As a result, the accurate calculation of the rolling bearing capacitance can improve the prediction of the harmful parasitic currents and help to develop preventive measures against them.

Kurzfassung

Mit dem Ausbau der Elektromobilität und der Windenergie steigt die Zahl der umrichtergesteuerten Elektromotoren und Generatoren. Parallel dazu steigt auch die Zahl der Wälzlagerausfälle, die durch umrichterinduzierte parasitäre Ströme verursacht werden. Um den elektrischen Zustand von Wälzlagern zu bestimmen, vorbeugende Maßnahmen gegen Schäden durch parasitäre Ströme zu entwickeln und elektrische Berechnungen auf Systemebene zu unterstützen, wurden elektrische Wälzlagermodelle entwickelt. Die Modelle beruhen auf der elektrischen Isolierfähigkeit des Schmierfilms, der sich in den Wälzkontakten ausbildet. Für die Berechnung der Wälzlagerkapazität wurden verschiedene Korrekturfaktoren entwickelt, um die komplexen tribologischen und elektrischen Wechselwirkungen in diesem Bereich zu vereinfachen. Die aktuellen Korrekturfaktoren und ihre Gültigkeitsbereiche variieren deutlich, was zu Unsicherheiten in deren allgemeinen Anwendung führen kann und weitere Untersuchungen auf diesem Gebiet erfordert. In der vorliegenden Arbeit wurde ein kombiniertes Simulationsverfahren entwickelt, mit dem die Wälzlagerkapazität von axial belasteten Wälzlagern berechnet werden kann. Die Simulation besteht aus einer elektrisch erweiterten EHD Simulation zur Berechnung der Kapazität des Wälzkontakts und einer elektrischen FEM Simulation zur Kapazitätsberechnung der weiteren Bereiche. Durch die Kombination der resultierenden Kapazitätswerte der beiden Simulationsverfahren kann die gesamte Wälzlagerkapazität mit hoher Genauigkeit und ohne Verwendung von Korrekturfaktoren berechnet werden. Darüber hinaus werden durch experimentelle Untersuchungen die verschiedenen Kapazitätsquellen des Wälzlagers identifiziert. Nach der Validierung der kombinierten Simulationsmethode kann diese zur Untersuchung der verschiedenen Kapazitätsquellen eingesetzt werden, d.h. um deren Bedeutung im Vergleich zur gesamten Wälzlagerkapazität zu ermitteln. Die entwickelte Simulationsmethode ermöglicht eine detaillierte Analyse der Wälzlagerkapazitäten unter Berücksichtigung von Einflussfaktoren, die bisher nicht berücksichtigt werden konnten (z.B. Ölmenge in der lagernahen Umgebung). Durch die genaue Berechnung der Wälzlagerkapazitäten können schädliche parasitäre Ströme besser vorhergesagt und Präventivmaßnahmen dagegen entwickelt werden.

Contents

Nomenclature V

1 Introduction 1

2 Fundamentals and state of the art 3

- 2.1 Fundamentals of bearing currents 3
  - 2.1.1 "Classical" bearing currents 3
  - 2.1.2 "Modern" bearing currents 4
  - 2.1.3 Damages due to bearing currents 11
  - 2.1.4 Preventive measures 13
- 2.2 Basics of rolling bearings 14
  - 2.2.1 Function and design 14
  - 2.2.2 Loads and hertzian contact 16
  - 2.2.3 Rolling bearing kinematic 20
  - 2.2.4 Lubrication and lubricant properties 22
  - 2.2.5 Elastohydrodynamic lubrication 26
- 2.3 The electrical modelling of rolling bearings 32
  - 2.3.1 Electrical contact model 32
  - 2.3.2 Electrical rolling bearing model 35

3 Motivation and objectives 39

4 Experimental investigation methods 40

- 4.1 Measurement set-up and testing conditions 40
  - 4.1.1 Measurement set-up 40
  - 4.1.2 Investigated rolling bearings and test oils 42
- 4.2 Measurement methods 43
  - 4.2.1 Charging curve measurement 43
  - 4.2.2 Impedance measurement 50

5 Simulation and modelling strategies 58
- 5.1 Electrically extended EHL simulation 58
  - 5.1.1 Numerical EHL simulation 58
  - 5.1.2 Electrical extension of the EHL simulation 66
- 5.2 Capacitance simulation with finite element method 73
- 5.3 Combined simulation method 78

6 Systematic investigation of rolling bearing capacitances 82
- 6.1 Capacitance sources in rolling bearings 82
  - 6.1.1 Rolling element dependent and independent capacitances 83
  - 6.1.2 Environmental influences 85
  - 6.1.3 Rolling element related capacitances 90
  - 6.1.4 Capacitance structure of rolling bearings 93
- 6.2 Validation of the combined simulation method 95
  - 6.2.1 Influence of the axial load 96
  - 6.2.2 Influence of the rotational speed 97
  - 6.2.3 Influence of the temperature 98
  - 6.2.4 Influence of the oil quantity 100
  - 6.2.5 Validation and evaluation of the results 102
- 6.3 Investigations with axially loaded angular contact ball bearing 111

7 Summary and outlook 114

A Appendix 118
- A.1 Rolling bearing data 118

Bibliography 119

Nomenclature

List of Symbols

Variable	Unit	Description
a, b	mm	Semi-axes of the hertzian contact ellipse
$a_1 \dots a_5$	-	Lubricant-specific constants of the Bode equations
d_{ir}	mm	Diameter of the inner ring raceway
d_{or}	mm	Diameter of the outer ring raceway
d_p	mm	Pitch diameter
d_{re}	mm	Diameter of the rolling element
f	Hz	Frequency
h	µm	Gap height
h_0	µm	Central lubricant film thickness
$\tilde{h}_0$	µm	Mutual approach
$h_{0,isoth}$	µm	Central lubricant film thickness assuming isothermal contact conditions
$h_{0,th}$	µm	Central lubricant film thickness with thermal correction
h_{min}	µm	Minimum lubricant film thickness
$h_{min,isoth}$	µm	Minimum lubricant film thickness assuming isothermal contact conditions
$h_{min,th}$	µm	Minimum lubricant film thickness with thermal correction
i	-	Imaginary unit
k_1, k_2, k_3	-	Lubricant-specific constants of the Bode equations
k_C	-	Correction factor of the contact capacitance
k_R	-	Correction factor of the contact resistance

Variable	Unit	Description
n	min^{-1}	Rotational speed
n_{cage}	min^{-1}	Rotational speed of the cage
n_{ir}	min^{-1}	Rotational speed of the inner ring
n_{or}	min^{-1}	Rotational speed of the outer ring
n_{re}	min^{-1}	Rotational speed of the rolling element
p	MPa	Pressure
p_{cav}	MPa	Cavitation pressure
p_{max}	MPa	Maximum hertzian contact pressure
r	mm	Radius
$r_{1x,}\ r_{2x}$	mm	Radius of the contacting bodies in x-direction
r_{1y}, r_{2y}	mm	Radius of the contacting bodies in y-direction
r_{ir}	mm	Radius of the inner ring raceway
r_{or}	mm	Radius of the outer ring raceway
$r_{rw,ir}$	mm	Groove radius of the inner ring raceway
$r_{rw,or}$	mm	Groove radius of the outer ring raceway
u_o	m/s	Hydrodynamic velocity
u_1, u_2	m/s	Velocities of the contacting surfaces
u_{ir}	m/s	Hydrodynamic velocity of the inner ring contact
u_{or}	m/s	Hydrodynamic velocity of the outer ring contact
t	msec	Time
t_1, t_2	msec	Time points
v	m/s	Velocity, Circumferential velocity
v_1, v_2	m/s	Velocities of the contacting surfaces
v_{cage}	m/s	Circumferential velocity of the cage
v_{ir}	m/s	Circumferential velocity of the inner ring
v_{or}	m/s	Circumferential velocity of the outer ring
Δv	m/s	Relative velocity
x, y, z	-	Cartesian coordinates

Variable	Unit	Description
A	mm²	Area
A	pF	Rolling element independent capacitance
$A_1 \ldots A_4$	-	Lubricant-specific constants of the Bode equations
A_{Hertz}	mm²	Area of the hertzian contact ellipse
B	pF	Capacitance increase per rolling element
C	pF	Capacitance
$C_{11}^{l}, C_{12}^{l} \ldots$	V	Lumped capacitances of a multi-conductor system
$C_{11}^{g}, C_{12}^{g} \ldots$	V	Ground capacitances of a multi-conductor system
C_C	pF	Cable capacitance
C_{con}	pF	Contact capacitance
C_{Hertz}	pF	Capacitance of the hertzian contact region
C_{inlet}	pF	Capacitance of the inlet region
C_{outlet}	pF	Capacitance of the outlet region
$C_{outside}$	pF	Capacitance of the outside region of the contact
$C_{RE,Cont,ir}^{EEHL}$	pF	Capacitance of the inner ring contact obtained by the electrically extended EHL simulation
$C_{RE,Cont,or}^{EEHL}$	pF	Capacitance of the outer ring contact obtained by the electrically extended EHL simulation
$C_{RE,Env,ir}^{FEM}$	pF	Capacitance of the surroundings of the inner ring contact obtained by FEM simulation
$C_{RE,Env,or}^{FEM}$	pF	Capacitance of the surroundings of the outer ring contact obtained by FEM simulation
C_{RB}	pF	Rolling bearing capacitance
$C_{RB,A}, C_{RB,B}$	pF	Rolling bearing capacitances of the electric motor
C_{RS}	pF	Rotor-Stator stray capacitance
C_S	pF	Substitutive capacitance
C_{Seg}	pF	Segment capacitance of the rolling bearing
$C_{Seg,Env}^{FEM}$	pF	Environmental capacitance of the rolling bearing segment obtained by FEM simulation
C_{th}	-	Thermal correction factor of the lubricant film thickness

Variable	**Unit**	**Description**
C_{WR}	pF	Winding-Rotor stray capacitance
C_{WS}	pF	Winding-Stator stray capacitance
D_i	mm	Outer diameter of the rolling bearing
D_o	mm	Inner or bore diameter of the rolling bearing
E_0	GPa	Reduced modulus of elasticity
E_1, E_2	GPa	Modulus of elasticity of the contact bodies
E_D	V/m	Dielectric strength
F	N	Load
F_{ax}	N	Axial load
F_N	N	Normal load
F_{rad}	N	Radial load
G	-	Dimensionless material parameter
H	-	Dimensionless lubricant film thickness
H_0	-	Dimensionless central lubricant film thickness
$\widetilde{H}_0$	-	Dimensionless mutual approach (iteration constant)
H_{min}	-	Dimensionless minimum lubricant film thickness
I	A	Electric current
I_0	A	Charging current (first instant)
O	-	Mid-point of the intermediate circuit in the inverter
P	-	Dimensionless pressure
Q	N	Load of the rolling element or the contacting bodies
Q	C	Electric charge
$Q_1, Q_2 \dots$	C	Electric charges of a multi-conductor system
Q_j	N	Individual load of the rolling element
R	Ω	Electric resistance
R'	Ω	Simplifying resistance for the calculations
R^2	-	Coefficient of determination
$R_{a,1}, R_{a,2}$	µm, mm	Arithmetic average roughness of the surfaces

Variable	Unit	Description
R_C	Ω	Electric resistance of the cable
$R_{con,oil}$	Ω	Electric resistance of the lubricated rolling contact
R_{eff}	Ω	Effective resistance
$R_{Hertz,oil}$	Ω	Electric resistance of the hertzian contact region
R_O	Ω	Internal resistance of the oscilloscope
$R_{q,1}$, $R_{q,2}$	µm, mm	Root-mean-square roughness of the surfaces
R_R	Ω	Regulating resistance
R_{RB}	Ω	Electric resistance of the rolling bearing
R_S	Ω	Substitutive resistance
R_x	mm	Equivalent radius of the contacting bodies in x direction
R_y	mm	Equivalent radius of the contacting bodies in y direction
T	°C, K	Temperature
U	-	Dimensionless speed parameter
U	V	Voltage
U_0	V	Supply voltage
U_1, U_2 …	V	Voltages of a multi-conductor system
U_1, U_2 …	V	Voltages at different time points
U_C	V	Charging voltage
U_{CM}	V	Common-mode voltage
U_{IC}	V	Intermediate circuit voltage of the frequency inverter
U_{max}	V	Maximum of the charging voltage
U_{RB}	V	Voltage acting on the rolling bearing
U_U, U_V, U_W	V	Phase voltages
U, V, W	-	Phases of the electric motor
W	mm	Width of the rolling bearing
W	-	Dimensionless load parameter
X	Ω	Reactance
X	-	Dimensionless x-coordinate

Variable	**Unit**	**Description**
Y	-	Dimensionless y-coordinate
ΔX, ΔY	-	Dimensionless element sizes of the EHL simulation
Z	-	Number of rolling elements
$\overline{\boldsymbol{Z}}$	Ω	Complex impedance vector
$\overline{\boldsymbol{Z}}_C$	Ω	Impedance vector of a capacitor
$\overline{\boldsymbol{Z}}_R$	Ω	Impedance vector of a resistor
α	°	Contact angle
α_0	°	Nominal contact angle
α_j	°	Individual contact angle of the rolling element
α_p, α_p^*	1/Pa	Pressure-viscosity coefficient
α_s	1/K	Lubricant-specific constant of the Bode equations
β	°	Angle of the external load on the rolling bearing
β_T	1/K	Isothermal compressibility (Bode equations)
β_{th}	1/K	Temperature-viscosity coefficient
γ	-	Geometric parameter
$\dot{\gamma}$	1/s	Shear rate
δ	µm, mm	Depth of indentation
$tan(\delta)$	-	Dielectric loss factor
ε_0	F/m	Vacuum permittivity
ε_r	-	Relative permittivity
$\varepsilon_{r,air}$	-	Relative permittivity of air
$\varepsilon_{r,oil}$	-	Relative permittivity of the oil
η	Pa·s	Dynamic viscosity
$\hat{\eta}$	-	Dimensionless dynamic viscosity
η_0	Pa·s	Dynamic viscosity at atmospheric pressure
θ	-	Cavity fraction
κ	-	Ellipticity parameter (ratio of the semi-axes)

$\bar{\kappa}$	-	Approximation of ellipticity parameter
λ	-	Specific lubricant film thickness
λ_{th}	W/(m·K)	Thermal conductivity
μ_{min}	-	Minimum value of the coefficient of friction
ν	m^2/s	Kinematic viscosity
ν_1, ν_2	-	Poisson's ratios of the contact bodies
ρ	1/mm	Curvature of the body
ρ	kg/m^3	Density
$\hat{\rho}$	-	Dimensionless density
ρ_0	kg/m^3	Density at atmospheric pressure
ρ_{ave}	kg/m^3	Average density of oil and gas
ρ_{el}	Ω·m	Electrical resistivity (or specific electrical resistance)
$\rho_{el,oil}$	Ω·m	Electrical resistivity of the oil
ρ_g	kg/m^3	Solidification density parameter of the Bode equations
ρ_s	kg/m^3	Lubricant-specific constant of the Bode equations
σ	µm, mm	Combined roughness of the contacting surfaces
τ	MPa	Shear stress
τ	sec	Time constant
φ	°	Phase angle
ω	rad/s	Angular velocity, angular frequency
ω_{cage}	rad/s	Angular velocity of the cage
ω_{ir}	rad/s	Angular velocity of the inner ring
ω_{or}	rad/s	Angular velocity of the outer ring
ω_{re}	rad/s	Angular velocity of the rolling element

$\mathcal{F}$	-	Elliptic integral of the first order
$\bar{\mathcal{F}}$	-	Approx. of the elliptic integral of the first order
$\mathcal{E}$	-	Elliptic integral of the second order
$\bar{\mathcal{E}}$	-	Approx. of the elliptic integral of the second order
$\mathcal{L}$	-	Thermal load parameter

Subscripts

Index	Description
1, 2	Body 1, 2
ax	Axial
i, j	Index of vector and matrix elements
ir	Inner ring
max	Maximum
min	Minimum
or	Outer ring
rad	Radial
RB	Rolling bearing
re	Rolling element

Abbreviations

Abbreviation	Description
AC	Alternating current
BVR	Bearing voltage ratio
CFD	Computational fluid dynamics
DC	Direct current
DIN	Deutsches Institut für Normung
EDM	Electric discharge machining
EEHL	Electrically extended EHL simulation
EHL	Elastohydrodynamic lubrication
FBNS	Fischer-Burmeister-Newton-Schur (algorithm)
FEM	Finite element method
GESA	Gerät zur erweiterten Schmierstoffanalyse (German) Device for extended lubricant analysis (English)

GTO	Gate-turn-off (thyristor)
IGBT	Insulated gate bipolar transistor
ISO	International Organization for Standardization
JFO	Jakobsson-Floberg-Olsson (cavitation model)
LMA	Levenberg-Marquardt algorithm
MEGT	Institute of Machine Elements, Gears and Transmission
PTFE	Polytetrafluoroethylene
PVC	Polyvinyl chloride
PWM	Pulse-width modulation
RC	Resistance-capacitance (circuit)
SVM	Space vector modulation
WEC	White etching cracks

1 Introduction

Rolling bearings are among the most widely used machine components and the demand for their stable and high performance in diverse applications is constantly present. It can be explained by their essential function, which is to ensure relative motion between components next to the transmission of the related forces and torques with minimal losses. Today, there is a wide range of different types of rolling bearings, designed for specific operating conditions or environments, i.e., to ensure high efficiency in various applications. In addition to higher efficiency, the aim of the rolling bearing development process is to achieve a long service life. The correct service life prediction of the rolling bearings is a significant task at the design stage of the machines, since the failure of a rolling bearing can lead to the failure of the whole machine. To prevent such undesired events, there are various calculation methods – rolling bearing standards (e.g., [DIN ISO 281], [DIN 26281]), catalogues with design guidelines (e.g., [Skf18], [Sch18]), and further empirical or numerical calculation processes – that allow the design engineer to determine the expected service life and critical conditions of the bearings. These calculation methods develop in parallel with the rolling bearing itself and can take more and more influencing factors into account. In addition, the computer-aided design and optimisation of mechanical systems enables further improvement of the performance and quality of the individual components. Through the coupling of different simulation levels (system, subsystem, element), i.e., by considering the system level interactions between the components (e.g., the interactions between the rolling bearings and the supported gears in a drive unit), more accurate predictions can be made about the conditions of each individual component in the machine.

A large proportion of rolling bearing applications is related to the mobility and energy sectors, which are currently undergoing a major transformation. As sustainability comes increasingly to the fore, so do the modern electric motor and generator systems, which brings challenges in the related rolling bearing applications. With the increasing number of frequency inverter-controlled electric motors and generators, the number of bearing failures caused by parasitic currents is also increasing. Depending on the mechanical and electrical conditions of the bearing, different type of parasitic currents can appear, which influence the failure mode and thus the service life of the bearing. In order to predict such harmful electric conditions, and to elaborate possible preventive measures, complex multi-level (rolling contact, rolling bearing, electric drive) multi-field (tribological, mechanical, electrical) calculations and simulations are necessary, where the interactions of the different components can be taken into account. An essential part of these investigations is the correct electrical modelling of the mechanical subsystems, such as the rolling bearings. In the rolling contacts of the bearings, a lubricating film develops. It can act as an electrical insulation between the conductive surfaces and thus can be described and quantified electrically. Since the accurate mechanical and fluid dynamical modelling of this area is already a complex task, simpler calculation methods in combination with various correction factors are often used to derive the corresponding electrical values. The currently used correction factors and functions vary over a wide range, depending on different conditions (e.g., type of the rolling bearing, electrical properties of the lubricant), and their validity range also varies considerably. This leads to uncertainty in their general application and to the demand for further investigations in this field. Due to the electrical consideration of the insulating lubricant film in the contacts and the surrounding conductive components, the rolling bearings can be modelled with equivalent electric circuits, and lastly with operating point-dependent electrical values, such as capacitance, resistance, and impedance. It allows the integration of the rolling bearings as an electrical subsystem into the system-level electrical simulations. The present work is focusing on the improvement of the capacitance modelling of rolling bearings, in parallel with the general investigation of the phenomena in the background of the correction factors. The results provide the possibility to improve the accuracy of system-level modelling of electric motors and generators, and to develop preventive measures against parasitic current-induced damages in the mechanical subsystems.

2 Fundamentals and state of the art

The appearance of parasitic currents in rolling bearings has necessitated the electrical investigation and modelling of this basically mechanical component. In this chapter, the fundamentals are discussed, starting from the sources and types of bearing currents, through the related mechanical description of rolling bearings, and closing with the state-of-the-art electrical modelling of rolling bearings using different correction factors.

2.1 Fundamentals of bearing currents

Although the phenomenon of harmful bearing currents has been known and investigated for decades, the number of bearing damages caused by parasitic currents has increased in recent years. It can be explained by the increasing application of frequency inverter-controlled electric machines. Thereby, in addition to the "classical" bearing currents, "modern", frequency inverter-induced bearing currents have appeared. These "modern" bearing currents are in the focus of numerous scientific works, such as in [Müt04], [Gem16], [Rad16], [Tis17], [Fur17] and [Bec20], among others.

2.1.1 "Classical" bearing currents

The "classical" bearing currents, compared to "modern" bearing currents, have lower frequencies and can potentially occur in any electric motor or generator. Typically, two sources can be distinguished, which are briefly presented in the following based on [Zik10]:

- **Electrostatic charging**: It can occur due to frictional electricity (e.g., in pumps and fans), which leads to the development of a DC voltage between the shaft and the machine frame, and thus across the bearing. If this potential difference exceeds the insulating ability of the lubricant film in the rolling contact, an electrical discharge can occur, which can lead to damages on the contact surfaces and in the lubricant.

- **Magnetic asymmetries**: The asymmetries of the magnetic field can be caused by various reasons, such as the inaccuracies of the production process, imperfections in the design, material inhomogeneities or the bending of the shaft in case of large machines. The resulted magnetic asymmetries induce an alternating voltage along the shaft. If the shaft voltage is high enough, it can discharge through the lubricant film and leads to a low frequency circulating current across one bearing, through the frame, across the other bearing, back to the shaft. Bearing currents due to magnetic asymmetries are more typical of large-size electric machines.

Due to the improved manufacturing processes and optimised motor designs, the electrical bearing loads caused by "classical" bearing currents and the number of the resulted failures have been reduced [Zik10].

2.1.2 "Modern" bearing currents

In case of damages related to "modern" frequency inverter-induced bearing currents, an increasing trend can be observed, which can be explained by the increasing application of frequency inverter-controlled motors and generators. To describe the origin of the "modern" bearing currents, the operating principle of a voltage source DC-link frequency inverter is briefly explained in the following based on [Jag05] and [Pre02]. The inverter controls the rotational speed of a three-phase induction motor with the pulse-width modulation (PWM) method.

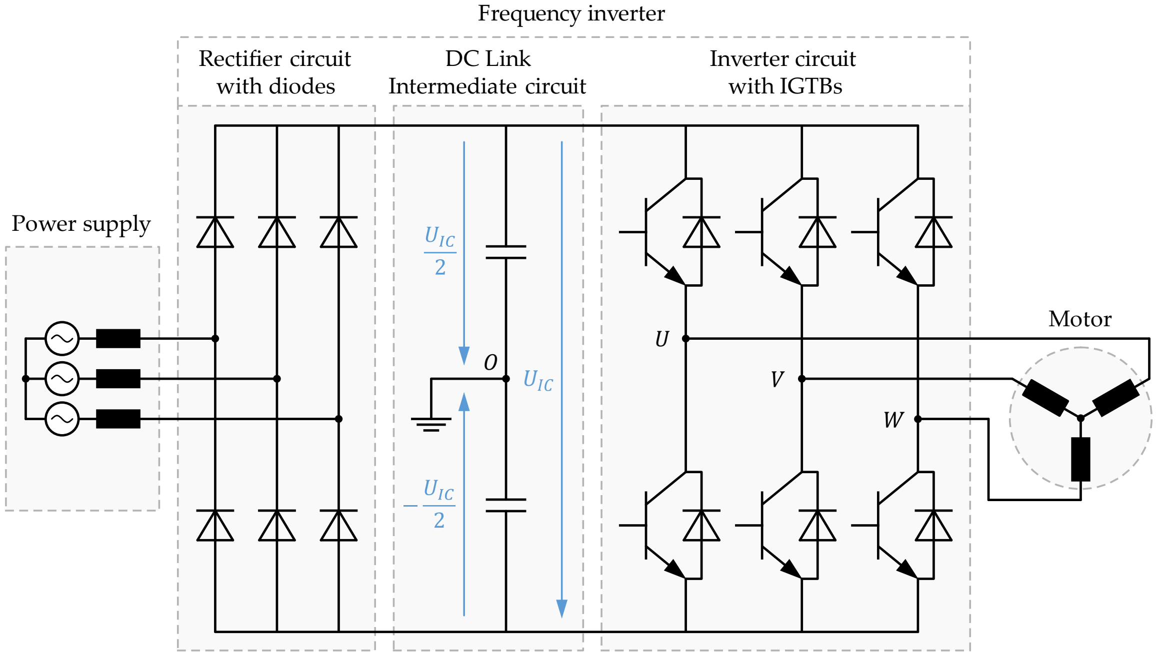

Figure 2.1: Schematic representation of a voltage source DC-link frequency inverter (based on [Jag05])

As shown in Figure 2.1, the frequency inverter consists of three main parts. First, the three-phase diode rectifier bridge converts the incoming three-phase AC power supply to a DC voltage. In the DC link there are smoothing capacitors, which are connected at the mid-point 0 to the ground and thereby define a positive ($+U_{IC}/2$) and a negative ($-U_{IC}/2$) voltage rail, respectively. These discrete voltage levels are combined by the fast-switching semiconductors (nowadays they are predominantly insulated gate bipolar transistors (IGBT)) to generate the control voltage signals for the phases (U, V, W) of the electric motor. Therefore, the phase voltages are not sinusoidal but square wave signals, which are defined by the pulse-width modulation (PWM) and its control algorithm, the space vector modulation (SVM). (These modulation techniques have different variations that result in different signal quality and computational requirements.) The PWM controls the IGBT switching elements and varies the width of the discrete voltage levels, i.e., the shape of the square wave signals. For this purpose, a reference sine wave and a triangular carrier signal are compared, as it is illustrated on Figure 2.2. If the reference signal is greater than the carrier signal, the corresponding pulse-width modulated voltage signal is in high state, otherwise it is in low state.

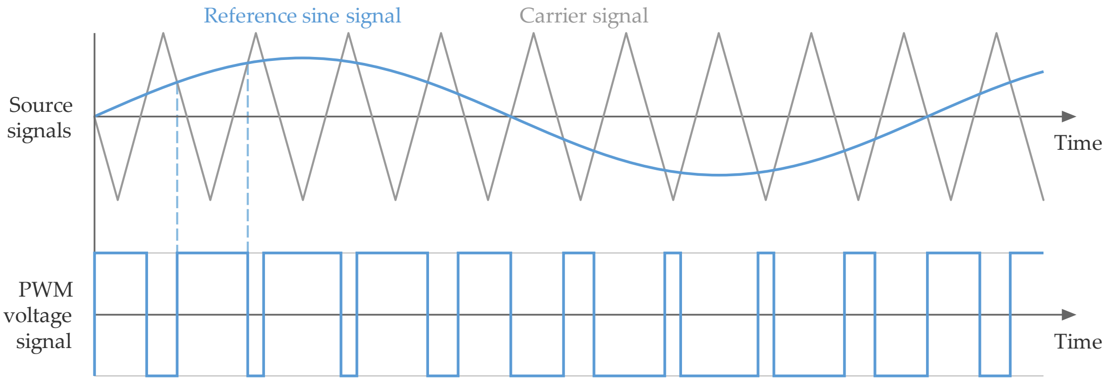

Figure 2.2: Operating principle of the pulse-width modulation based on [SM19]

Due to the inductances of the motor winding, a sinusoidal current is generated by the rectangular voltage pulses of the phase signal. The phase voltages are then synchronised by the SVM depending on the desired rotational speed and load. In case of three 120° phase-shifted sinusoidal voltage signals, the sum of the signals would be zero at every time point. In contrast, the sum of the pulse-width modulated voltage signals is generally not zero, but a stair-shaped signal, with three rising and three falling levels. This characteristic signal is the common-mode voltage U_{CM}, which represents the star point-to-ground voltage of the motor. The common-mode voltage does not impair the electromechanical performance of the motor, but it has a significant role in the generation of bearing currents [Zik10]. The pulse-width modulated phase voltage signals, and the corresponding common-mode voltage are illustrated on Figure 2.3.

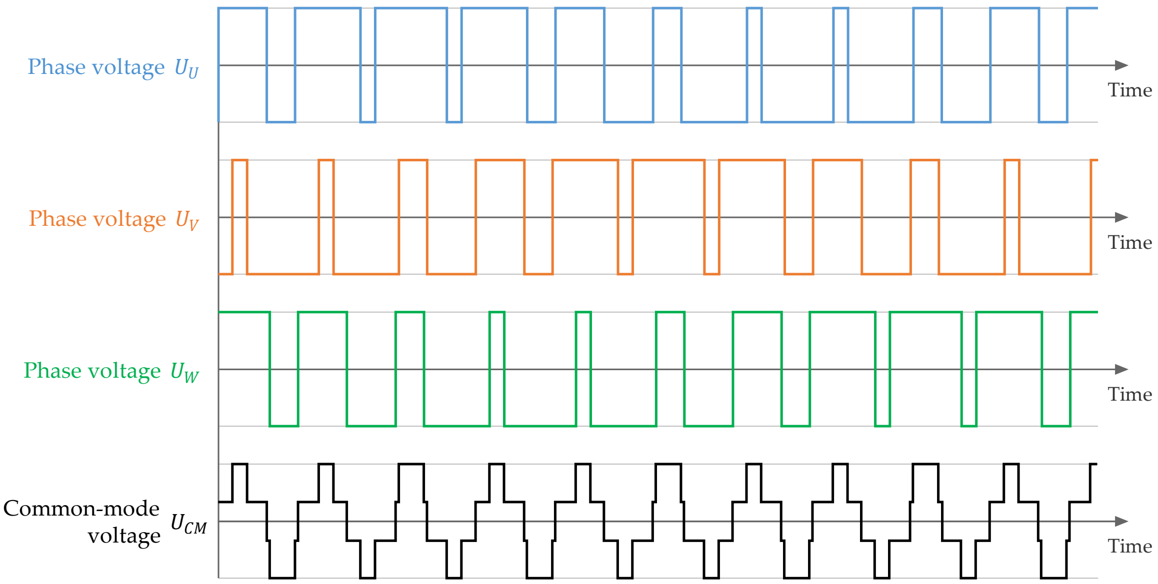

Figure 2.3: Pulse-width modulated phase voltage signals, and the common-mode voltage (based on [SM19])

The electric machines comprise inherent stray capacitances, which represent capacitive coupling between certain components of the motor. These stray capacitances interact with the high-frequency common-mode voltage and influence the generation of parasitic bearing currents. The air gaps and further insulating materials between the conductive components of different potentials are able to store electrical charge and thus can act as local stray capacitances. In case of electric motors, there are stray capacitances at the winding-rotor C_{WR}, rotor-stator C_{RS} and winding-stator C_{WS} couplings (Figure 2.4). In this regard, also the rolling bearings act as stray capacitances $C_{RB,A}$, $C_{RB,B}$, considering the lubrication film between their conductive components. Based on the location of the stray capacitances in the motor, an equivalent circuit diagram can be obtained, which is shown in Figure 2.4 b). It can be observed that the capacitances form a voltage divider, which allows to describe the ratio between the voltage acting on the rolling bearing U_{RB} and the common-mode voltage U_{CM}. This relation is the "bearing voltage ratio" (BVR) [Müt04]:

$$BVR = \frac{U_{RB}}{U_{CM}} = \frac{C_{WR}}{C_{WR} + C_{RB,A} + C_{RS} + C_{RB,B}} \tag{2.1}$$

The BVR can be used to approximate the maximum induced voltage on the bearing related to the common-mode voltage of the motor. The investigations in [Müt04] and [Tis17] showed that the BVR for most standard electric motors is between 1 % and 10 %. For example, in case of a maximum common-mode voltage of 400 V, a maximum bearing voltage of 40 V can be expected [Rad16].

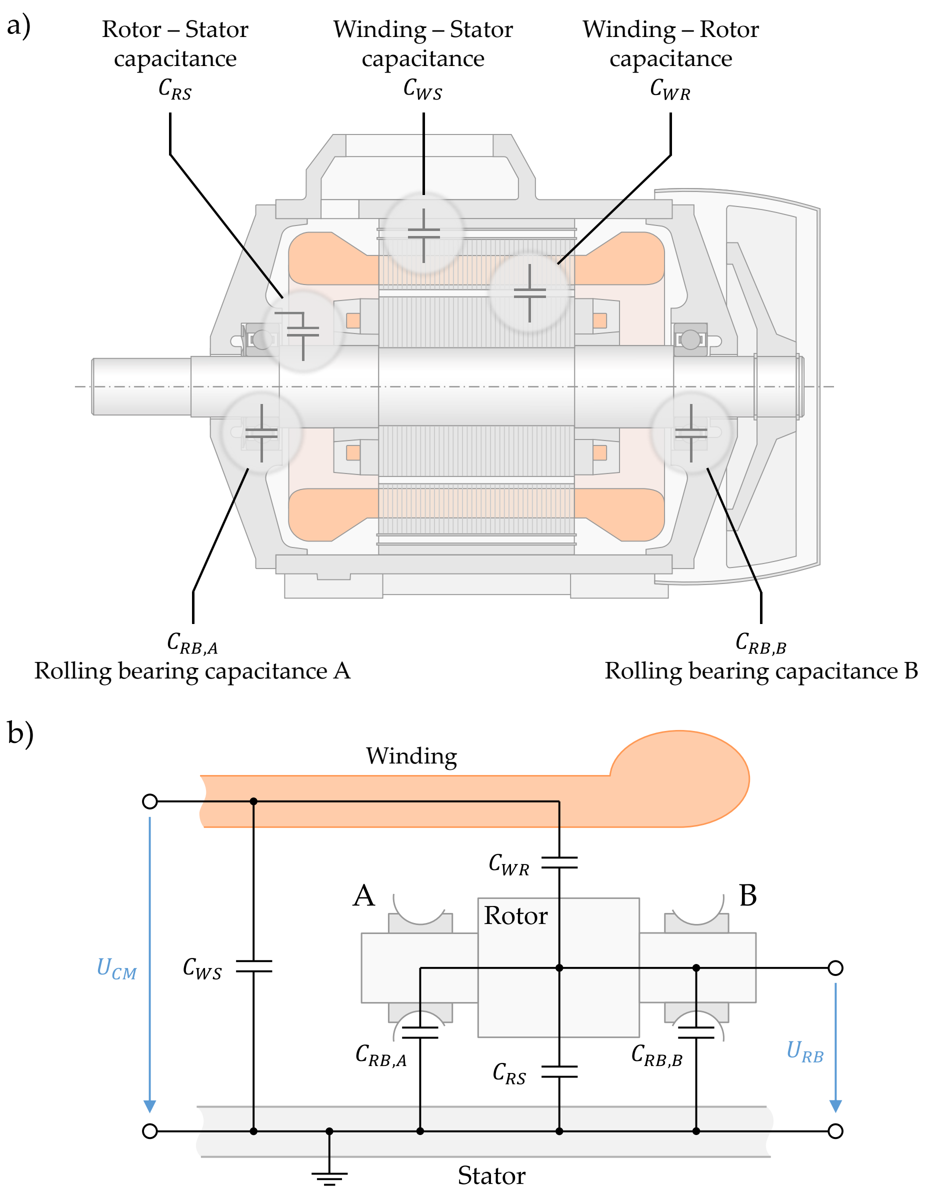

Figure 2.4: a) Stray capacitances of the electric motor (based on [Rad16]); b) Equivalent circuit diagram of the motor using the stray capacitances [Tis17]

After the brief description of the operating principle of modern frequency inverter-controlled electric motors (focusing on the rolling bearing-related electrical effects), the induced "modern" bearing currents can be presented in the following, categorised into four groups based on [Zik10], [Jag05] and [Fur17]:

- **dU/dt currents**: The application of IGBTs as fast-switching semiconductors improves the switching rate, and thus the approximation of the desired sinusoidal voltage signals (compared to the previously used gate-turn-off (GTO) thyristors), and at the same time leads to an increased steepness of the voltage pulses. These fast voltage transients, combined with the stray capacitances, cause current pulses according to the $I = C \cdot dU/dt$ relation at each transition of the phase voltages, i.e., at each switching event of the frequency inverter [Zik10]. In case of a well-developed lubricating film in the rolling contacts, the bearing is in a capacitive state. Therefore, the voltage can build up and the currents passing the bearing – with an amplitude of approx. 10 mA [Fur17] – do not lead to damages, since they are in a reactive state. If the bearing operates with insufficient lubrication condition, i.e., the insulating effect cannot be achieved in the rolling contacts, active currents are draining to the ground through the bearing at the switching events in the range of 5 mA to 200 mA [Fur17]. Examples for dU/dt current paths are illustrated on Figure 2.5 a).

- **Electric discharge machining (EDM) currents**: As shown in Figure 2.4, the common-mode voltage U_{CM}, which acts between the winding and the stator, and the stray capacitances, which serve as a voltage divider, define the bearing voltage U_{RB}. This voltage has a similar course as the common-mode voltage but scaled according to the BVR. If the bearings of the motor operate with insulating lubricant film in the rolling contacts, they act like capacitors and are charged at every switching operation due to the dU/dt currents. In this case the bearing voltage can build up until the point, where the breakdown voltage of the lubricant film is exceeded. At this moment, the energy stored in the stray capacitances will be discharged and an EDM current pulse occurs, which can lead to damages in the rolling bearing. In contrast to dU/dt currents, which can only occur during the switching operations of the frequency inverter, EDM currents can appear independently of them at any time, when the breakdown voltage of the lubricant film is exceeded [Jag05]. Depending on the amplitude of the common-mode voltage, on the stray capacitances of the motor and especially on the operating-point-dependent lubrication condition in the roller bearing, the EDM-breakdown can occur at a few volts up to several tens of volts, and the corresponding current can reach several amperes [Fur17]. Figure 2.5 a) shows examples for EDM current paths in the motor.

- **Grounding currents**: The steep edges of the common-mode voltage interact with the winding-stator stray capacitance C_{WS}, and thereby high-frequency currents are generated. These currents, which leave the winding through the capacitance C_{WS}, flow back to the source, i.e., to the ground potential of the frequency inverter and called grounding currents [Fur17]. Since the current follows the path with the lowest impedance, the grounding conditions have a great importance regarding the affected components. If the motor is installed with a low-impedance stator grounding, most of the grounding current flows as "*stator-to-ground*" current through this grounding back to the inverter (i.e., to its ground potential). In this case, the bearings are not affected. If the rotor shaft is connected to a well-grounded driven machine (next to a possible poor grounding of the stator or the inverter), an alternative current path may form, which provides lower impedance than the previously defined. Therefore, the high-frequency currents flow from the stator through one of the bearings to the shaft, then along the shaft to the driven machine and back to the grounding potential. These "*rotor-to-ground*" currents are in the range of several amperes [Fur17], and they can lead to damages in the rolling bearings of the motor or in the components of the driven machine. Figure 2.5 b) represents possible current paths for both the "*stator-to-ground*" and the "*rotor-to-ground*" currents.

- **High frequency circulating currents**: As it was mentioned previously, high-frequency grounding currents can leave the winding through the capacitance C_{WS} due to the steep edges of the common-mode voltage. Consequently, the current flowing into the stator winding is higher than the current flowing out [HXL20], [CLN98]. The resulted non-constant (both in space and time) current-flow in the stator winding generates a tangential magnetic field around the motor shaft. This rotating magnetic field can induce an alternating shaft voltage in axial direction (similar to the shaft voltages generated by the magnetic asymmetries at the "classical" bearing currents). As a result, high-frequency circulating currents can flow from the motor shaft across one bearing, along the motor frame and across the other bearing back to the motor shaft. It is illustrated in Figure 2.5 c). The circulating currents appear on the bearings with the same magnitude but with opposite polarity. Since they are coupled with the dU/dt currents, they do not flow continuously, but synchronised with the switching operations of the frequency inverter [Zik10]. The high-frequency circulating currents, such as the grounding currents, can also reach values of several amperes [Fur17]. The investigations described in [Tis17] show that the electrical bearing load due to circulating currents increases with increasing motor power, and typically occurs from a motor power of 50 kW [RG15].

a) dU/dt and EDM currents

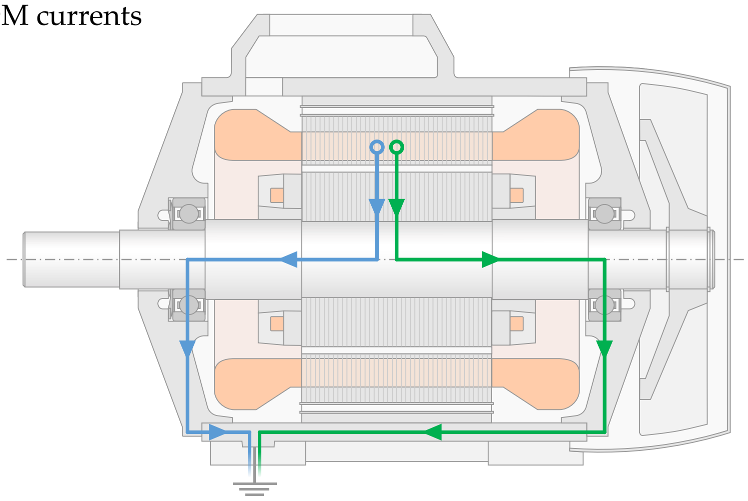

b) Grounding currents

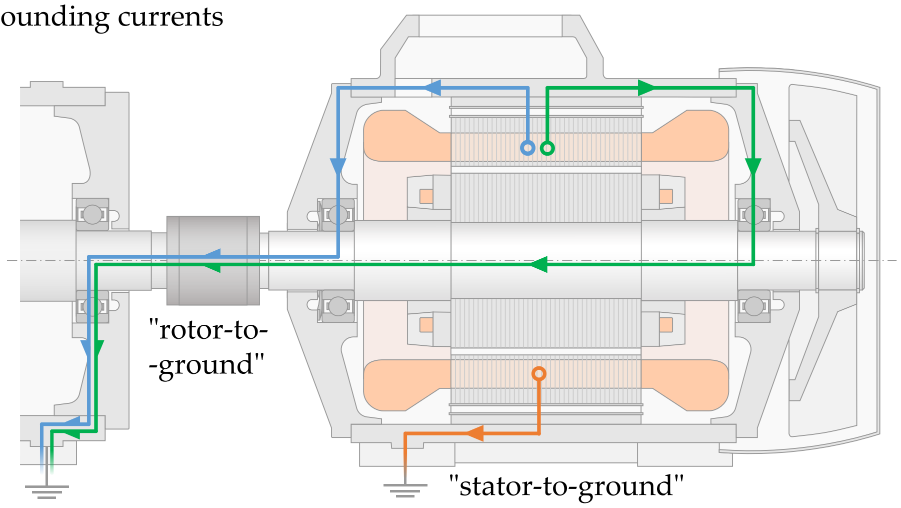

c) Circulating currents

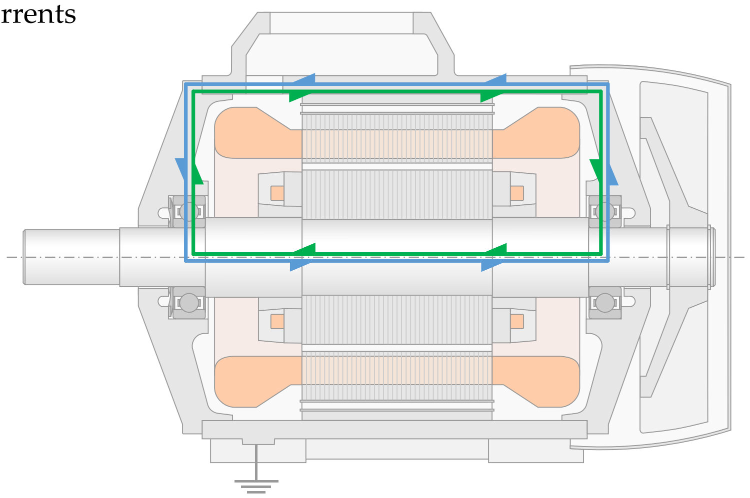

Figure 2.5: Frequency inverter-induced bearing currents represented by their paths: a) dU/dt and EDM currents; b) Grounding currents; c) Circulating currents (based on [PBCN18] and [Sch20])

2.1.3 Damages due to bearing currents

The presented parasitic currents can lead to different types of rolling bearing damages (Figure 2.6), which can significantly reduce the service life of the component, and thus the service life of the whole machine. The current related rolling bearing damages are described in the following:

- **Crater formation and grey frosting**: Due to the high energy of the electrical discharges, metallic particles can leave the surfaces, resulting in crater-like formations. In parallel, local melting can occur, which is then rolled over by the rolling element leading to a hardened material layer and macroscopically matt-looking surface [Furt17]. The resulted surface structure is also known as "grey frosting". (Figure 2.6 a))

- **Fluting**: The fluting is a typical current-related damage of rolling bearings, which is also referred to as "ripple" formation in the literature. The fluting is characterised by a multitude of heterochromatic grey lines perpendicular to the raceway [Tis17b]. These lines form a nearly periodic ridge-valley structure on the running traces of the rings (or in rare cases on the rolling elements). The fluting leads to increased vibration and thus significantly higher wear of the rolling bearing. (Figure 2.6 b))

- **Lubricant degradation**: The high local temperature generated by electrical discharges in the rolling contact leads to the degradation of the lubricant. Due to oxidation processes, the lubricant discolours and its lubricating properties deteriorate, which can lead to bearing damages. In addition, during the crater formation, the metal particles that leave the surfaces accumulate in the lubricant, thereby changing its electrical properties. (e.g., conductivity, permittivity) [Bec20]. These effects can be observed for both lubricating oils and greases. (Figure 2.6 c))

- **White etching cracks (WEC)**: The WECs are cracks in the microstructure of the bearing steel, which appear with localised white areas when the microsection is polished and etched. The formation mechanism of WECs is a complex and diverse process and the subject of ongoing research. The WECs lead to material spalling and thus to an early failure of the rolling bearing. Current research shows that the presence of bearing currents helps the formation of WECs [LBG16], [LBG21]. (Figure 2.6 d))

a) Crater formation and grey frosting

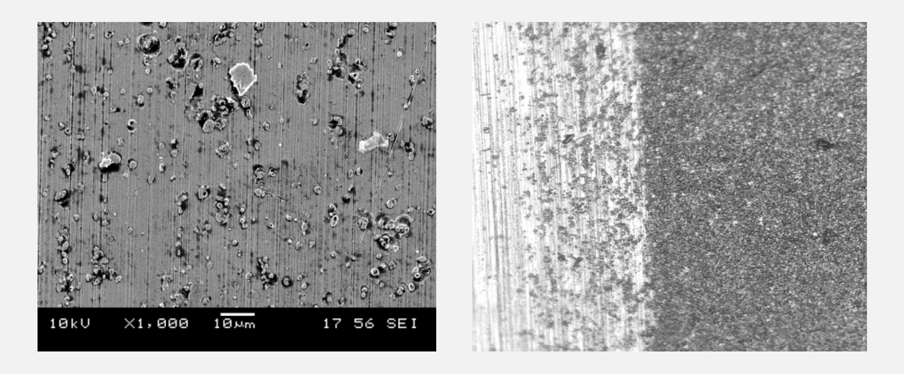

b) Fluting

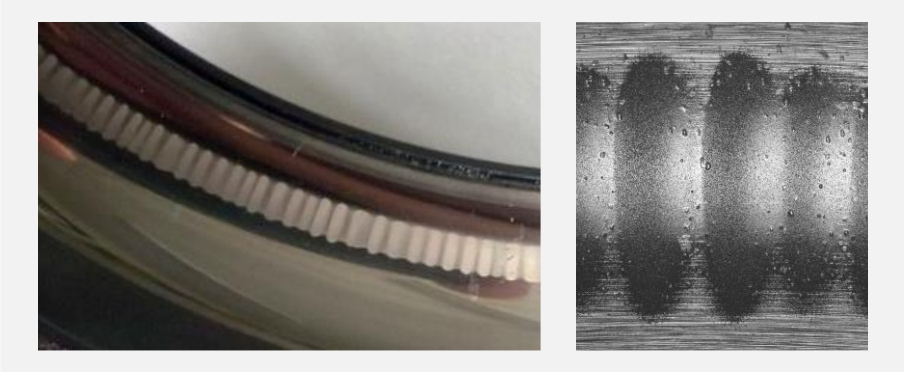

c) Lubricant oxidation and accumulated particles

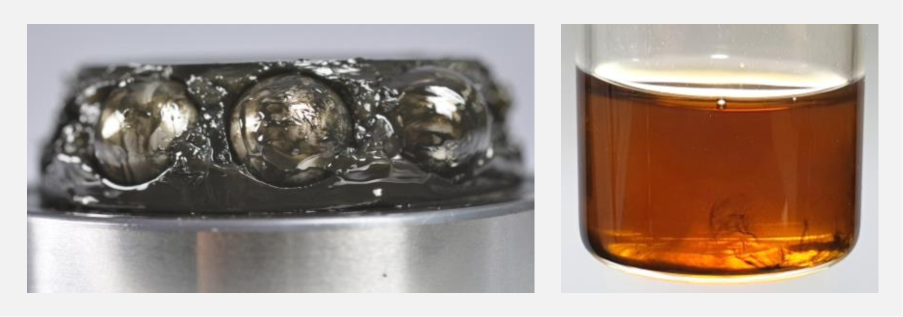

d) White etching cracks

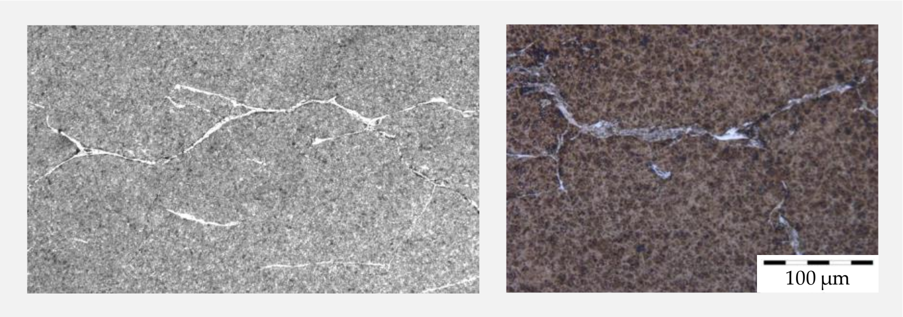

Figure 2.6: Rolling bearing damages caused by parasitic currents: a) Crater formation and grey frosting [Rad16], [Bec20]; b) Fluting [Rad16]; c) Lubricant degradation; d) White etching cracks [MSMK19], [LBG16]

2.1.4 Preventive measures

The damages caused by the parasitic bearing currents can lead to the downtime of the entire machine. In order to avoid this outcome, different preventive measures have been developed and are currently being researched. Focusing on the manipulation of harmful currents and their paths, different preventive strategies can be distinguished. These strategies and the components, developed for their practical application, are summarised in [Bec20], and are presented accordingly in the following:

Strategy 1: The rolling bearings and their surroundings are designed in such a way that no harmful currents can flow through the bearings.

- Insulated bearings (hybrid bearings or ceramic bearings)
- Insulated bearing rings
- Insulated clutches

Strategy 2: The harmful currents are limited or avoided before they would reach the rolling bearing by influencing the electrical system.

- Sine-wave filters
- Nanocrystalline or ferrite rings
- Current-limiting chokes

Strategy 3: The harmful currents are conducted through an alternative path, thereby avoiding the rolling bearing.

- Shaft grounding rings
- Contact brushes
- Conductive sealings
- Conductive lubricants

The listed strategies and components have inherent advantages and disadvantages. While some methods only protect against certain type of bearing currents, others lead to one-time or regular additional costs (due to additional parts and/or mounting), which make their application financially disadvantageous. Furthermore, reducing certain type of harmful currents can lead to an increase in other types of parasitic currents. The manipulation of current paths, and thereby avoiding the bearing currents, can also shift the harmful effects to other mechanical components, such as to the gears. These facts underline the need for the electrical modelling of mechanical components and contacts, which allows the observation and investigation of the system-level electrical interactions.

2.2 Basics of rolling bearings

To discuss the state-of-the-art electric bearing models, it is first necessary to present the related rolling bearings and their relevant aspects. Accordingly, this chapter focuses on the mechanical description of rolling bearings, and the lubricant film in the rolling contact.

2.2.1 Function and design

The function of rolling bearings is to transfer forces between parts moving relative to each other and to define their relative position. The friction that arises between moving components is reduced with the help of intermediate rolling elements, which replace sliding motion with rolling (next to a small amounts of residual sliding) [SS12]. Today, a large variety of rolling bearings is available, with bearing designs optimised for specific applications and environments. Rolling bearings can be distinguished, among others, according to the direction of the carried load (axial, radial or combined) or the shape of the rolling elements (ball, cylindrical-, tapered- or further special roller). Figure 2.7 provides a brief overview of typical rolling bearing designs, showing their target load conditions and contact angles.

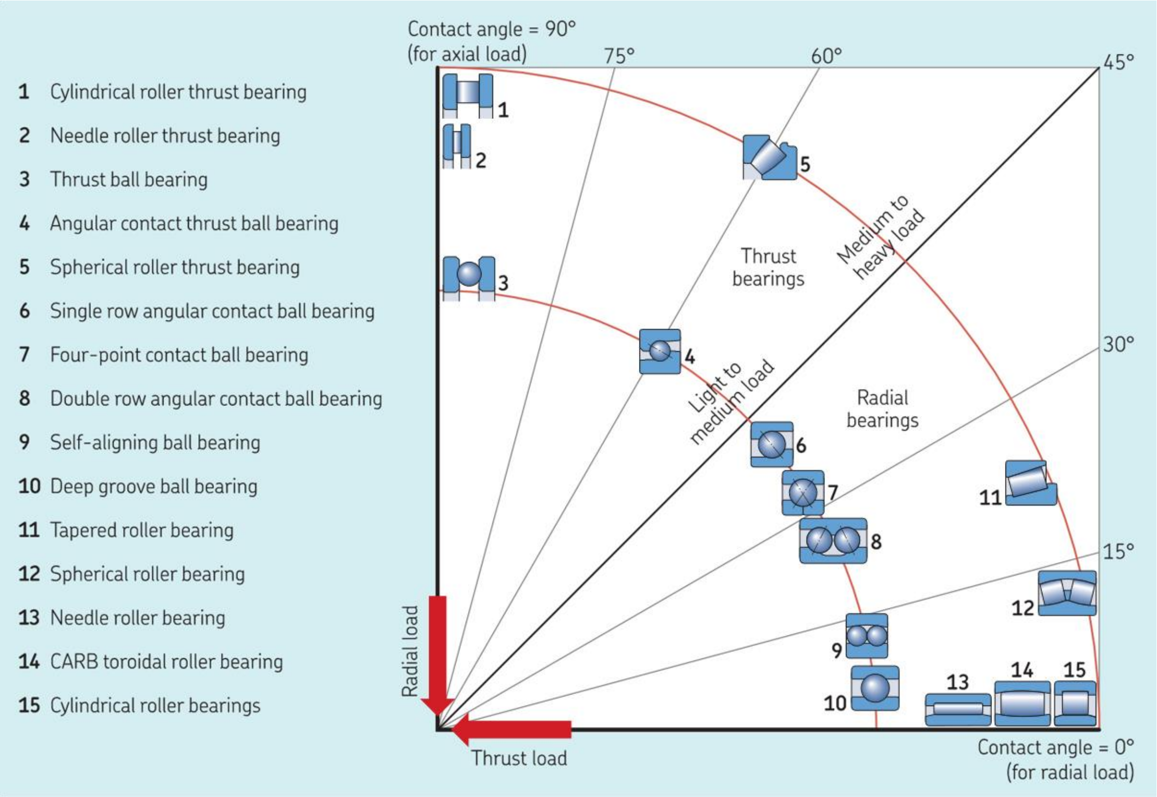

Figure 2.7: Typical designs of rolling bearings with targeted load conditions and contact angles [Skf18]

Generally, the rolling bearings consist of the following parts: inner ring, outer ring, rolling elements, cage, and lubricant. The rolling elements move on the raceways of the inner and outer rings and are kept evenly spaced by the cage. The rings and the rolling elements are made of bearing steel (in special cases ceramic or plastic materials are also applied), and the cages can be made of steel, brass, or different plastic variants. To reduce frictional losses, lubricating oils, greases, and in special applications solid lubricants are used. The rolling bearing can also be equipped with sealing rings to keep the lubricant between the inner and outer rings and to avoid contamination.

In the following, the work focuses on deep groove ball bearings, angular contact ball bearings and thrust ball bearings. The first two are of particular importance for electric motors and generators, while the third has a significant role in investigations because of its favourable modelling possibilities. Figure 2.8 illustrates the main parts and the mounting dimensions of the rolling bearings through the example of an angular contact ball bearing and a thrust ball bearing.

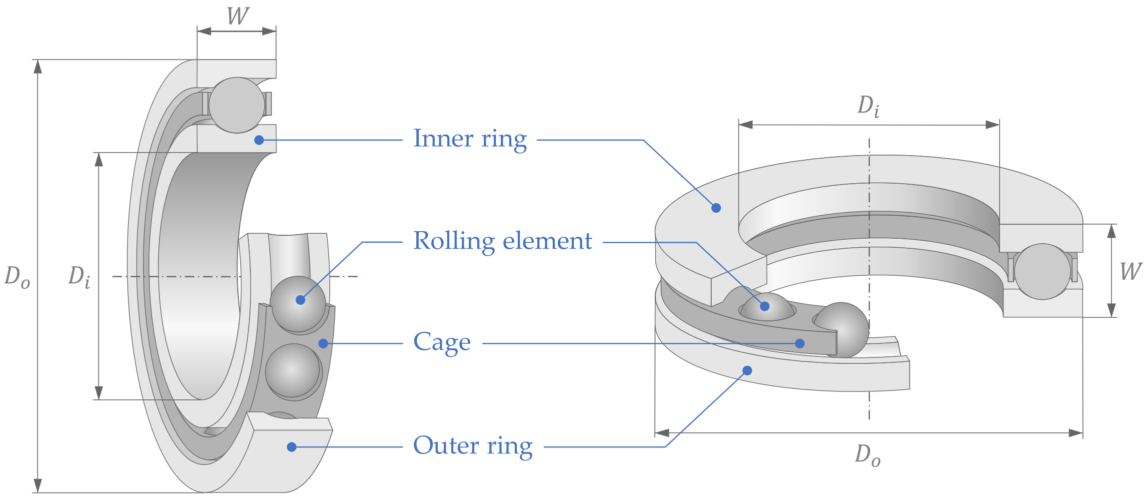

Figure 2.8: Main parts and mounting dimensions of rolling bearings through the example of an angular contact ball bearing and a thrust ball bearing

The rolling bearings are mounted with the bore diameter D_i of the inner ring and the outside diameter D_o of the outer ring. In the case of thrust ball bearings, the inner and outer rings can be defined by their positioning surfaces, i.e., the ring mounted with its inner diameter D_i is referred to as inner ring. Furthermore, the width W of the bearing is a further mounting dimension. Another group of bearing dimensions is related to the operation of the bearing. This includes, among others, the diameter of the rolling element d_{re} and the groove radius of the raceway on the inner ring $r_{rw,ir}$ and outer ring $r_{rw,or}$. The dimensions related to the rolling element and its direct environment are shown in Figure 2.9.

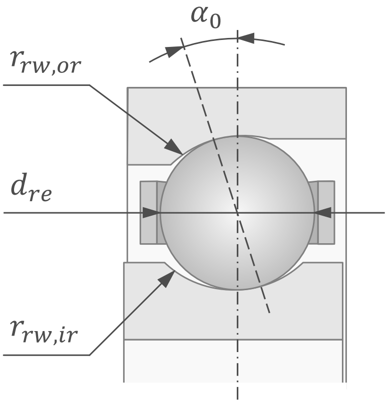

Figure 2.9: Rolling bearing dimensions related to the rolling element and its direct environment

During the operation of the rolling bearing, the external load is transmitted inside the bearing from one raceway through the rolling elements to the other raceway. The direction of the load is described by the line connecting the contact points of the bearing rings with the centre of the rolling element. This line closes an angle with the radial mid-plane of the bearing, which is called contact angle [Bal05]. Depending on the operating condition of the bearing, a distinction can be made between nominal contact angle α_0 and operating contact angle α. The nominal contact angle, which depends only on the geometry of the bearing, is present in unloaded condition. When the bearing is loaded by external forces, it operates with the operating contact angle that considers the change of the angle due to the load-dependent deformations. Furthermore, at high rotational speeds, additional centrifugal forces act on the rolling elements, resulting in different loads and contact angles in the inner and outer ring contacts. A detailed description of the rolling bearing dimensions, and the related calculations can be found in [Sch19] or [Bar96], among others.

2.2.2 Loads and hertzian contact

If a rolling bearing is subjected to external forces or tilting moments, the inner ring of the bearing can shift and tilt relative to the outer ring due to the clearance and the elastic deformation of the components. The resulted displacement leads to an individual operating contact angle α_j for each rolling element j (Figure 2.10 a)), and accordingly to an individual load Q_j. Depending on the external loads, different load distributions can be observed on the rolling elements, which are illustrated in Figure 2.10 b). In the case of purely radial loading of the bearing ($\beta = 0°$), a load zone is formed inside the bearing and only the rolling elements located within this zone are subjected to it. With an increasing axial component of the external load (0° < β < 90°), more and more rolling elements are involved with their unique contact angle α_j and load Q_j. For bearing loads acting only in the axial direction F_{ax} ($\beta = 90°$), the load is distributed evenly on all rolling elements with the same operating contact angle α as:

$$Q = \frac{F_{ax}}{Z \cdot \sin\alpha} \tag{2.2}$$

where Z is the number of rolling elements. To calculate the load distribution and contact angles in general cases, there are different calculation methods that take into account the balance of external forces and the forces acting on the rolling elements. For low to medium rotational speeds the assumption of static equilibrium is generally used (e.g., [DIN 26281]). For higher rotational speeds, the calculations can be extended to take centrifugal forces into account [HK06].

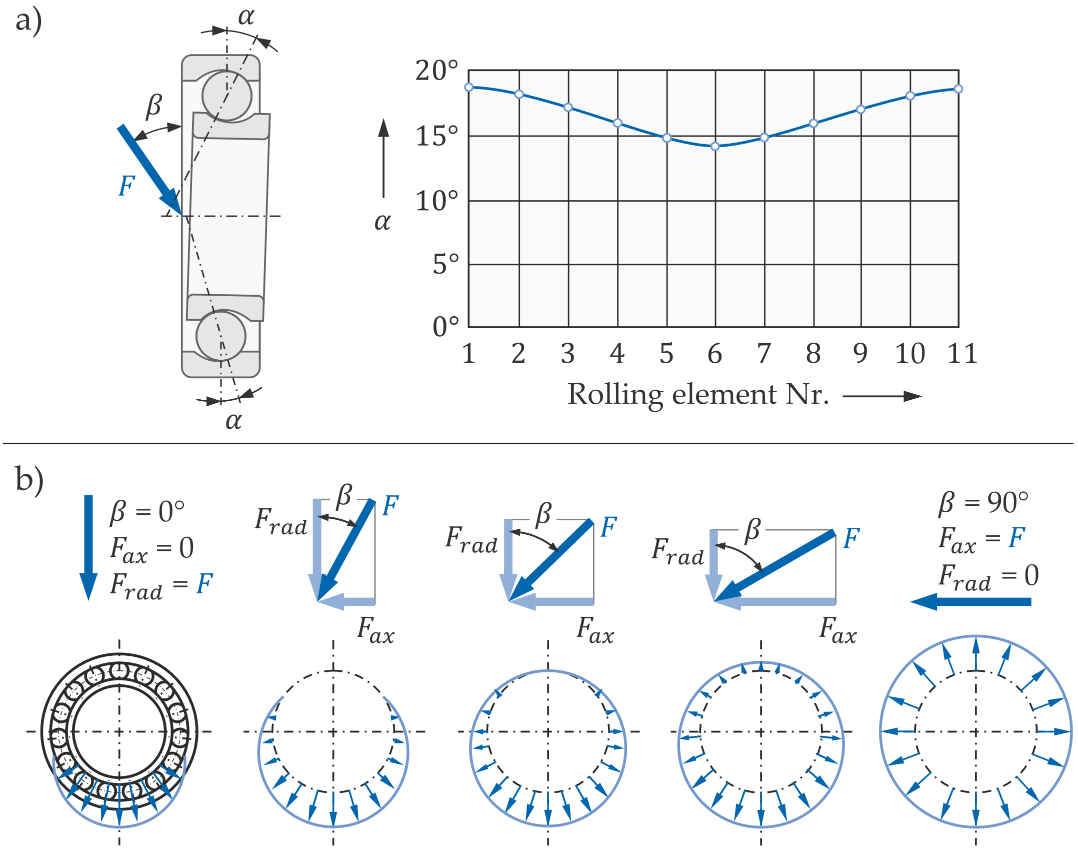

Figure 2.10: a) Operating contact angles of the individual rolling elements in case of a combined bearing load; b) Distribution of the bearing load on the rolling elements under different load conditions of the rolling bearing [Sch10]

Knowing the load on the rolling element, the deformation and the area of the contact surface can be approximated using the hertzian contact theory [Her81], which is described in the following based on [Wan15]. Although this calculation method applies certain simplifications (e.g., the surfaces are assumed to be frictionless and only normal forces are transmitted between them), it is well suited to general problems, and is still widely used today. In the case of ball bearings, the contacts can be generally described as point contacts between elastic ellipsoids, where a contact ellipse is formed due to the acting load Q. The corresponding semi-major and semi-minor axes are denoted by a and b. The geometries of the contact partners are described with their curvatures in two perpendicular planes, which are also perpendicular to the plane of the contact ellipse and defined by the semi-axes. The coordinates are chosen to satisfy the following condition of the radii in accordance with Figure 2.11:

$$\frac{1}{r_{1y}} + \frac{1}{r_{2y}} > \frac{1}{r_{1x}} + \frac{1}{r_{2x}} \tag{2.3}$$

The convex surfaces are represented by a positive radius, while the concave surfaces are represented by a negative radius.

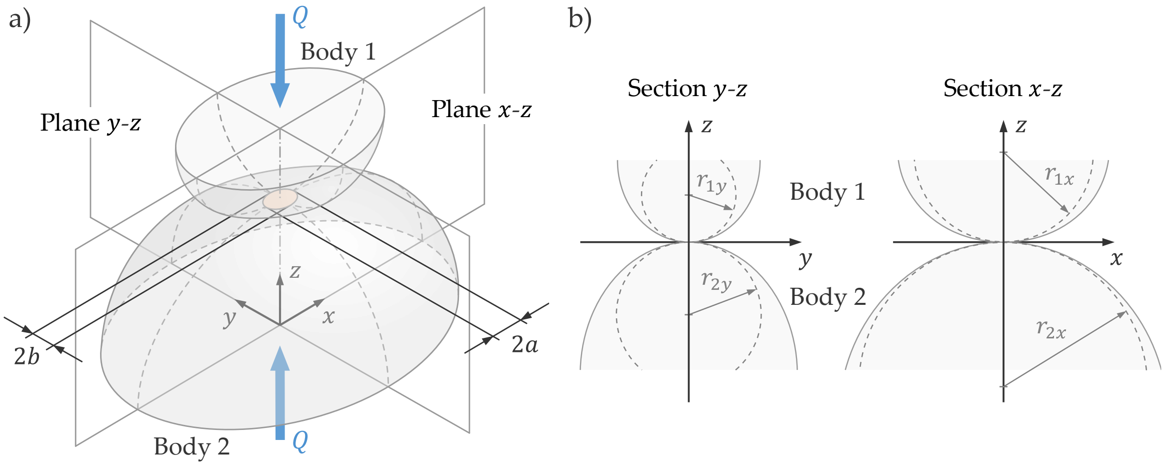

Figure 2.11: a) Representation of the hertzian contact of elliptic bodies; b) Section views of the contact before the deformation with the corresponding coordinates and dimensions (based on [Wan15])

In this system the semi-major and semi-minor axes a and b, the depth of indentation δ, and the maximum contact pressure p_{max} can be calculated as:

$$p_{max} = 1.5 \cdot \frac{Q}{\pi \cdot a \cdot b} \tag{2.4}$$

$$\delta = \mathcal{F} \cdot \sqrt[3]{\frac{9 \cdot \sum \rho}{2 \cdot \mathcal{E}} \cdot \left(\frac{Q}{\pi \cdot \kappa \cdot E_0}\right)^2} \tag{2.5}$$

$$a = \sqrt[3]{\frac{6 \cdot \kappa^2 \cdot \mathcal{E} \cdot Q}{\pi \cdot \sum \rho \cdot E_0}} \tag{2.6}$$

$$b = \sqrt[3]{\frac{6 \cdot \mathcal{E} \cdot Q}{\pi \cdot \kappa \cdot \sum \rho \cdot E_0}} \tag{2.7}$$

where $\sum \rho$ is the sum of the curvatures:

$$\sum \rho = \frac{1}{r_{1x}} + \frac{1}{r_{2x}} + \frac{1}{r_{1y}} + \frac{1}{r_{2y}} \tag{2.8}$$

The material properties of the contact bodies are described with the reduced modulus of elasticity E_0, using the modulus of elasticities E_1 and E_1, and Poisson's ratios ν_1 and ν_2 of the bodies:

$$E_0 = \frac{2}{\frac{1-\nu_1^2}{E_1} + \frac{1-\nu_2^2}{E_2}} \tag{2.9}$$

The ratio of the semi-axes (or ellipticity parameter) is denoted by κ:

$$\kappa = \frac{a}{b} \tag{2.10}$$

Furthermore, $\mathcal{F}$ and $\mathcal{E}$ are the complete elliptic integrals of the first and second order. Since iterative calculations are required to solve the presented form of the hertzian equations, several methods have been proposed to simplify and speed up the computational process. A possible method for the replacement of the elliptic integrals was presented by Brewe and Hamrock [BH77], where the parameters $\mathcal{E}$, $\mathcal{F}$ and κ are described by regression-based analytic approximation formulas as the function of the curvature radii. The provided fits for $\mathcal{E}$, $\mathcal{F}$ and κ are denoted by $\bar{\mathcal{E}}$, $\bar{\mathcal{F}}$ and $\bar{\kappa}$:

$$\bar{\mathcal{E}} = 1.0003 + 0.5968 \cdot \frac{R_x}{R_y} \tag{2.11}$$

$$\bar{\mathcal{F}} = 1.5277 + 0.6023 \cdot ln\left(\frac{R_y}{R_x}\right) \tag{2.12}$$

$$\bar{\kappa} = \frac{a}{b} = 1.0339 \cdot \left(\frac{R_y}{R_x}\right)^{0.636} \tag{2.13}$$

where

$$\frac{1}{R_x} = \frac{1}{r_{1x}} + \frac{1}{r_{2x}} \tag{2.14}$$

$$\frac{1}{R_y} = \frac{1}{r_{1y}} + \frac{1}{r_{2y}} \tag{2.15}$$

Once the elliptic semi-axes are known, the area of the hertzian contact surface A_{Hertz} can be calculated, which has significant role in the electrical modelling of the contact (described in Chapter 2.3.1).

$$A_{Hertz} = \pi \cdot a \cdot b \tag{2.16}$$

2.2.3 Rolling bearing kinematic

For the calculation of the lubricant film thickness in the rolling contacts of the bearing, it is necessary to know the kinematic conditions of the related components. In the following, the calculation of the required velocities and rotational speeds is presented using the example of an angular contact ball bearing. It is assumed that the rolling elements roll slip-free on the raceways, while the deformation of the contacts and the effect of centrifugal forces are neglected. The kinematic conditions and the related geometric dimensions are shown in Figure 2.12.

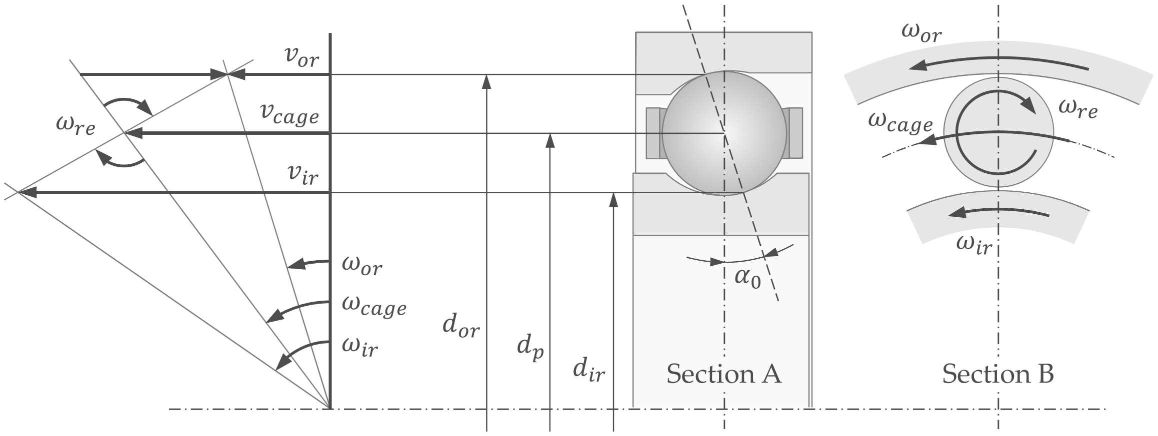

Figure 2.12: Kinematic conditions of an angular contact ball bearing (based on [Bar96] and [Aul14])

The circumferential velocity of a body rotating around its axis can be calculated as:

$$v = r \cdot \omega = r \cdot \frac{2 \cdot \pi \cdot n}{60} \tag{2.17}$$

Where ω is the angular velocity, n is the rotational speed, and r is the distance between the axis of rotation and the circumferential point. For the subsequent equations, the pitch diameter d_p and the geometric parameter γ are first defined:

$$d_p = \frac{d_{ir} + d_{or}}{2} = r_{ir} + r_{or} \tag{2.18}$$

$$\gamma = \frac{d_{re}}{d_p} \cdot \cos\alpha_0 \tag{2.19}$$

Using the presented parameters, the circumferential velocity at the contact point of the inner and outer ring can be calculated as:

$$\begin{aligned} v_{ir} = r_{ir} \cdot \omega_{ir} &= \frac{1}{2} \cdot \left(d_p - d_{re} \cdot \cos\alpha_0\right) \cdot \omega_{ir} = \\ &= \frac{1}{2} \cdot d_p \cdot (1-\gamma) \cdot \omega_{ir} = \frac{\pi \cdot n_{ir}}{60} \cdot d_p \cdot (1-\gamma) \end{aligned} \tag{2.20}$$

$$\begin{aligned} v_{or} = r_{or} \cdot \omega_{or} &= \frac{1}{2} \cdot \left(d_p + d_{re} \cdot \cos\alpha_0\right) \cdot \omega_{or} = \\ &= \frac{1}{2} \cdot d_p \cdot (1+\gamma) \cdot \omega_{or} = \frac{\pi \cdot n_{or}}{60} \cdot d_p \cdot (1+\gamma) \end{aligned} \tag{2.21}$$

The circumferential velocity of the cage v_{cage}, which also represents the translational velocity of the centre of the rolling elements, can be determined with the help of the previously defined contact velocities:

$$\begin{aligned} v_{cage} &= \frac{1}{2} \cdot d_p \cdot \omega_{cage} = \frac{1}{2} \cdot (v_{ir} + v_{or}) = \\ &= \frac{\pi \cdot d_p}{120} \cdot [n_{ir} \cdot (1-\gamma) + n_{or} \cdot (1+\gamma)] \end{aligned} \tag{2.22}$$

Then, the rotational speed of the cage n_{cage} and the rotational speed of the rolling elements (relative to their centre) n_{re} can be expressed as:

$$n_{cage} = \frac{1}{2} \cdot [n_{ir} \cdot (1-\gamma) + n_{or} \cdot (1+\gamma)] \tag{2.23}$$

$$n_{re} = \frac{1}{2} \cdot \frac{d_p}{d_{re}} \cdot (n_{or} - n_{ir}) \cdot (1-\gamma^2) \tag{2.24}$$

For the calculation of the lubricant film thickness (Chapter 2.2.5), the hydrodynamic velocity is necessary. It can be calculated by the averaged sum velocity of the contact surfaces considering an equivalent system, where the cage and the set of rolling elements are stationary fixed, and the velocities of the components are assigned accordingly [Aul14]. Thereby, the lubricant is conveyed into the lubrication gap due to the rotation of the contact partners around their axis of rotation.

In this way, the hydrodynamic velocity of the inner ring contact and the outer ring contact can be calculated:

$$u_{ir} = \frac{\pi}{120} \cdot d_p \cdot \left[(1-\gamma) \cdot \left(n_{ir} - n_{cage}\right) - \gamma \cdot n_{re}\right] \tag{2.25}$$

$$u_{or} = \left| \frac{\pi}{120} \cdot d_p \cdot \left[(1+\gamma) \cdot \left(n_{or} - n_{cage}\right) + \gamma \cdot n_{re}\right] \right| \tag{2.26}$$

The presented calculations can also be applied to a driven shaft with a non-rotating outer ring. In this case, the circumferential velocity of the outer ring v_{or} and the rotational speed of the outer ring n_{or} must be substituted with zero in the equations. Similarly, the calculations can also be applied for thrust ball bearings if the contact angle α_0 is defined as 90°. A detailed description and calculation of the kinematic conditions of rolling bearings (e.g., considering different contact angles at the inner ring and outer ring contact) can be found, among others, in [Bar96].

2.2.4 Lubrication and lubricant properties

Friction occurs between contacting components that move relative to each other and are subjected to contact loads. It leads to wear, heating, and it could reduce the service life of the parts. To ensure a long service life, lubrication is applied, which can reduce friction and reduce or avoid wear between the components [SS12]. In addition, lubrication is used to improve heat dissipation, to transfer wear particles from the contact and to prevent corrosion. These beneficial factors make it an essential part of the rolling bearings. The lubricants can be solid (e.g., PTFE, graphite), plastic (grease), liquid (oil) or gaseous (air). In electric motors, generators and in the related applications predominantly lubricating oils and greases are used. The lubricating oils can be divided into mineral oils and synthetic oils. During their production, certain properties are specifically adjusted, such as viscosity and density. Other properties such as flash point, corrosion resistance, foaming behaviour or electric conductivity can be influenced by different additives. Lubricating greases consist of base oil, thickener, and additives. Due to its structure, the thickener can absorb the base oil and deliver it to the bearing components in small quantities over a long period of time. In this way, even a small amount of grease can provide sufficient lubrication for a considerable time. Additives are also used in case of lubricant greases to influence some targeted properties. Commonly used additives, their influence, and a detailed description of the composition of lubricants can be read in [SS12].

The electrical energy storing ability of the rolling bearing strongly depends on the thickness of the lubricant film in the rolling contacts, and thereby on the rheological and electrical properties of the lubricant. Since the present work focusing on oil-lubricated rolling bearings, the relevant properties of lubricating oils, which are taken into account in the subsequent modelling, are presented below.

In terms of the description and modelling of lubricants, viscosity is one of their most important rheological properties. The dynamic viscosity η describes the internal friction of the fluid, i.e., its resistance to relative movement. It is defined as the shear force F required to move two parallel, plane surfaces of unit area A with a constant relative velocity Δv against each other, in case of an infinitesimally thin h fluid layer between them. For Newtonian fluids under these conditions, a linear velocity profile dv/dy develops, as it is depicted in Figure 2.13.

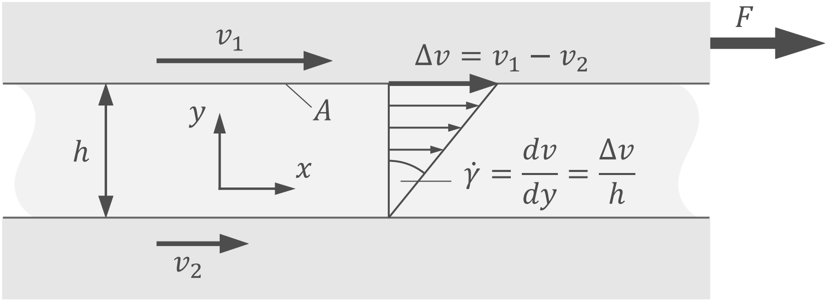

Figure 2.13: Gap flow with velocity gradient in case of a Newtonian fluids [SS12]

Thus, the dynamic viscosity is the ratio of the shear stress τ to the shear rate $\dot{\gamma}$ in the fluid. Since the shear force F per unit area A corresponds to the shear stress τ, and the velocity gradient dv/dy corresponds to the shear rate $\dot{\gamma}$, the dynamic viscosity can be expressed as:

$$\eta = \frac{F/A}{dv/dy} = \frac{\tau}{\dot{\gamma}} \tag{2.27}$$

Another quantity used to describe the internal friction of a fluid is the kinematic viscosity ν, which is defined as the ratio of the dynamic viscosity η to the density ρ of the fluid:

$$\nu = \frac{\eta}{\rho} \tag{2.28}$$

The viscosity changes as a function of temperature and pressure. With increasing temperature, the viscosity decreases, while increasing pressure leads to increasing viscosity. To describe these relationships, different calculation methods have been developed. In case of dynamic viscosity, the equation of Vogel can take the temperature dependence into account using lubricant-specific constants [SS12], which must be determined by measurements. The change of the dynamic viscosity as a function of the pressure can be described by the Barus equation [Bar93] with the help of the oil viscosity at atmospheric pressure and the pressure-viscosity coefficient α_p, which itself depends on both the pressure and the temperature [CH10]. Using the equation derived by Rodemund [Rod80], the effect of both parameters can be taken into account using the coefficients of Vogel (for temperature dependence) and additional parameters from Rodemund (for pressure dependence).

Similar to viscosity, density also depends on temperature and pressure. The increasing temperature leads to decreasing density, while increasing pressure leads to increasing density. The [DIN 51757] offers a calculation method for the determination of the density of lubricants considering their temperature-dependence at atmospheric pressure. Another calculation method was developed by Vogelpohl, which uses separate formulae for the density-temperature and density-pressure relationships [SS12]. Gundrum derived an equation [Gun91] with which both parameters can be considered using lubricant-specific constants.

In the present work, a set of equations developed by Bode [Bod84], [Bod89] is applied to describe the pressure- and temperature-dependence of density and dynamic viscosity in case of the investigated oils. Similar to some of the previously mentioned methods, the equations require lubricant-specific constants (α_s, ρ_s, $a_1 \ldots a_5$, and $A_1 \ldots A_4$) that must be determined experimentally using a high-pressure viscometer. Knowing these values, the temperature and pressure dependent density $\rho(p,T)$ and dynamic viscosity $\eta(p,T)$ of the lubricant can be calculated with the help of the following equations:

$$\rho(p,T) = \frac{\rho(T)}{1 - a_1 \cdot ln\left(\frac{a_2 + a_3 \cdot T + a_4 \cdot T^2 + a_5 \cdot T^3 + p}{a_2 + a_3 \cdot T + a_4 \cdot T^2 + a_5 \cdot T^3}\right)} \tag{2.29}$$

where

$$\rho(T) = \rho_s \cdot (1 - \alpha_s \cdot T) \tag{2.30}$$

and

$$\eta(p,T) = A_1 \cdot e^{\left(\frac{A_2 \cdot \rho(p,T)}{\rho_g(T) - \rho(p,T)}\right)} \tag{2.31}$$

where

$$\rho_g(T) = A_3 \cdot (1 + A_4 \cdot T) \tag{2.32}$$

Using the measurement results of the high-pressure viscometer, the pressure-viscosity coefficient α_p^* can also be determined [VB14] (which is necessary for the calculation of the lubricant film thickness):

$$\alpha_p^* = \left(\int_{0,1}^{\infty} \frac{\eta_0}{\eta(p)} dp \right)^{-1} \tag{2.33}$$

Besides pressure and temperature, viscosity can also depend on the shear rate. If the shear stress is proportional to shear rate, then the viscosity is a proportionality constant (Eq. (2.27)). Fluids showing this behaviour are known as Newtonian fluids. However, certain fluids (and most lubricating oils) show a non-linear relationship between shear stress and shear rate, i.e., the viscosity changes as the function of the shear rate. A fluid is called shear thickening (or dilatant) if its viscosity increases as the shear rate increases, and a fluid is called shear thinning (or pseudoplastic) if its viscosity decreases as the shear rate increases. In rolling bearing applications, lubricating oils often behave as pseudoplastic fluid. To describe these viscosity and flow behaviours, different fluid models were elaborated. The fluid models and further rheological descriptions of the lubricants, which are not the subject of the present work, can be found, among others, in [SS12] and [Kie17].

In addition to the rheological description, the electrical properties of lubricants also play a significant role in the electrical modelling of rolling bearings. Since in the past, the electrical properties of lubricants were not part of the selection criteria used in rolling bearing applications, there are currently no standards or prescribed test methods for characterizing them under relevant conditions of high pressure, temperature, and shear [Rad16]. There are standards only for the determination of the electrical properties of transformer oils (e.g., [DIN 51412], [DIN EN 60156], [DIN EN 60247]). Accordingly, the number of investigations focusing on this field in rolling bearing applications has increased in recent years (e.g., [BKRS18], [BCGS19], [GCBS19]). In the work of Bechev, a test methodology was elaborated for the characterization of the electrical properties of rolling bearing lubricants [Bec20]. The developed test method allows the determination of the related electrical properties of the lubricants directly in the rolling bearing. The relevant electrical properties of the rolling bearing lubricants are the relative permittivity ε_r, the dielectric loss factor $tan(\delta)$, the resistivity ρ_{el} and the dielectric strength E_D. These parameters depend, among others, on the temperature, the pressure, the electric field strength, and the frequency of the applied electric load in case of alternating current [Rad16], [Bec20]. For a detailed description of the mentioned parameters, see [Küc09].

Focusing on the determination of the electrical capacitance of the rolling bearings, the relative permittivity of the lubricant is of particular importance. The relative permittivity (or dielectric constant) is a relative measure, which describes the ability of a material (as dielectric) to store electric energy in an electrical field. It is expressed as a ratio of the permittivity of vacuum (ε_0 = 8.854 · 10^{-12} F/m), i.e., it represents the factor by which the capacitance of a capacitor is increased by the application of the dielectric medium compared to vacuum. The relative permittivity also depends on the temperature and pressure. To describe these dependencies, the modified Clausius-Mossotti equation can be used based on the work of Bondi [Bon51] and Schrader [Sch88], which requires a reference density and a reference relative permittivity for the calculations. A different approach was provided by Bode, using an extended set of material-specific constants (k_1, k_2, k_3) determined by measurements with a quartz viscometer [Fur17]. In the present work, the calculation method of Bode and the corresponding equations are applied to describe the relative permittivity of the lubricants:

$$\varepsilon_r(p,T) = \varepsilon_r(T) + k_3 \cdot [\rho(p,T) - \rho(T)] \tag{2.34}$$

$$\varepsilon_r(T) = k_1 \cdot \beta_T(T)^{-0{,}5} \cdot \rho(T)^{1/6} + k_2 \cdot T \tag{2.35}$$

$$\beta_T(T) = \frac{a_1}{a_2 + a_3 \cdot T + a_4 \cdot T^2 + a_5 \cdot T^3} \tag{2.36}$$

2.2.5 Elastohydrodynamic lubrication

When two lubricated contact bodies move relative to each other under high load, a lubricant film can develop between them. The thickness of the lubricating film greatly influences the frictional losses and the electrical behaviour of the contact. Based on the deformation of the contact bodies (rigid or elastic) and the pressure dependence of the lubricant viscosity (constant or pressure-dependent), different lubrication regimes are defined [Joh70]:

- Rigid - Isoviscous or hydrodynamic lubrication

  The pressure in the film does not cause elastic deformation of the bodies and does not change the viscosity of the lubricant.
  (Rigid bodies, constant viscosity)

- Elastic - Isoviscos lubrication

  The pressure in the film causes elastic deformation of the bodies but does not influence the viscosity of the lubricant.
  (Elastic bodies, constant viscosity)

- Rigid - Piezoviscous lubrication
  The pressure in the film does not cause elastic deformation of the bodies but influences the viscosity of the lubricant.
  (Rigid bodies, pressure-dependent viscosity)
- Elastic - Piezoviscos or elastohydrodynamic lubrication (EHL)
  The pressure in the film causes elastic deformation of the bodies and influences the viscosity of the lubricant.
  (Elastic bodies, pressure-dependent viscosity)

Since in typical high loaded rolling element-raceway contacts EHL lubrication is present, the current work and the following description focus on this regime. To determine the relevant contact variables, such as pressure and lubricant film thickness, the solution of the following coupled equations is required:

- Reynolds differential equation (represents the continuity equation of the lubricant)
- Lubrication gap equation (represents the contact geometry and the elastic deformation)
- Lubricant equations of state (represent the temperature and pressure dependence of the lubricant density and viscosity)
- Energy equation (represents the energy equilibrium in the lubrication gap)

The resulted lubricant film thickness- and pressure distributions of the high loaded EHL rolling contact have characteristic courses, which are illustrated in Figure 2.14. In the central area of the contact, a relative wide, nearly constant lubrication gap can be observed between the deformed surfaces, which can be described by the central lubricant film thickness h_0. In this region, the pressure distribution shows a similar course like the pressure distribution described by the hertzian contact theory. In the outlet direction, it is followed by a second pressure peak (the so-called Petrusevitz peak) and a characteristic constriction of the lubrication gap due to the corresponding deformation. The minimum lubricant film thickness h_{min} is located in this area, which is of particular importance from both tribological and electrical point of view.

The analytical solution of the aforementioned coupled equations is not possible in most cases, and their simultaneous numerical solution is a time-consuming task [Mag12]. Therefore, to calculate analytically the central and the minimum lubricant film thickness (thereby reducing the computational time and effort), numerous approximate equations have been developed over the last decades.

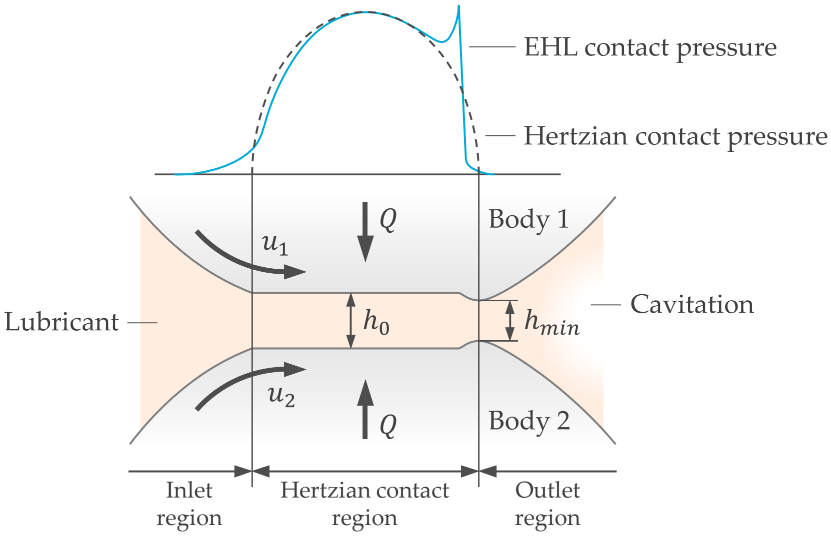

Figure 2.14: Lubrication gap and pressure distribution in EHL rolling contact (based on [Mag12] and [Aul14])

In case of point contact, the best-known approximate equations were derived by Hamrock and Downson in 1977 from a series of numerical calculations [HD77]. The elaborated analytical formulae (Eq. (2.37) - (2.38)) use dimensionless parameters and describe the minimum and central film thickness with rolling direction along the minor semi-axis of the elliptical contact surface, assuming perfectly smooth contact surfaces and isothermal condition:

$$H_{min} = 3.63 \cdot G^{0.49} \cdot U^{0.68} \cdot W^{-0.073} \cdot (1 - e^{-0.68 \cdot \kappa}) \tag{2.37}$$

$$H_0 = 2.69 \cdot G^{0.53} \cdot U^{0.67} \cdot W^{-0.067} \cdot (1 - 0.61 \cdot e^{-0.73 \cdot \kappa}) \tag{2.38}$$

The equations contain the following dimensionless parameters:

- Dimensionless film thickness:

$$H = \frac{h}{R_x} \tag{2.39}$$

- Dimensionless material parameter:

$$G = \alpha_p^* \cdot E_0 \tag{2.40}$$

- Dimensionless load parameter:

$$W = \frac{Q}{E_0 \cdot R_x^2} \tag{2.41}$$

- Dimensionless speed parameter:

$$U = \frac{\eta_0 \cdot u_0}{E_0 \cdot R_x} \tag{2.42}$$

In the equations κ is the elliptic parameter (Eq. (2.10)), R_x is the reduced radius of the contacting bodies in rolling direction, α_p^* is the pressure-viscosity coefficient (Eq. (2.33)), E_0 is the reduced modulus of elasticity (Eq. (2.9)), Q is the load of the contact, η_0 is the dynamic viscosity of the lubricant at atmospheric pressure and sump temperature and u_0 is the hydrodynamic velocity (Eq. (2.25) and (2.26)).

Another group of approximate equations were derived by Chittenden et al. [CDDT85a], [CDDT85b], which extended the previous approach by considering the flow direction of the lubricant in the contact (Eq. (2.43) and (2.44)). For this purpose, an additional term was introduced, which can take into account the ratio of the radii transversal to and in flow direction of the lubricant.

$$H_{min} = 3.68 \cdot G^{0.49} \cdot U^{0.68} \cdot W^{-0.073} \cdot \left[1 - e^{-0.67 \cdot \left(\frac{R_s}{R_e}\right)^{2/3}}\right] \tag{2.43}$$

$$H_0 = 4.31 \cdot G^{0.49} \cdot U^{0.68} \cdot W^{-0.073} \cdot \left[1 - e^{-1.23 \cdot \left(\frac{R_s}{R_e}\right)^{2/3}}\right] \tag{2.44}$$

The ratio R_s/R_e is defined using the angle ξ of the inflow direction to the minor semi-axis as:

$$\frac{R_s}{R_e} = \frac{\frac{R_y}{R_x} \cdot \cos^2 \xi + \sin^2 \xi}{\cos^2 \xi + \frac{R_y}{R_x} \cdot \sin^2 \xi} \tag{2.45}$$

The presented approaches were developed using a series of complex numerical calculations. In order to solve them and to reduce the computational effort, different simplifications had to be made, which are also valid for the resulted analytical formulae. Accordingly, various correction factors have been developed to overcome the modelling inaccuracies caused by these simplifications, and to extend their range of validity. The assumption of an isothermal condition in the rolling contact, which was applied during the development of the presented analytical formulae, is not valid for the actual formation of the lubricant film. To correct the calculated lubricant film thickness values, different thermal correction factors were elaborated. Applying them, the corrected lubricant film thickness values can be obtained as:

$$h_{0,th} = C_{th} \cdot h_{0,isoth} \tag{2.46}$$

$$h_{min,th} = C_{th} \cdot h_{min,isoth} \tag{2.47}$$

With the thermal correction factor of Murch and Wilson [MW75]:

$$C_{th,[MW75]} = \frac{3.94}{3.94 + \mathcal{L}^{0.62}} \tag{2.48}$$

where

$$\mathcal{L} = \frac{\eta_0 \cdot \beta_{th} \cdot u_0^2}{\lambda_{th}} \tag{2.49}$$

The thermal load parameter $\mathcal{L}$ can be calculated with the help of the dynamic viscosity at atmospheric pressure η_0, the temperature-viscosity coefficient β_{th}, the thermal conductivity λ_{th} and the hydrodynamic velocity u_0. Although the mentioned thermal correction of Murch and Wilson was developed for line contacts, it can also be applied to point contacts as an approximation [Kie17]. Further correction factors and methods have been developed to consider the lubricant compressibility (e.g., [VB94], [CVL10]), shear-thinning of the lubricant (e.g., [JKB08]), surface roughness (e.g., [Kre13]) and further influencing effects. Within their validity range, the presented approaches for the determination of the central and minimum film thickness show good agreement with the results of different studies and their measurements [JDY06], [CDV07]. Over the years, numerous approximate equations were developed, which differ in their range of validity or can consider certain additional factors in the modelling of the lubricated rolling contact. Their description, the comparison of their validity range and the developed correction factors are summarised in [MBWR20].

Based on the ratio of the lubricant film thickness to the surface roughness of the contacting bodies, and on the related coefficient of friction, different lubrication and friction conditions can be distinguished. To represent them, the Stribeck-curve can be used (Figure 2.15), which was developed from a systematic study of the coefficient of friction in case of plain bearings [Str02]. The Stribeck-curve describes the relationship between the coefficient of friction and the relative speed of the contacting surfaces (and hence the thickness of the lubricant film). The different lubrication and friction conditions are described in the following based on [SS12].

- **No Lubrication / Solid body friction**
  If there is no lubricant between the contacting surfaces, solid state friction occurs.
- **Boundary lubrication / Boundary friction**
  In this case the lubricant is present between the bodies, but because of its insufficient quantity or the disadvantageous operating conditions no hydrodynamic effects occur. This region can be described by a relatively constant and high coefficient of friction.

- **Mixed lubrication / Mixed friction**
  In mixed lubrication, the quantity of the lubricant and the operating conditions support the formation of a lubricating film, but its thickness is not sufficient to completely separate the surfaces, i.e., the contact of the asperities is present. The behaviour of the tribological system is partly defined by the mechanisms occurring in boundary lubrication and partly by the mechanisms of the full film lubrication. With the increasing relative velocity, the coefficient of friction first decreases until a minimum value μ_{min} due to the decreasing solid body friction. Thereafter, it increases due to the increasing fluid friction in the contact.

- **Full film lubrication / Fluid friction**
  The surfaces of the contacting bodies are completely separated from each other by the lubricant film. The frictional resistance that counteracts the movement is generated solely by the shearing of the viscous fluid, i.e., by fluid friction. It provides quasi wear-free operation.

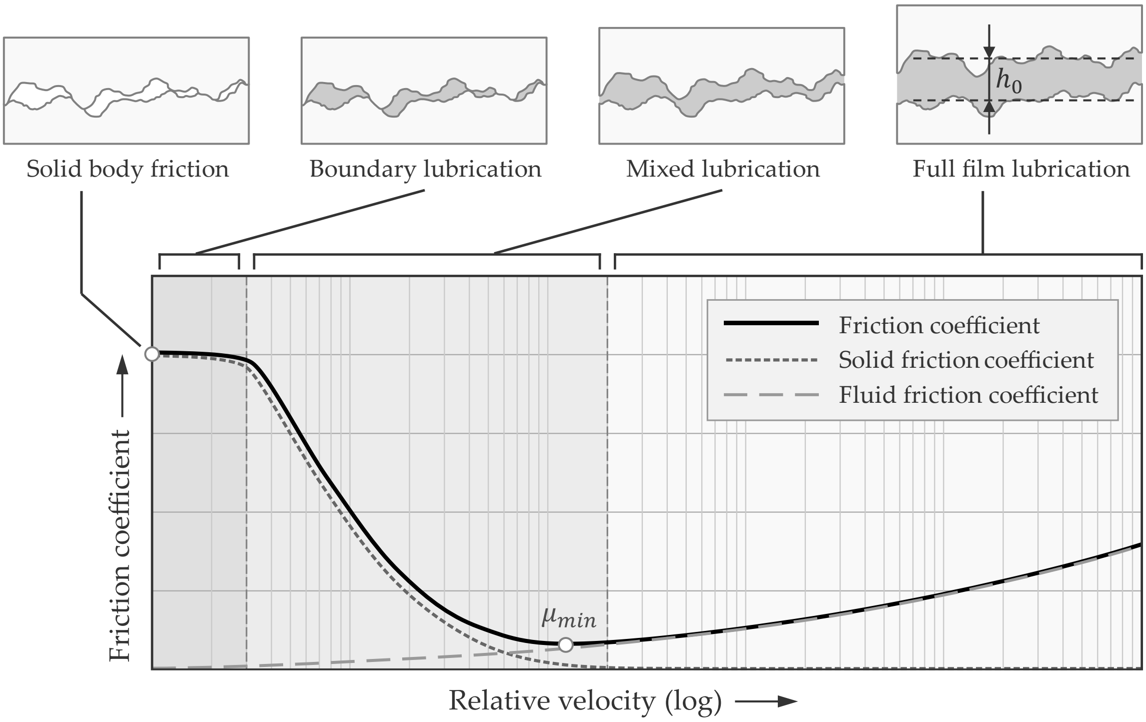

Figure 2.15 Stribeck-curve with the schematic representation of the different friction and lubrication conditions (based on [Kie17])

In order to describe the lubrication conditions quantitatively, a dimensionless parameter, the specific lubricat film thickness can be used. It is defined as the ratio of the minimum or central lubricant film thickness and a representative roughness measure of the contact surfaces. In the work of Tallian [Tal68] the specific lubricant film thickness λ is defined as:

$$\lambda = \frac{h_0}{\sigma} = \frac{h_0}{\sqrt{R_{q,1}^2 + R_{q,2}^2}} \tag{2.50}$$

where the central lubricant film thickness h_0 is normalised by the combined roughness σ of the contacting surfaces. The parameter σ is calculated from the root-mean-square roughness R_q value of the surfaces. Assuming a gaussian normal distribution of the roughness heights, an approximation of σ is possible with the help of the arithmetic average roughness R_a values [Aul14]:

$$\sigma = \sqrt{R_{q,1}^2 + R_{q,2}^2} \approx \sqrt{\frac{\pi}{2}} \cdot \sqrt{R_{a,1}^2 + R_{a,2}^2} \tag{2.51}$$

It is assumed that for $\lambda < 1$, the roughnesses of the bodies cause solid contact or they are only separated by a thin boundary layer (boundary lubrication), while for $3 < \lambda$ the surfaces are completely separated by the lubricating film (full film lubrication). In the range $1 < \lambda < 3$, the interactions between the roughness peaks decisively influence the lubricating film formation (mixed lubrication) [Eng02]. There are also other boundary values in the literatur. For example in the work of Bartel [Bar10], the boundary between the full film lubrication and the mixed lubrication regimes is defined by $\lambda = 3...5$. For the boundary between the mixed and boundary lubrication, the assumption value $\lambda = 0.25$ can be also found [CH10]. In addition, there are other definitions of the specific lubricant film thickness where other film thickness or roughness values are used (e.g., [ZW12]).

2.3 The electrical modelling of rolling bearings

2.3.1 Electrical contact model

The electrical models of the lubricated rolling contact were originally developed for the determination of the lubricant film thickness. The models provide the connection between the film thickness and the electrical parameters such as capacitance, resistance and impedance, which can be determined by different electrical measurement methods (e.g., impedance- or charging curve measurement). Later, these models became the basis for the electrical description of rolling bearings used in electrical system simulations. The models are based on the capacitive behaviour of the lubricated rolling contact, where the developed lubricant film separates the contact surfaces. As a result, the rolling contact can be considered as a capacitor, where the separated conductive surfaces are the capacitor plates and the lubricant film between them acts as a dielectric.

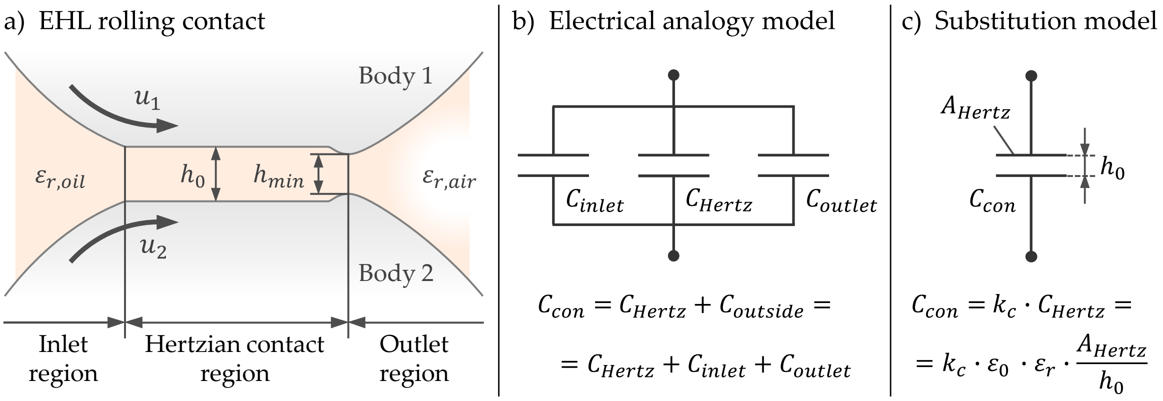

Figure 2.16: Electrical description of the EHL rolling contact focusing on the capacitances: a) EHL rolling contact; b) Electrical analogy model; c) Substitution model (based on [Brü72] and [Fur17])

The electrical rolling contact, similar to the EHL description, can be divided into three regions: inlet region, hertzian contact region and outlet region. Accordingly, it can be modelled with three capacitors connected in parallel [Brü72], as it is illustrated in Figure 2.16. Thus, the total contact capacitance C_{con} is the sum of the capacitances of the contact regions:

$$C_{con} = C_{Hertz} + C_{outside} = C_{Hertz} + C_{inlet} + C_{outlet} \tag{2.52}$$

This modelling approach is often used in related scientific works, such as in [Bar96], [JGB12] and [Fur17], among others. The capacitance of the hertzian contact region can be calculated as a parallel plate capacitor, where the area of the capacitor plates is approximated by the hertzian contact area A_{Hertz}, and the distance between the plates is approximated by the central lubricant film thickness h_0:

$$C_{Hertz} = \varepsilon_0 \cdot \varepsilon_r \cdot \frac{A_{Hertz}}{h_0} \tag{2.53}$$

In this equation, ε_0 is the vacuum permittivity, ε_r is the relative permittivity of the lubricant, and it is assumed that the electric field is homogeneous, i.e., the electric field lines are parallel in the entire region. The electrical influence of the surface geometry in the area of the minimum lubricant film thickness is neglected. The other two regions cannot be properly approximated by the equation of a parallel plate capacitor. While in the inlet region the curvature of the partially deformed surfaces makes the modelling problematic, in the outlet region it is combined with the presence of a two-phase dielectric (air and lubricant) caused by the cavitation phenomena. To avoid these modelling difficulties and to define the capacitance of the whole contact, different correction factors and functions were developed. The correction factors describe the ratio between the total capacitance of the contact and the capacitance of the hertzian contact region as:

$$k_C = \frac{C_{con}}{C_{Hertz}} \tag{2.54}$$

$$C_{con} = k_C \cdot C_{Hertz} = k_C \cdot \varepsilon_0 \cdot \varepsilon_r \cdot \frac{A_{Hertz}}{h_0} \tag{2.55}$$

Based on the experimental investigations of spindle bearings, Barz [Bar96] defined the correction factor $k_C = 3.5$, which showed a good agreement in the investigated cases, but the subsequent studies concluded that this relation is not valid in general. In the work of Jablonka et al. [JGB12], the relation of the total contact capacitance, the hertzian contact capacitance and the capacitance of the outside region (inlet and outlet region) were investigated with the help of a ball-on-disk apparat.

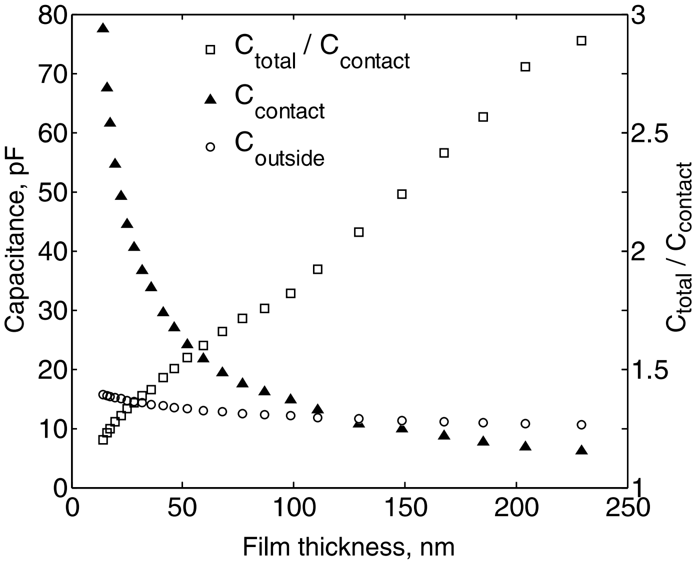

Figure 2.17: Hertzian contact ($C_{contact}$) and outside ($C_{outside}$) capacitances, as a function of optically measured lubricant film thickness [JGB12]

The results (Figure 2.17) show that low lubricant film thickness values lead to high capacitance values, while increasing film thickness results in lower capacitances. It can also be observed that with increasing film thickness, the capacitance of the hertzian contact region (denoted by $C_{contact}$) decreases more significantly than the capacitance of the outside region (denoted by $C_{outside}$). After a certain point, the capacitance of the outside region exceeds the value of the hertzian contact region, which shows the significance of the operating point dependent investigation of the electrical rolling contact, focusing on the different contact regions.

From electrical point of view, the EHL rolling contact can be characterised not only by its capacitance but also by its resistance. The resistance of the hertzian contact region can be calculated analogously to the capacitance with the help of the hertzian contact area A_{Hertz} and the central lubricant film thickness h_0 as:

$$R_{Hertz,oil} = \rho_{el,oil} \cdot \frac{h_0}{A_{Hertz}} \tag{2.56}$$

where $\rho_{el,oil}$ is the specific resistance of the lubricant. Using the k_R correction factor, the electric resistance of the total contact is:

$$R_{con,oil} = k_R \cdot R_{Hertz,oil} \tag{2.57}$$

By connecting the obtained capacitance and resistance in parallel, the EHL rolling contact can be electrically described in general for full film lubrication conditions [Pra06]. Further studies, which investigate the electrical discharge phenomena and the related damages, often add additional elements to this model (e.g., resistors and switching components that are activated by the discharge event), such as [GSRS14], [RG15], or [Rad16].

2.3.2 Electrical rolling bearing model

The electrical modelling of the rolling bearings is built on the electrical contact model. By connecting two electrical contact models in series, which represent the contact points of a rolling element with the inner- and outer rings, the electrical model of a rolling bearing segment is obtained. Then, by connecting the segment models in parallel according to the number of rolling elements, the electrical rolling bearing model is obtained (Figure 2.18). This is the basic idea of the electrical modelling of rolling bearings, which is used in numerous scientific works such as in [Fur17] and [Bec20]. In some studies, it is extended with the resistance of the rolling contact and other conductive parts (rolling elements, inner- and outer ring), while in others they are omitted. Since the present work investigates the capacitances of rolling bearings, the following description focuses on the capacitive modelling and neglects the resistances.

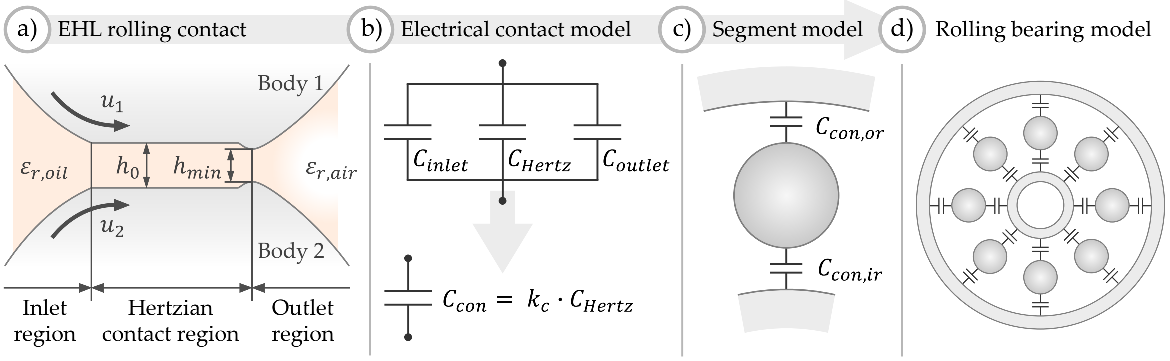

Figure 2.18: Modelling strategy of the rolling bearing capacitances: a) EHL rolling contact; b) Electrical contact model; c) Segment model; d) Electrical rolling bearing model (based on [Bec20])

An influencing factor of the electrical modelling of rolling bearings is the cage material, which can be either insulating (e.g., polyamide) or conductive (e.g., steel, brass) [Fur17]. Using conductive cage, the rolling elements are electrically connected among each other (assuming that the rolling elements are in contact with the cage and no insulating lubricant film develops between them), while in case of an insulating cage, the rolling elements are electrically connected only through the inner and outer rings. The electrical circuit diagrams of the rolling bearings with conductive and insulating cage materials are illustrated in Figure 2.19.

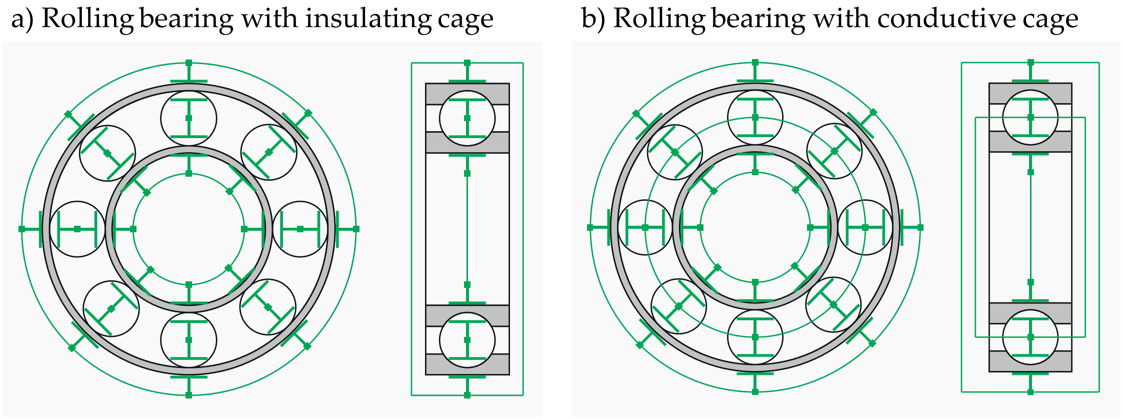

a) Rolling bearing with insulating cage

b) Rolling bearing with conductive cage

Figure 2.19: Electric circuit diagrams of the rolling bearings: a) Rolling bearing with insulating cage; b) Rolling bearing with conductive cage [Fur17]

Based on the circuit diagrams, the total bearing capacitance can be derived [Fur17]:

- For conductive cage:

$$C_{RB} = \frac{\sum_{i=1}^{Z} C_{con,ir,i} \cdot \sum_{i=1}^{Z} C_{con,or,i}}{\sum_{i=1}^{Z} C_{con,ir,i} + \sum_{i=1}^{Z} C_{con,or,i}} \tag{2.58}$$

- For insulating cage:

$$C_{RB} = \sum_{i=1}^{Z} \frac{C_{con,ir,i} \cdot C_{con,or,i}}{C_{con,ir,i} + C_{con,or,i}} \tag{2.59}$$

Where Z is the number of the rolling elements. Knowing the operating conditions of each rolling contact, the individual contact capacitances $C_{con,ir}$, $C_{con,or}$ can be calculated and used for the determination of the total rolling bearing capacitance C_{RB}. Since the electrical modelling of the unloaded rolling elements is not possible using the approach described in the previous section, they are usually taken into account by various simplifications. In [Fur17], it is assumed, that the unloaded rolling elements are located at the middle of the radial clearance, and the related capacitances are calculated with the resulted distances and the undeformed geometries.

A key part of the electrical rolling bearing models is the application of the appropriate correction factor or function that describes the ratio between the total capacitance of the rolling contact and the capacitance of the hertzian contact region. By comparing the measured total capacitances of the rolling bearings (or the ball-on-disc apparat [JGB12]) with the capacitances calculated by the hertzian contact regions, different correction functions were derived (e.g., [JGB12], [Jab15], [BFT17], [Fur17]). In the work of Bechev [Bec20], some of the best-known correction functions are summarised and extended with additional ones, which were developed with the help of a thrust ball bearing using lubricants with different electrical properties ("*highohmic*" and "*lowohmic*"). As it can be observed in Figure 2.20, the magnitude of the correction factors can reach significant values even for small lubricant film thicknesses, which are even larger for radially loaded bearings. With increasing film thickness, the correction factors show larger values, i.e., the measurement results lead to larger deviation from the capacitances of simple capacitor model of the hertzian contact regions. Accordingly, the role of the outside region in the total capacitance of the rolling contact increases with the increasing film thickness. It can also be observed that the load case (axial or radial loaded rolling bearing) and the permittivity of the lubricant ("*highohmic*" and "*lowohmic*") play significant role in the course of the correction functions.

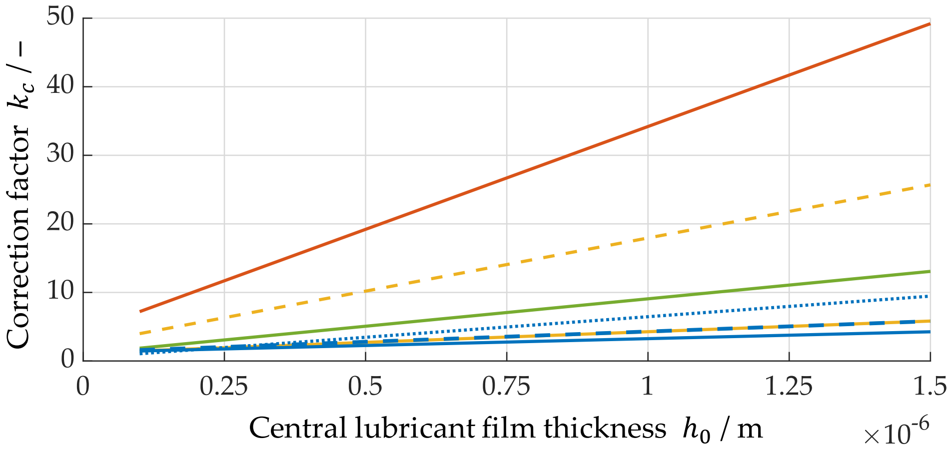

	Correction factor	Source	Remark
——	$k_c = 8 \cdot 10^6 \cdot h_0 + 1.07$	[JGB12]	Ball-on-disc
——	$k_{c,radial} = 3 \cdot 10^7 \cdot h_0 + 4.2$	[BFT17]	Radial load
——	$k_{c,axial} = 3.11 \cdot 10^6 \cdot h_0 + 1.16$	[Fur17]	Axial load
- - -	$k_{c,radial} = 1.55 \cdot 10^7 \cdot h_0 + 2.44$	[Fur17]	Radial load
- - -	$k_{c,highohmic} = 6 \cdot 10^6 \cdot h_0 + 0.46$	[Bec20]	Axial load
········	$k_{c,lowohmic} = 2 \cdot 10^6 \cdot h_0 + 1.26$	[Bec20]	Axial load
——	$k_{c,total} = 3 \cdot 10^6 \cdot h_0 + 1.3$	[Bec20]	Axial load

Figure 2.20: Different correction factors as the function of the central lubricant film thickness (based on [Bec20])

In general, the values provided by the correction functions vary over a wide range, which is not specified in physical terms, and thus leads to uncertainty in the electrical modelling of rolling bearings. In addition, it is possible that further factors (other than the ratio of the total contact capacitance to the capacitance of the hertzian contact region) are included in the correction functions due to the applied measurement method during their elaboration. Consequently, the state-of-the-art electrical rolling bearing models can provide a good approximation for simpler cases, but depending on the type of bearing, the direction of the applied load, the electrical properties of the lubricant and further unknown factors, they can still lead to significant deviations. To understand the underlying factors behind the uncertainty of the electrical modelling of rolling bearings and to improve the validity range of the electrical bearing models, further investigations are necessary.

3 Motivation and objectives

The rapid expansion of electromobility, wind power and further applications related to frequency inverter-controlled electric motors and generators has led to new challenges and requirements in the development of rolling bearings. Due to the presence of parasitic currents in rolling bearings, electrical damages can occur. The rolling bearing is therefore no longer just a mechanical component in such systems, but also an electrical component, making its electrical characterization essential. In order to determine the electrical state of the bearing, to develop preventive measures against electrical damages, and to support system-level electrical calculations, electrical bearing models have been developed, as described in the previous chapter. The state-of-the-art electrical rolling bearing models are based on the electrical contact models that use different correction factors or functions. Although these correction factors can help to describe the regions of the contact, where the electrical modelling is problematic, their validity is usually limited by different factors (e.g., geometry, lubricant properties). In general, the values of the correction factors vary over a wide range, are influenced by numerous known and unknown factors, and thus their application can lead to uncertainty in the electrical modelling of rolling bearings.

The main objective of the present work is to develop a computational method for the determination of rolling bearing capacitance under full film lubrication condition without applying correction factors. In addition, through systematic investigations using experimental and numerical techniques, the capacitance sources in rolling bearings must be identified and then considered in the developed calculation method. The results must be validated and compared with calculations using correction function. The developed computational method is intended to serve as the basis for deriving physically based electrical rolling bearing models in the future for axially, and subsequently for combined loaded rolling bearings. The work focuses on the full film lubrication condition and is limited to the capacitance modelling of axially loaded rolling bearings. Accordingly, the investigation of rolling bearings with combined loads and the modelling of rolling bearing resistances are not part of the studies.

4 Experimental investigation methods

In this chapter, the measurement setup and the measurement methods applied for the experimental investigations are described. Some results are also presented for the explanation of the measurement methods, but the comprehensive analysis of the experimental and numerical results is discussed in Chapter 6.

4.1 Measurement set-up and testing conditions

4.1.1 Measurement set-up

For the experimental investigations, a test cell called GESA (from the German "*Gerät zur erweiterten Schmierstoffanalyse*", i.e., "*device for extended lubricant analysis*") was adjusted and used. The GESA cell was developed at the Institute of Machine Elements, Gears, and Transmissions (MEGT) of the University of Kaiserslautern, as part of a scientific research work [Bec20]. The cell, which involves a thrust ball bearing 51208 as test bearing and the investigated lubricant, can be integrated in a commercially available four-ball-tester (Figure 4.1).

Figure 4.1: Test bench for the experimental investigations: a) Four-ball-tester [HP19]; b) GESA cell installed in the four-ball-tester [Bec20]

In this work, a slightly modified variant of the GESA cell was applied, which is shown in Figure 4.2. The non-rotating ring of the thrust ball bearing is installed in the cell base, while the rotating ring is mounted on a shaft, which is driven by the electric motor of the four-ball-tester. The shaft is centred with the help of a ceramic ball and tapered bores. It leads to a smooth and low-vibration operation of the system, which is essential for the investigation of phenomena related to the lubricant film in the rolling contact.

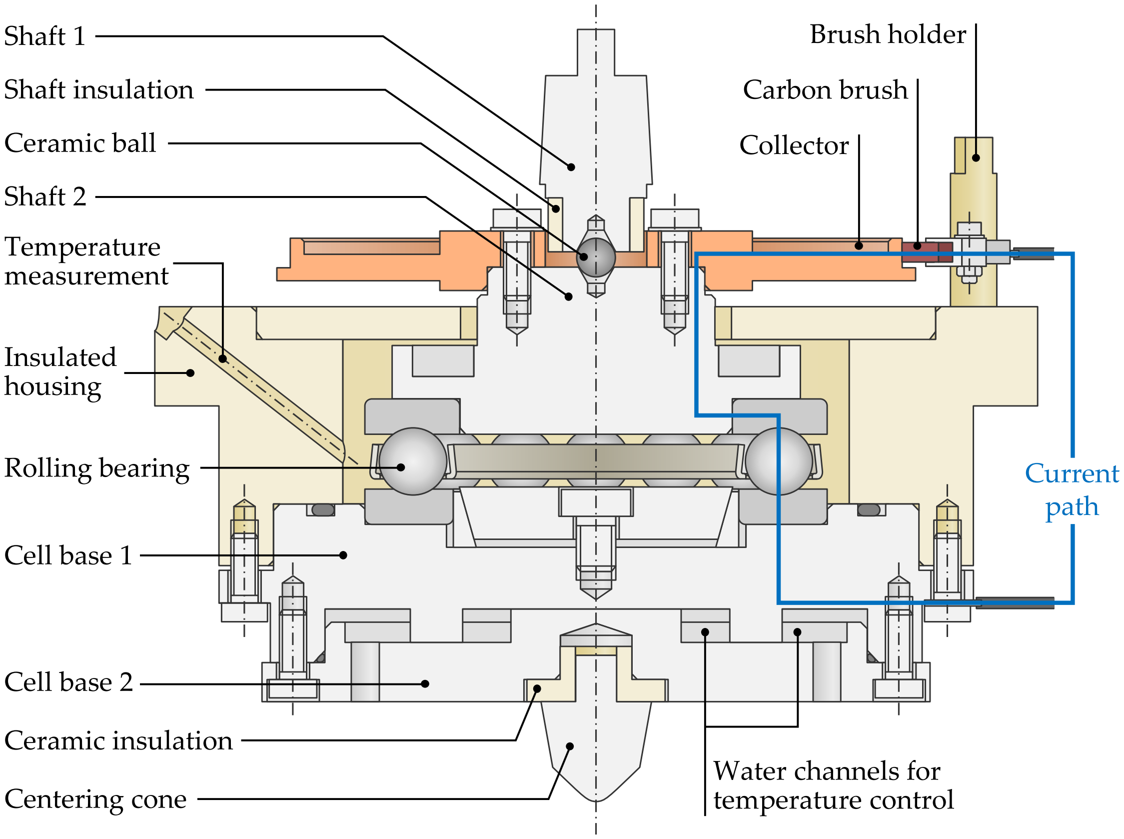

Figure 4.2: Modified GESA cell with its main components

The axial load of the bearing is adjusted by the load unit of the four-ball-tester. The cell can be cooled by a water-cooling system or heated by cartridge heaters, which are regulated by a temperature control system leading to stable operating temperature. The temperature of the oil sump and the non-rotating ring can be measured close to the rolling contact. The rotational speed (100 to 6000 min^{-1}), axial load (0 to 12 kN), and temperature (10 to 90 °C) can be varied and adjusted to the desired operating conditions by the presented setup. The test cell is electrically insulated from both the motor and the frame of the four-ball tester using insulating components. The desired electric load, or the measurement signal is transmitted to the rolling bearing with the help of a special slipring (i.e., collector) mounted on the shaft. The obtained electrical path through the rolling bearing is illustrated in Figure 4.2. In addition to the smooth running and the precisely adjustable operating condition, a significant advantage of the measurement set-up is that the electrical path is defined by a limited number of conductive components and using only one rolling bearing. This minimises the influence of undesired external factors, resulting in more accurate examinations. The presented GESA cell serves as the basic instrument for the investigations, but in some special cases minor modifications have been applied (see later in Chapter 6.1.2).

4.1.2 Investigated rolling bearings and test oils

In most of the investigations, the thrust ball bearing 51208 was applied as test bearing, which was used in the development of the GESA cell [Bec20]. The application of this bearing has various experimental and modelling advantages. The bearing can be quickly installed and de-installed, and the rings can be easily separated even between measurements to change the number of rolling elements. The vertical arrangement ensures that the axial load and oil quantity are evenly distributed on and between the rolling elements, which is beneficial for both the modelling and for the comparison of the experimental and numerical results. In addition, due to the geometrical and operational similarities, it can be assumed that under sufficient lubrication and steady-state operating conditions, the lubricant film thicknesses in the rolling contacts are identical. For further simplification of the subsequent electrical modelling, the geometric dimensions of the steel cage of the bearing were measured and a 3D-printed plastic replica was made and mounted in the bearing. The aim of using thrust ball bearing in the tests was to investigate the electrical rolling contact and to determine the capacitance sources of the bearing. Afterwards, an angular contact ball bearing (type 7206) was applied, which is of practical relevance in the field of electromobility. The aim was to demonstrate the general validity of the experiences gained by the investigation of the thrust ball bearing in a more complex case, where the contact geometries at the inner and outer ring contacts are different. The data of the bearings are summarised in Appendix A.1.

During the investigations carried out in this work, two electrical insulating test oils were used as lubricants. They were selected on the basis of having different base oils, no additives and significantly different relative permittivities. The different base oils (mineral oil and polyglycol) and the different relative permittivities increase the range of validity of the investigations. The relevant properties of the lubricants are summarised in Table 4.1. In addition, the viscosity, density, and relative permittivity of the test oils were determined as a function of pressure and temperature by external high-pressure measurements. With the help of these measurements, the lubricant-specific coefficients of Bode, presented in Chapter 2.2.4, were also determined.

Table 4.1: Investigated lubricants with their basic properties

Lubricant	Test oil 1	Test oil 2
Base oil	Mineral oil	Polyglycol
Additives	No	No
Density at 15 °C [kg/m^3] *	890.6	1043.9
Dynamic viscosity at 40 °C [mm^2/s] *	97.3	107.7
Dynamic viscosity at 100 °C [mm^2/s] *	8.8	18.8
Relative permittivity at 40 °C [-] *	2.2	6.3

* at atmospheric pressure

4.2 Measurement methods

The presented measurement setup allows the application of different measurement methods to determine the capacitance of the rolling bearings. In this work, two methods were applied, the charging curve measurement and the impedance measurement. Due to their parallel application, the uncertainties related to the measurement techniques can be reduced. In addition, their range of applicability, the differences in their results and possible influencing factors can be compared.

4.2.1 Charging curve measurement

The first measurement method is based on the charging characteristic of capacitors. If a capacitor is connected in series with a resistor (thus forming an RC-circuit) and then loaded by a DC supply voltage, the capacitor is gradually charged through the resistor until its voltage reaches the supply voltage. In parallel, the charging current has a high initial value at the first instant, which then asymptotically approaches zero as the capacitor becomes fully charged. The described serial RC-circuit, the charging voltage and the charging current are shown in Figure 4.3.

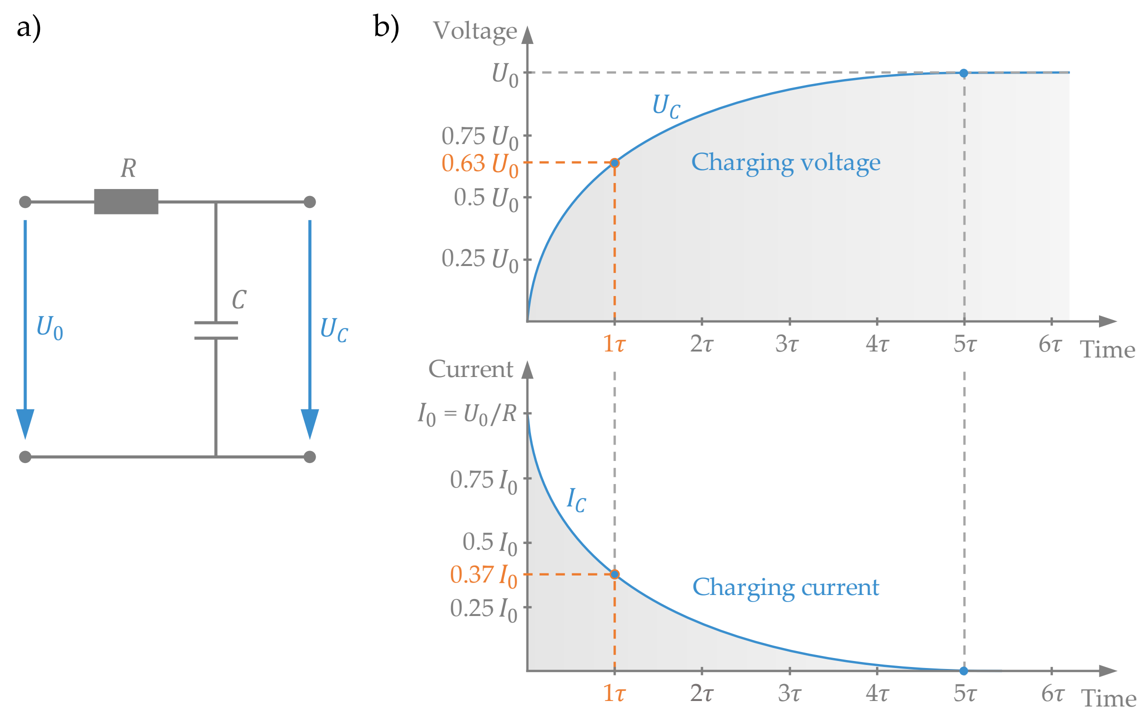

Figure 4.3: a) Serial RC-circuit; b) Charging voltage and charging current of the RC circuit with the introduction of the time constant τ

The charging processes can be described by the following equations, which are derived from the differential equation underlying the charging process of the capacitor in the presented RC-circuit:

$$U_C(t) = U_0 \cdot \left(1 - e^{-\frac{t}{\tau}}\right) = U_0 \cdot \left(1 - e^{-\frac{t}{R \cdot C}}\right) \tag{4.1}$$

$$I_C(t) = \frac{U_0}{R} \cdot e^{-\frac{t}{\tau}} = \frac{U_0}{R} \cdot e^{-\frac{t}{R \cdot C}} \tag{4.2}$$

Where U_0 is the supply voltage, and τ is the time constant:

$$\tau = R \cdot C \tag{4.3}$$

If the resistance is expressed in Ohms and the capacitance in Farads, the time constant is defined in seconds. At the time point determined by τ, the actual capacitor voltage reaches 63 % of the applied supply voltage U_0. The capacitor is fully charged at approx. 5 times the value of the time constant (Figure 4.3 b)).

To determine the rolling bearing capacitance, measurements of its charging characteristic can be used. For this purpose, a signal generator and an oscilloscope are required. In this work, the "*HAMEG - HM 8035*" pulse generator and the "*LeCroy - WaveSurfer 424*" oscilloscope were applied. The signal generator provides the voltage supply by generating predefined square wave signals, and the oscilloscope is used to measure the charging voltage across the rolling bearing as a function of time. Based on the measurement setup, an equivalent electrical circuit can be defined (Figure 4.4 a)), which considers the capacitance C_{RB} and resistance R_{RB} of the rolling bearing, the internal resistance R_O of the oscilloscope, the cable capacitance C_C and resistance R_C, and a regulating resistance R_R [Bec20]. By combining the electrical components, a substitutive circuit can be created (Figure 4.4 b)) for the simplification of the evaluating calculations. This circuit involves the regulating resistance R_R, the substitutive resistance R_S, and the substitutive capacitance C_S.

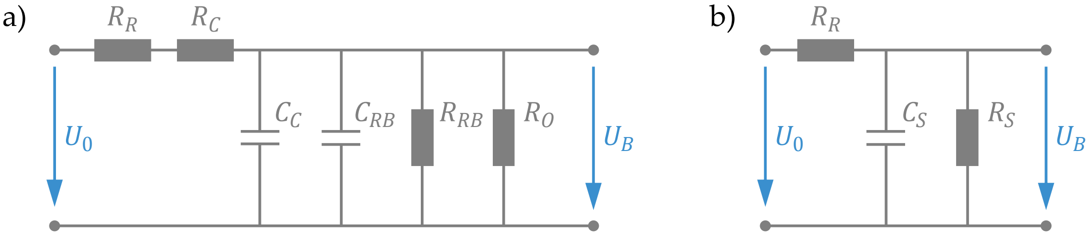

Figure 4.4: a) Equivalent electrical circuit of the measurement setup; b) Simplified substitutive circuit of the measurement setup [Bec20]

The resistance of the cable can be omitted, as its magnitude is negligible compared to the regulating resistance. With this assumption the substitutive components are:

$$R_S = \frac{R_{RB} \cdot R_O}{R_{RB} + R_O} \tag{4.4}$$

$$C_S = C_C + C_{RB} \tag{4.5}$$

In accordance with the simplified substitutive circuit, the equation describing the charging voltage can be written in the following form:

$$U_C(t) = U_0 \cdot R' \cdot \left(1 - e^{-\frac{t}{R_R \cdot R' \cdot C_S}}\right) \tag{4.6}$$

where

$$R' = \frac{R_S}{R_S + R_R} \tag{4.7}$$

For the evaluation of the measured charging curves, two different methods can be used [Fur17]. In the first method (which is used in [WKT10] and [Wit17]), the substitutive resistance is calculated with the help of the supply voltage U_0, the regulating resistance R_R, and the measured maximum voltage level of the charging process U_{max} as:

$$R_S = \frac{U_{max}}{U_0 - U_{max}} \cdot R_R \tag{4.8}$$

Then, the rolling bearing resistance can be obtained by the rearrangement of Eq. (4.4):

$$R_{RB} = \frac{R_S \cdot R_O}{R_O - R_S} \tag{4.9}$$

For the determination of the bearing capacitance, the time constant is necessary. It can be approximated with the help of two time point of the charging period t_1, t_2, and the two corresponding voltage values U_1, U_2, according to Figure 4.5 a). The time constant can be expressed as [Wit17]:

$$\tau = \frac{t_2 - t_1}{\ln \frac{U_2/U_0}{U_1/U_0}} \tag{4.10}$$

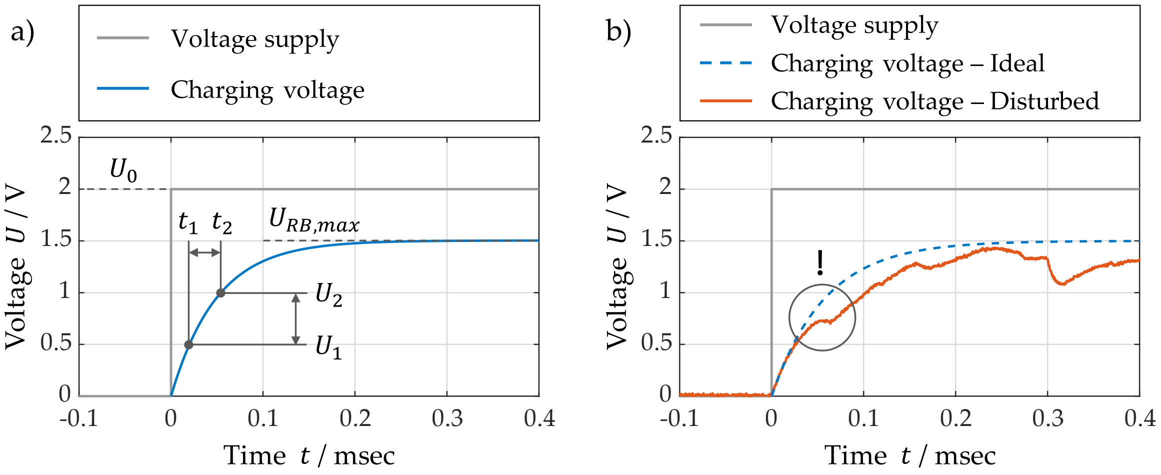

Figure 4.5: a) Parameters for the calculation of the time constant; b) Charging voltage of a measurement with disturbances compared to an ideal charging curve (based on [Wit17])

After calculating the time constant, the substitutive- and rolling bearing capacitances can be determined:

$$C_S = \tau \cdot \frac{R_S + R_R}{R_S \cdot R_R} \tag{4.11}$$

$$C_{RB} = C_S - C_C \tag{4.12}$$

With the help of charging curve measurements on model circuits, where the rolling bearing is replaced with capacitor and resistor components of known values, the capacitance of the cable can be determined. For the measurements performed during the work, the cable capacitance was 170 pF, the value of the regulating resistance was 110 kOhm and the internal resistance of the oscilloscope was 1 MOhm. The amplitude of the square wave voltage supply was 2 V.

The second method for the evaluation of the measurements is based on the Eq. (4.6) describing the charging voltage as a function of time. By substituting Eq. (4.7), (4.4) and (4.5), the only unknown parameters are the capacitance and the resistance of the rolling bearing, which can be determined by curve fitting algorithms [Bec20]. The Levenberg-Marquardt algorithm (LMA) [Lev44], [Mar63], also known as the damped least-squares method, can be applied for this purpose. Accordingly, the searched values are determined by minimizing the residuals, i.e., the difference between the measured values of the charging voltage and the fitted values provided by the presented equation of the charging voltage. It is important to note that in both evaluation methods, partial or complete discharges during the charging period (e.g., by momentary asperity contacts) can significantly distort the results due to the extended charging time (Figure 4.5 b)). Therefore, measurements with disturbances (especially if they are in the initial charging period) should be omitted, or the evaluated range of the measured voltage signal should be limited. For the evaluation of the charging curve measurements, the LMA curve fitting method is applied in this work.

As shown in the circuit diagram in Figure 4.4 a), the rolling bearing is modelled as a parallel connection of a capacitor and a resistor. To support the interpretation of the measured charging curves, the independent influences of the bearing capacitance and resistance are compared analytically in case of the presented measurement setup. For this purpose, Figure 4.6 a) shows three calculated charging curves with the same bearing capacitance and different bearing resistances, while Figure 4.6 b) shows three charging curves with the same bearing resistances and different bearing capacitances.

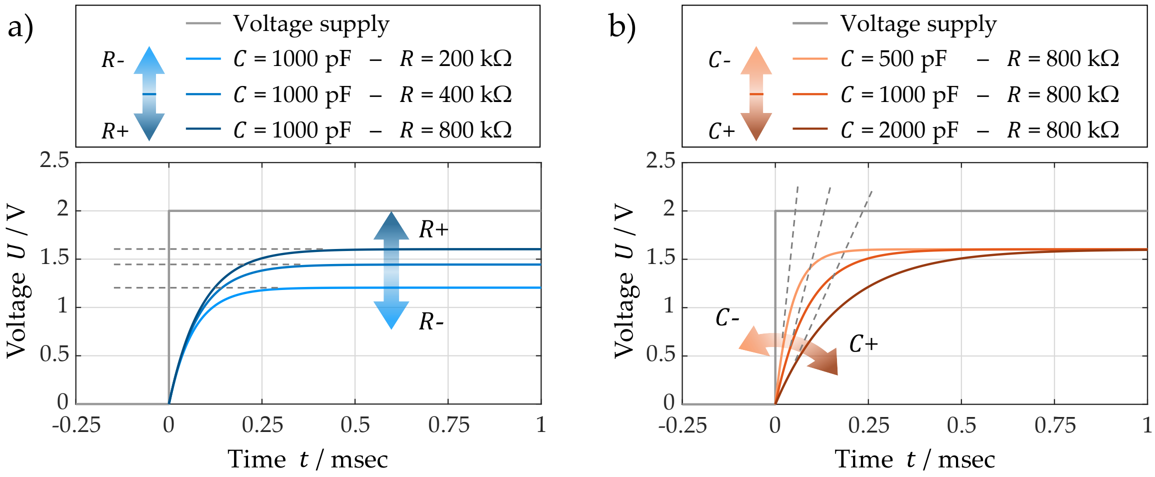

Figure 4.6: a) Influence of the bearing resistance on the charging voltage at constant bearing capacitance; b) Influence of the bearing capacitance on the charging voltage at constant bearing resistance

It can be observed that the resistance of the bearing mainly affects the maximum voltage level of the charging curve, and it has influence also on the charging time. The capacitance of the bearing affects the time constant, i.e., how long it takes to reach the maximum charging voltage. The curves show that for the determination of the bearing capacitance, the initial part of the charging curve is particularly important.

The lubrication condition of the rolling bearing has a significant influence on the quality of the measurement evaluation and thus on the resulted capacitance values. For the representation of this relationship, Figure 4.7 shows measured charging voltage curves of the investigated rolling bearing 51208 with test oil 2 in case of full film lubrication (Figure 4.7 a)), mixed lubrication (Figure 4.7 b)), and boundary lubrication condition (Figure 4.7 c)). Each diagram provides three measured charging curves of a defined operation condition and the corresponding fitted curves using the LMA evaluation method. In addition, the resulted rolling bearing capacitances, resistances, and the coefficients of determination R^2, which indicates the quality of the curve fitting, are also presented. The lubrication condition, which is quantified by the specific lubricant film thickness parameter λ, is influenced by the operating conditions of the rolling bearing, namely by the axial load F_{ax}, the oil temperature T, and the rotational speed n.

In full film lubrication condition, the measurements show good reproducibility and the coefficients of determination indicate a high degree of agreement between the measured and fitted curves. The difference between the resulted capacitance values is less than 5 %, and between the resistance values is less than 10 %. The results suggest that the measurement method suitable for the investigation of the full film lubrication condition.

In contrast, significant differences can be observed for mixed lubrication condition. The measured charging curves show disturbances that reduce the quality of the curve fitting and thus lead to a larger deviation of the results. The disturbances (partial or complete discharges) of the charging curves can be explained by momentary contacts between the asperities of the surfaces, or by the thin layer of oil between single asperity peaks, where the measurement voltage exceeds the isolation ability of the oil and a discharge occurs. Consequently, the magnitude of the measurement voltage can affect the quality of the measurement results and the range of applicability. The relative difference between the resulted resistance values is larger than the relative differences of the capacitances, which can be explained by the fact that there is less disturbance in the initial range of the presented curves. Avoiding discharges during the charging period is a key requirement for the accurate measurement of bearing capacitances. As a result, in addition to the full film lubrication condition, investigations can also be carried out in mixed lubrication condition, until the measured charging curves allow the determination of stable, reproducible capacitance values. With decreasing specific lubricant film thickness, more and more disturbances occur in the charging process, reducing the accuracy and applicability of the measurement method.

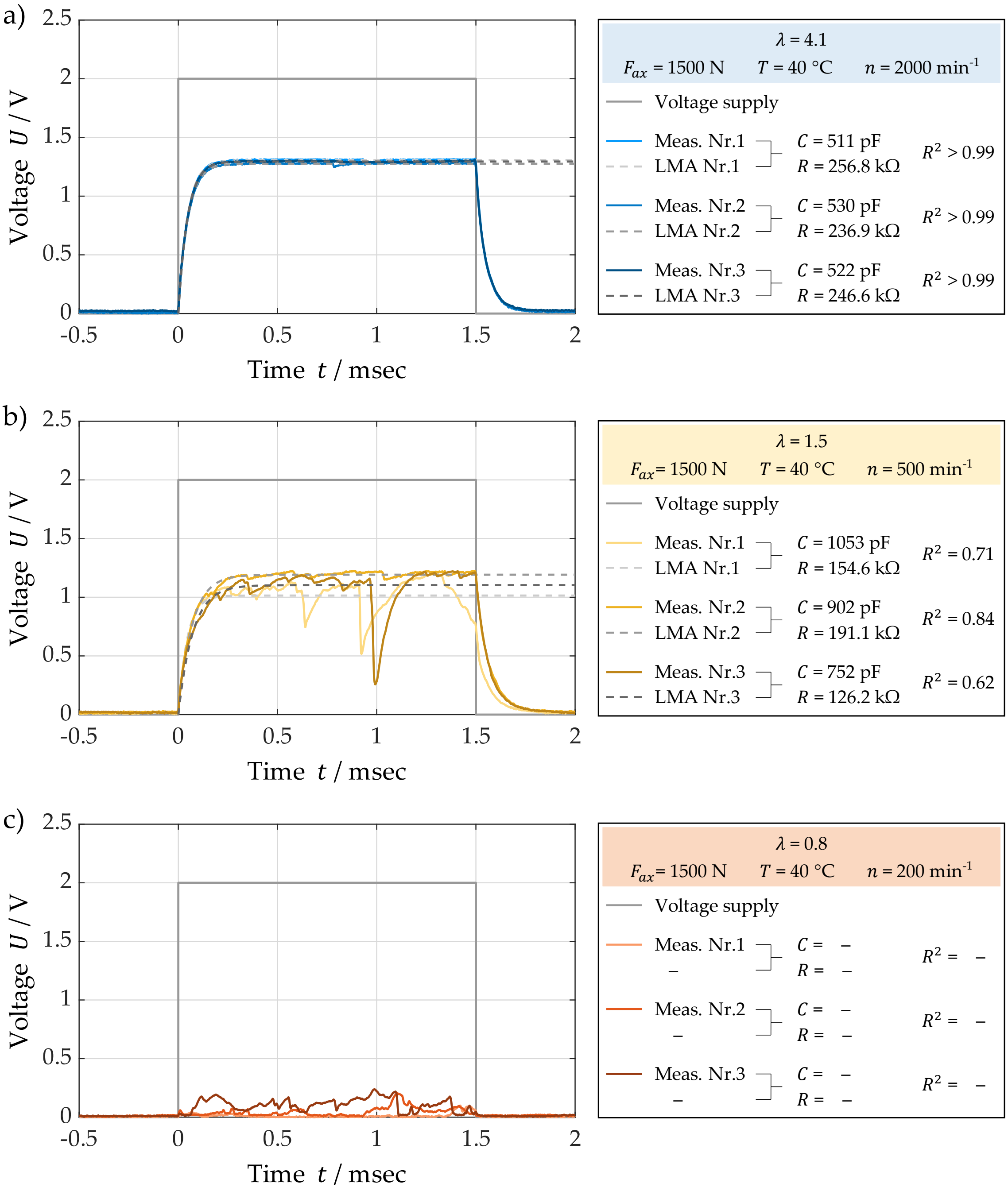

Figure 4.7: Charging curve measurement results with thrust ball bearing 51208 and test oil 2 for the representation of the relation between the lubrication condition and the quality of the measurement evaluation: a) Full film lubrication; b) Mixed lubrication; c) Boundary lubrication

In case of boundary lubrication condition, the rolling bearing capacitance cannot be determined by the presented measurement method. Between surfaces that are permanently in contact, the electrical insulating oil film cannot develop, thus the charging voltage curve cannot build up, and the LMA curve fitting method cannot be applied.

4.2.2 Impedance measurement

Another experimental method for the determination of the rolling bearing capacitances is based on the measurement of electrical impedance. The impedance $\overline{\boldsymbol{Z}}$ represents the complex-valued electrical resistance of AC circuits. The real part of the impedance is the effective resistance R_{eff}, and the imaginary part is the reactance X:

$$\overline{\boldsymbol{Z}} = R_{\mathrm{eff}} + i \cdot X \tag{4.13}$$

Accordingly, the impedance can be represented in complex plane, as it is shown in Figure 4.8.

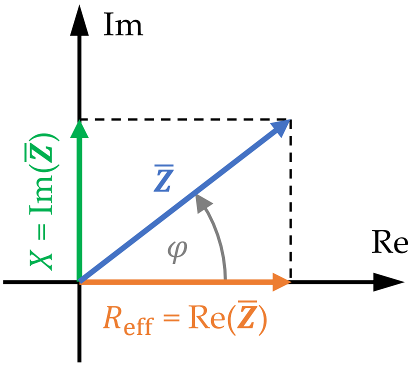

Figure 4.8: Representation of the impedance vector in complex plane

The effective resistance and the reactance can be expressed with the help of the impedance magnitude $|\overline{\boldsymbol{Z}}|$ and the phase angle φ:

$$R_{\mathrm{eff}} = |\overline{\boldsymbol{Z}}| \cdot \cos\varphi \tag{4.14}$$

$$X = |\overline{\boldsymbol{Z}}| \cdot \sin\varphi \tag{4.15}$$

where

$$|\overline{\boldsymbol{Z}}| = \sqrt{{R_{\mathrm{eff}}}^2 + X^2} \tag{4.16}$$

$$\tan\varphi = \frac{X}{R_{\mathrm{eff}}} \tag{4.17}$$

The impedance of an ideal resistor has only real part, its reactance and phase angle are zero and it is frequency independent. In contrast, the ideal capacitor has zero resistance, a phase angle of -90° and it is inversely proportional to the voltage frequency f. Their properties related to the complex impedance are summarised in Table 4.2, where ω is the angular frequency of the voltage signal, defined as:

$$\omega = 2 \cdot \pi \cdot f \tag{4.18}$$

Table 4.2: Impedance and related properties of ideal resistor and capacitor

Component	$\overline{\boldsymbol{Z}}$	R_{eff}	X	φ
Resistor	R	R	0	0°
Capacitor	$-i/\omega C$	0	$-1/\omega C$	-90°

Since the rolling bearing is modelled by connecting an ideal resistor and a capacitor in parallel, its impedance can be described using the impedance of the resistor $\overline{\boldsymbol{Z}}_R$ and capacitor $\overline{\boldsymbol{Z}}_C$ from Table 4.2 as:

$$\frac{1}{\overline{\boldsymbol{Z}}} = \frac{1}{\overline{\boldsymbol{Z}}_R} + \frac{1}{\overline{\boldsymbol{Z}}_C} = \frac{1}{R} + \frac{1}{-i/\omega C} = \frac{1}{R} + i\omega C \tag{4.19}$$

Thus, after rearrangement:

$$\overline{\boldsymbol{Z}} = R_{\text{eff}} + i \cdot X = \frac{R}{1 + (\omega \cdot C \cdot R)^2} - i \cdot \frac{\omega \cdot C \cdot R^2}{1 + (\omega \cdot C \cdot R)^2} \tag{4.20}$$

$$R_{\text{eff}} = \frac{R}{1 + (\omega \cdot C \cdot R)^2} \tag{4.21}$$

$$X = -\frac{\omega \cdot C \cdot R^2}{1 + (\omega \cdot C \cdot R)^2} \tag{4.22}$$

$$|\overline{\boldsymbol{Z}}| = \sqrt{{R_{\text{eff}}}^2 + X^2} = \frac{1}{\sqrt{\frac{1}{R^2} + \omega^2 \cdot C^2}} \tag{4.23}$$

$$\tan\varphi = \frac{X}{R_{\text{eff}}} = -\omega \cdot C \cdot R \tag{4.24}$$

With the help of the presented equations, the frequency-dependent impedance can be calculated for a parallel connected resistor and capacitor, i.e., for the rolling bearing model. Figure 4.9 a) shows the typical characteristic of the frequency-dependent impedance curves provided by this model in the complex plane.

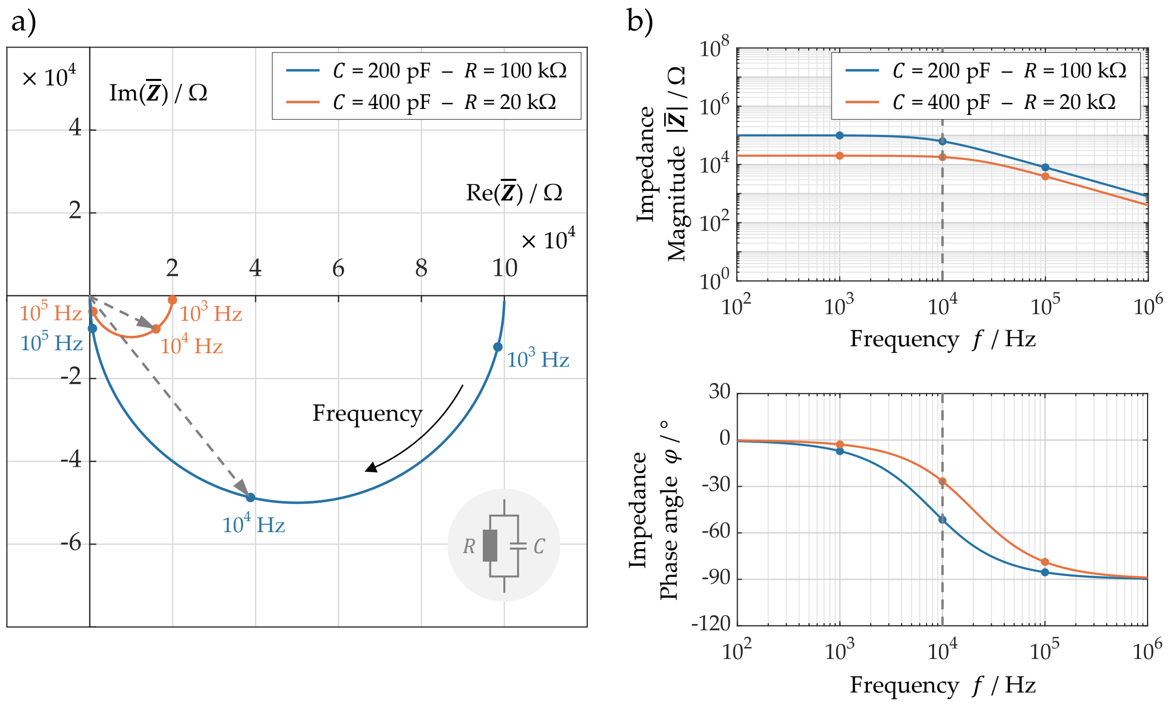

Figure 4.9: Different representations of the frequency-dependent impedance: a) Impedance curves in complex plane; b) Equivalent impedance magnitude and phase angle as the function of the frequency

The impedance curves form half circles in the fourth quadrant of the complex plane, which approach the origin with increasing frequency. The resistance defines the diameter of the half circle, while the capacitance defines the spacing of the frequencies along the curves. For the investigation of rolling bearings, another representation, the frequency-dependent magnitude and phase angle of the impedance are examined typically, which are shown in Figure 4.9 b). In this case, the frequency and the impedance magnitude are plotted on logarithmic scale. The marked values in the complex plane can be equivalently represented in the impedance magnitude and phase angle diagrams.

Similar to the introduction of the charging curve measurement method, it is beneficial to analyse the effect of capacitance and resistance on the impedance magnitude and phase angle curves in case of the parallel capacitor-resistor model of the rolling bearing. For this purpose, Figure 4.10 a) shows frequency-dependent impedance magnitude and phase angle curves with the same capacitance and different resistances, while curves with different capacitances and the same resistance are shown in Figure 4.10 b).

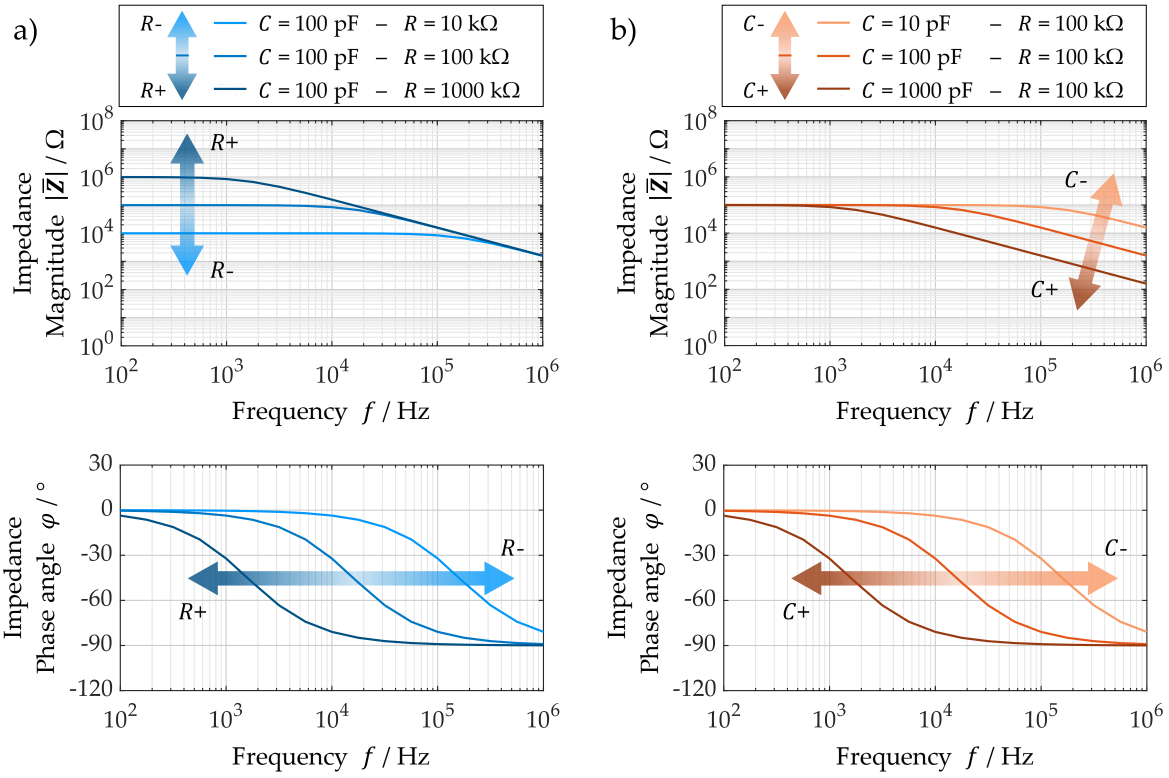

Figure 4.10: Impedance curves of parallel capacitor-resistor circuits: a) Influence of the resistance on the impedance magnitude and phase angle at constant capacitance; b) Influence of the capacitance on the impedance magnitude and phase angle at constant resistance

In general, the impedance magnitude curves can be divided into two regions. In the first region, the magnitude decreases slowly on logarithmic scale compared to the second region, and its starting value (at 0 Hz) is defined by the resistance. Subsequently, the second region shows a significant decreasing course, determined by the value of the capacitance. The transition between the two ranges is defined by the ratio of the resistance and capacitance values. The boundary frequency can be interpreted as the inflexion point of the phase angle curves. The increasing resistance increases the impedance magnitude of the first region, and at the same time the boundary frequency between the regions is shifted to lower frequencies. The increasing capacitance value shifts the second region of the impedance magnitude curve, and thus the boundary frequency, towards the lower frequencies.

For the interpretation of the impedance magnitude and phase angle in relation to the lubrication condition, a schematic representation is provided in Figure 4.11 from [GCBS19]. In general, a high impedance magnitude and a corresponding phase angle tending towards -90° indicate an insulating lubricant film in the rolling contact, while a low impedance magnitude value combined with a phase angle approaching 0° refers to boundary lubrication condition or dry contact.

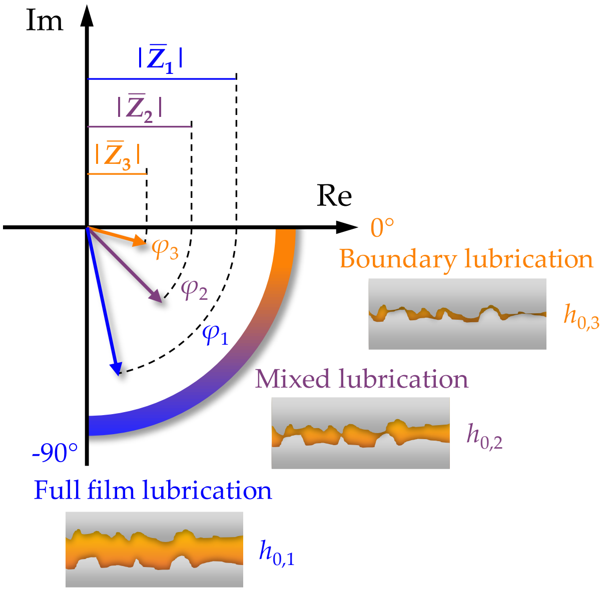

Figure 4.11: Schematic representation of the relationship between the lubrication condition of the rolling bearing and the corresponding complex impedance vector based on [GCBS19]

In case of a chosen frequency, the measured impedance values can be compared according to this scheme, but for the accurate determination of the rolling bearing capacitances, the measurement of frequency-dependent impedance magnitude and phase angle curves is necessary. For this purpose, the "*Omicron Lab - Bode 100*" vector network and frequency response analyser was used. The device allows the direct measurement of the aforementioned frequency-dependent curves by applying a frequency sweep voltage signal to the measured object and analysing the response. An advantage of the device is its internal calibration possibility, which can be used to filter out undesired external influences (for example cable capacitance and resistance).

In this work, the impedance measurements are evaluated by the LMA curve fitting method (similar to the evaluation of the charging curve measurements). The Eq. (4.23) of the impedance magnitude is used as the mathematical function of the curve fitting, where the capacitance and resistance of the rolling bearing are the searched parameters. The measurements are carried out in a frequency range of 10^2 - 10^6 Hz, and with a voltage amplitude of 0.5 V. The curve fitting is performed in frequency domain. To examine the applicability of the method, the results of measurements under different lubrication conditions were evaluated and compared. For this purpose, the same operating conditions were chosen, which were investigated in case of the charging curve measurement method in Figure 4.7. The Figure 4.12 shows measured impedance magnitude and phase angle curves of the investigated thrust ball bearing 51208 with test oil 2 in case of full film lubrication (Figure 4.12 a)), mixed lubrication (Figure 4.12 b)), and boundary lubrication condition (Figure 4.12 c)). Each diagram provides three measured curves of the specified operating condition and the corresponding fitted curves using the LMA method. The resulted rolling bearing capacitances, resistances, and the coefficients of determination are summarised in the legend of the diagrams.

In full film lubrication condition (similar to the charging curve measurement method), the results show a good reproducibility, and the regression curves follow the measured curves with high accuracy. Accordingly, the resulted capacitance and resistance values show only small deviations, with a maximum difference of less than 5 %.

In mixed lubrication condition, the measured curves follow a nearly identical course relative to each other with characteristic disturbances in the lower frequency range. The disturbances lead to stochastic peaks in the measured curves that point towards lower values in case of impedance magnitude and towards higher values in case of the phase angle. These disturbances can be explained by asperity contacts of the surfaces or by a momentary excess of the insulating ability of the oil film due to the measurement voltage. The undisturbed parts of the measured curves outline a covering curve, which help the evaluation of the results. Although the disturbances reduce the accuracy of the curve fitting, the undisturbed parts can be approximated well, as it is shown in Figure 4.12 b). As a result, the coefficients of determination for this method show higher values than for the charging curve measurement method with the same operating conditions in mixed lubrication condition. Furthermore, since the disturbances primarily affect the lower frequency range, they have less influence on the evaluated rolling bearing capacitance. With specific settings of the impedance analyser (such as the averaging factor or the measurement bandwidth), the effect of the described disturbances can be slightly reduced, but the further decrease of the specific lubricant film thickness (i.e., more frequent metallic contact between the surfaces) leads to the reduction of the measurement accuracy.

In case of boundary lubrication condition, the disturbances of the impedance magnitude and phase angle curves show a different characteristic. As the specific lubricant film thickness decreases, the disturbance peaks also appear in the higher frequency range, pointing towards both higher and lower values, thus preventing the identification of a covering curve. Although relatively stable capacitance and resistance values can be obtained by the LMA evaluation method, the measured curves are highly dependent on the measurement voltage. This lubrication condition is dominated by the metallic contact and the corresponding resistances. Accordingly, in this lubrication condition, the determination of the rolling bearing capacitance with the presented evaluation method is not recommended.

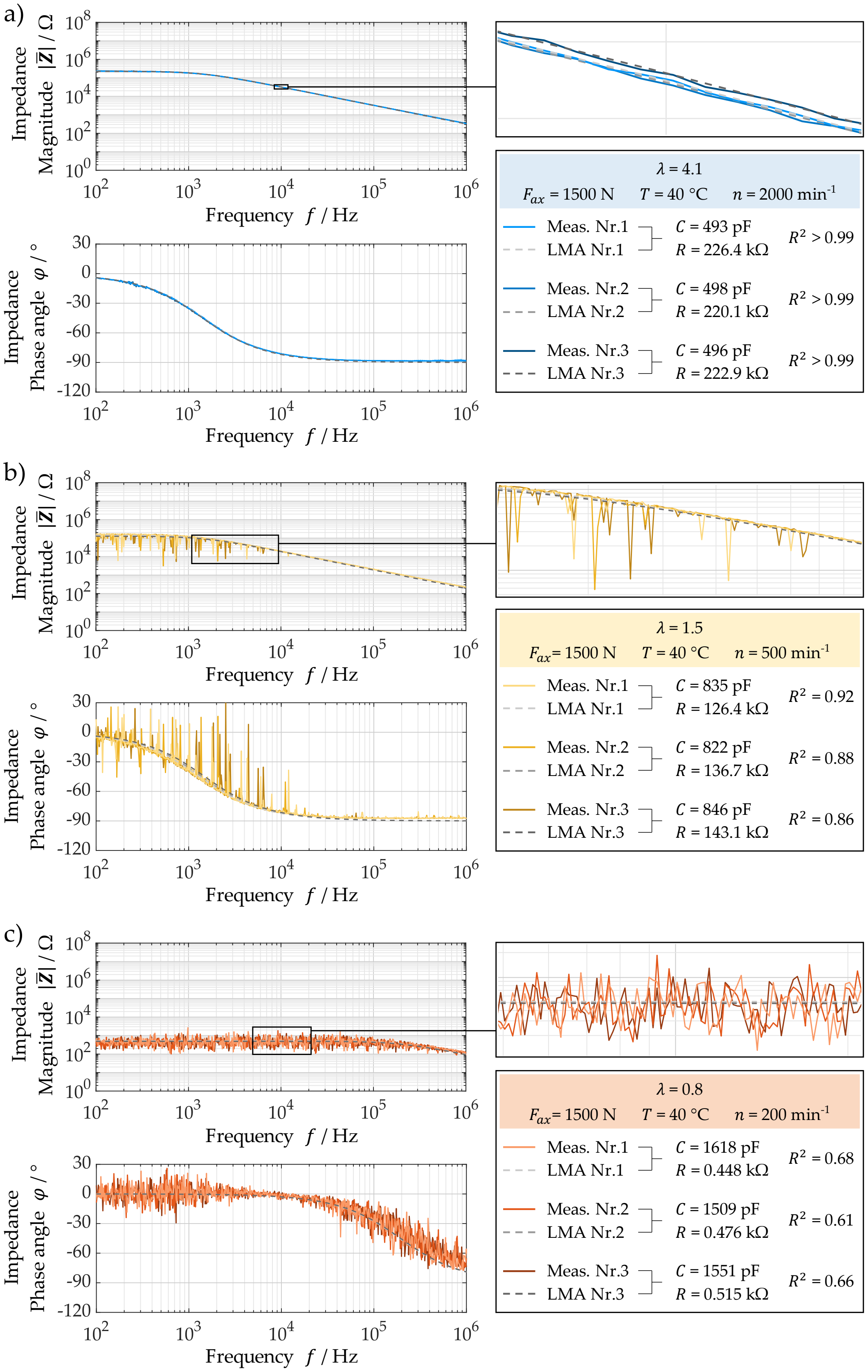

Figure 4.12: Impedance measurement results with thrust ball bearing 51208 and test oil 2 for the representation of the relation between the lubrication condition and the quality of the measurement evaluation: a) Full film lubrication; b) Mixed lubrication; c) Boundary lubrication

Based on the investigations of the presented measurement methods, both methods are suitable for the determination of rolling bearing capacitance in case of full film lubrication, and up to a certain range of the mixed lubrication condition. The charging curve measurement method is more sensitive to disturbances that appear with decreasing lubricant film thickness, and therefore its applicability is more limited. The determination of rolling bearing capacitances in boundary lubrication condition with the presented measurement methods shows uncertainties, which can be explained by the tribomechanical background phenomena (i.e., metallic contact), and therefore it is not recommended. Of the measurement methods, the impedance measurement can be applied over a wider range in terms of the lubrication conditions, requires fewer devices, and is more flexible to use. Because of these advantages, this measurement method is considered as the primary method of this work and certain investigations are carried out only with this method. Further comparison of the measurement methods is discussed in Chapter 6.2.

5 Simulation and modelling strategies

For the numerical investigations of rolling bearing capacitances, two computational methods were applied and combined. The first method is based on the numerical EHL simulation of the rolling contact. With the help of the resulting lubricant film-, phase- and pressure distributions, the calculation can be electrically extended to obtain a capacitance distribution over the investigated range of the contact. As second approach, finite element method (FEM) was applied to determine the capacitances between the conductive components of the rolling bearing as a multi-conductor system. By combining the electrically extended EHL simulation (for the contact domain) with the FEM simulation (for the surroundings of the contact), a detailed and systematic electrical analysis of the rolling bearing capacitances can be performed. In the following, the aforementioned simulation methods and the modelling strategy are presented.

5.1 Electrically extended EHL simulation

The electrical modelling of the rolling contact is presented in two parts. First, the numerical EHL simulation is described, and then the capacitance calculation is presented as the electrical extension of the EHL simulation.

5.1.1 Numerical EHL simulation

At the Institute of Machine Elements, Gears, and Transmissions (MEGT), numerical EHL simulations have been developed for the tribological investigation of rolling bearings, radial shaft seals [TMS20], gears [SOS21] and chain joints [MTLB18], among others. The developed simulation techniques form the basis of the calculations applied in the present work. Accordingly, the applied numerical EHL simulation is described below based on the works of Kamga et al. [SOMS18], [SOS21] for the investigation of elliptical point contact under isothermal lubrication conditions using a mass-conserving cavitation algorithm. To determine the lubricant film-, phase- (oil and air) and pressure distributions in the rolling contact, the solution of the following coupled equations is required:

Reynolds differential equation: The Reynolds differential equation is derived from the Navier-Stokes equations and describes the flow of a viscous fluid film between two surfaces, i.e., the dependence of the hydrodynamic pressure p on the lubricating gap high h, the velocities u_1 and u_2 of the contacting surfaces and the rheological properties of the lubricant (such as the density ρ and dynamic viscosity η). Based on various simplifications of these relations, different versions of the Reynolds equation have been proposed. The detailed derivation of the classical Reynolds equation and its assumptions can be found, for example, in [Bar10]. The Eq. (5.1) represents the stationary Reynolds equation used in this work, assuming isothermal conditions (based on [Dam03]).

$$\underbrace{\frac{\partial}{\partial x}\left(\frac{\rho \cdot h^3}{12 \cdot \eta} \cdot \frac{\partial p}{\partial x}\right) + \frac{\partial}{\partial y}\left(\frac{\rho \cdot h^3}{12 \cdot \eta} \cdot \frac{\partial p}{\partial y}\right)}_{\text{Poiseuille flow}} = \underbrace{\frac{u_1 + u_2}{2} \cdot \frac{\partial((1-\theta) \cdot \rho \cdot h)}{\partial x}}_{\text{Couette flow}} \tag{5.1}$$

The x indicates the direction of fluid flow and y is the direction perpendicular to it. The Reynolds equation consists of two flow components, the Poiseuille or pipe flow and the Couette or drag flow. The Poiseuille flow describes the flow of the fluid due to the pressure change dp/dx and dp/dy, while the Couette flow represents the flow due to the velocities of the moving contact bodies u_1 and u_2. These flow components are illustrated in Figure 5.1 based on [HSJ04].

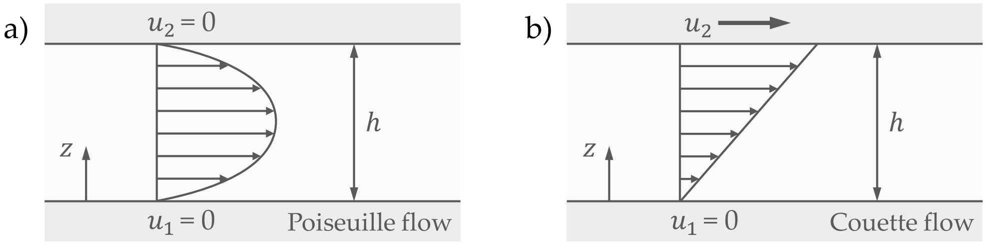

Figure 5.1: a) Velocity profile in the Poiseuille flow; b) Velocity profile in the Couette flow (based on [HSJ04])

To consider the cavitation phenomenon due to the rapid change of the pressure at the outlet region of the contact, the Jakobsson-Floberg-Olsson (JFO) mass-conserving cavitation model [JF57], [Ols65] is applied based on the work of [Elr81]. Accordingly, the cavity fraction θ is implemented as a solution variable of the cavitated domain. The cavity fraction can be expressed by the density of the lubricant ρ and the average density of the mix of oil and gas ρ_{ave} as $\theta = 1 - \rho_{ave}/\rho$. In the areas where no cavitation occurs, the gap is filled with oil, thus the cavity fraction is zero ($\theta = 0$), and the pressure is greater than the cavitation pressure ($p > p_{cav}$). In the cavitated areas, the pressure is assumed to be equal to the cavitation pressure ($p = p_{cav}$) and the cavity fraction is positive ($\theta > 0$). In addition, a complementary constraint is applied as $(p - p_{cav}) \cdot \theta = 0$, with $(p - p_{cav}) \geq 0$ and $\theta \geq 0$.

Rheological equations of the lubricant: For the solution of the Reynolds equation, knowledge of the rheological properties of the lubricant is required. Therefore, the density and dynamic viscosity values are provided in the calculations as the function of the temperature and the pressure using the Bode equations Eq. (2.34)-(2.36), which were presented in Chapter 2.2.4. The necessary lubricant-specific constants were determined by high-pressure measurements in an external laboratory. These coefficients are summarised in Table 5.1 for the investigated test oils.

Table 5.1: Lubricant-specific constants for the application of the Bode equations

	Test oil 1	Test oil 2
a_1	0.08970567	0.08610312
a_2	6348.426753	6248.006741
a_3	-27.52010404	-25.25302907
a_4	0.04547532	0.03691459
a_5	-0.00002769	-0.00001823
α_s	0.0005911	0.0006186
ρ_s	1073.465942	1270.435058

	Test oil 1	Test oil 2
A_1	0.03380703	0.38457417
A_2	2.82632938	2.27517931
A_3	785.285992	860.723564
A_4	0.00162619	0.00214144
k_1	0.00379557	0.01564958
k_2	0.00258151	-0.00034601
k_3	0.00130612	0.01316056

The results of the high-pressure measurements are shown in Figure 5.2 and Figure 5.3. In addition to the measured density and dynamic viscosity values, the corresponding results of the Bode equations are also presented. By using the experimentally determined lubricant-specific coefficients, the curves obtained by the Bode equations show a good agreement with the measured density and dynamic viscosity values for both test oils. Furthermore, the figures show that the density and dynamic viscosity of the two oils differ considerably.

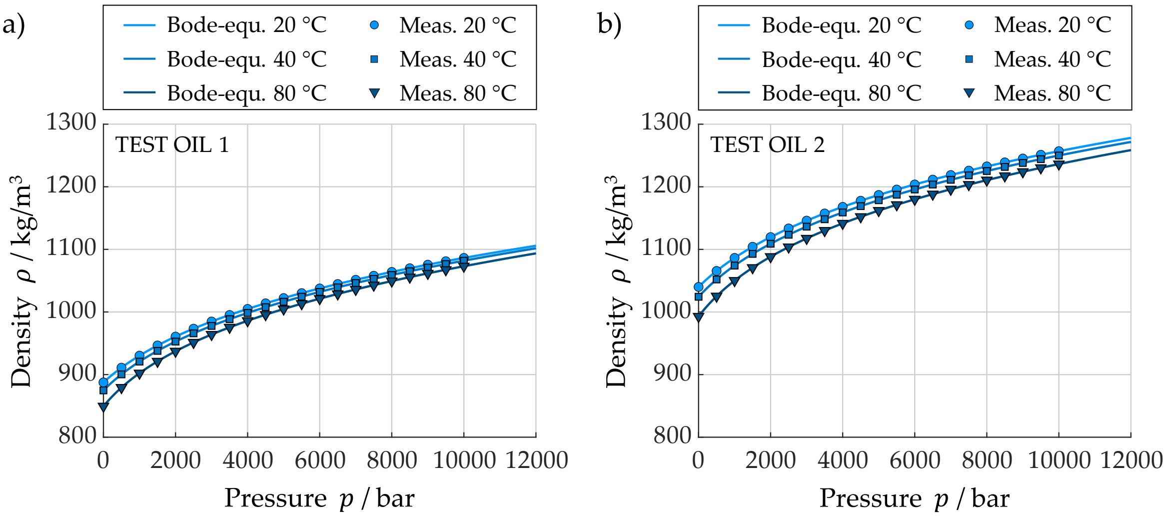

Figure 5.2: Pressure- and temperature dependence of the lubricant density by comparing the measured values with the results of Bode equations: a) Test oil 1; b) Test oil 2

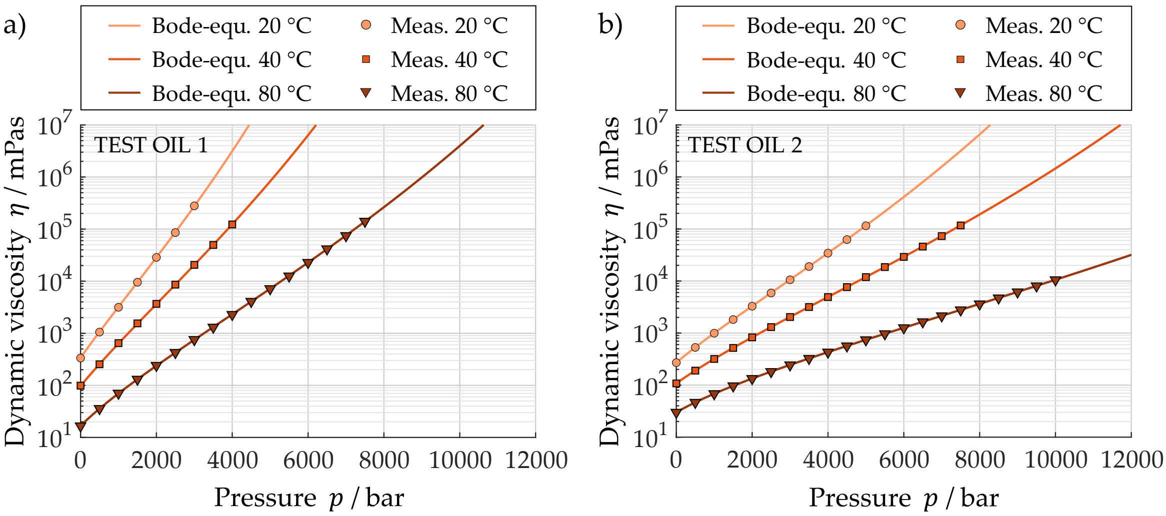

Figure 5.3: Pressure- and temperature dependence of the lubricant viscosity by comparing the measured values with the results of Bode equations: a) Test oil 1; b) Test oil 2

Lubrication gap equation: Due to the developed hydrodynamic pressure, the contact surfaces are deformed in the presence of the lubricating film between them. The resulting gap h can be calculated by the following equation:

$$h(x,y) = \tilde{h}_0 + \underbrace{\frac{x^2}{2 \cdot R_x} + \frac{y^2}{2 \cdot R_y}}_{\text{undeformed geometry}} + \underbrace{\frac{2}{\pi \cdot E_0} \cdot \iint_A \frac{p(x',y')\,dx'dy'}{\sqrt{(x-x')^2 + (y-y')^2}}}_{\text{elastic deformation}} \tag{5.2}$$

The first term is the mutual distance of approach $\tilde{h}_0$, which works as an iteration constant of the numeric calculation. It must be determined iteratively to achieve the equilibrium of forces in the lubrication gap. The second and third terms describe the reduced undeformed geometry of the contacting bodies, where R_x and R_y are the reduced radii in x and y directions, respectively. The fourth term describes the combined elastic deformation of the bodies using the Boussinesq equation [Bou85] with the assumption, that the deformation can be described by the theory of the elastic half-space [Joh85], [Bar10]. The (x', y') indicate the acting location of the pressure, and (x, y) indicate the evaluated location of the deformation inside the calculation domain A. The reduced modulus of elasticity E_0 has been presented in Chapter 2.2.2 by Eq. (2.9). The detailed derivation of the gap equation can be found in [Joh85].

Load balance equation: In the investigated tribological system, the external and internal forces must be in balance. Thus, the applied normal load F_N must be carried by the lubricant film. Consequently, the load resulting from the integration of the developed hydrodynamic pressure p over the investigated area A must be equal to the applied load F_N:

$$F_N = \iint_A p(x, y)\, dx\, dy \tag{5.3}$$

Since the analytical solution of the presented equation system of the EHL contact is not possible in the investigated cases, the application of numerical calculation method is necessary. The numerical calculations are carried out after the nondimensionalization of the equations, where the dimensional variables are replaced by the product of a dimensionless variable and a dimensional reference variable. In this way, the numerical errors (i.e., rounding errors due to the significant difference in the order of magnitude between the different variables) are damped, and the conditioning of the equations is improved [Dam03]. For the calculations, the following dimensionless variables were used:

$$X = \frac{x}{a} \tag{5.4}$$

$$Y = \frac{y}{b} \tag{5.5}$$

$$P = \frac{p}{p_{max}} \tag{5.6}$$

$$H = \frac{h}{\delta} \tag{5.7}$$

$$\hat{\eta} = \frac{\eta}{\eta_0} \tag{5.8}$$

$$\hat{\rho} = \frac{\rho}{\rho_0} \tag{5.9}$$

where p_{max} is the maximum hertzian pressure, a and b are the semi-axes of the hertzian contact ellipse in rolling direction and perpendicular to it (their notations may differ from those used in Chapter 2.2.2), and δ is the hertzian indentation depth, i.e., contact deformation. The η_0 and ρ_0 represent the dynamic viscosity and density of the lubricant at 40 °C and atmospheric pressure. The nondimensionalization of the Reynolds equation, the gap equation and the load balance equation can be found in [Dam03], among others. In the next step, the nondimensionalised equations are discretised. For this purpose, the finite volume method is used, where the calculation domain is divided into a finite number of control volumes, i.e., cells. At the derivation of the Reynolds equation, it is assumed that no flows occur in the direction of the lubrication gap height. With this assumption, the control volume is mathematically reduced into an area element. For the discretization of the calculation domain, a rectangular grid is defined, where constant element sizes ΔX and ΔY are used.

Since the location of the cavitation area is unknown at the beginning of the simulation, the simultaneous calculation of the pressure, gap height and the cavity fraction, i.e., the solution of the equation system, is not possible by direct calculation methods. Accordingly, an iterative solution method is applied. The main steps of the applied iterative solution method are shown in the flow chart of Figure 5.4. The calculations start with the initialization, where the input and initial parameters are defined, such as the geometric data, lubricant coefficients and operating conditions (load, velocity, temperature), and where an initial gap height is assumed. After the initialization, the hydrodynamic pressure distribution is determined iteratively taking into account the JFO cavitation model. For this purpose, the Fischer-Burmeister-Newton-Schur (FBNS) algorithm is used, which was proposed by Woloszynski et al. [WPS15]. Once the hydrodynamic pressure converged, the load balance equation is evaluated, and the mutual approach $\widetilde{H}_0$ is adjusted until the residue of the load balance equation is less than the discretization error.

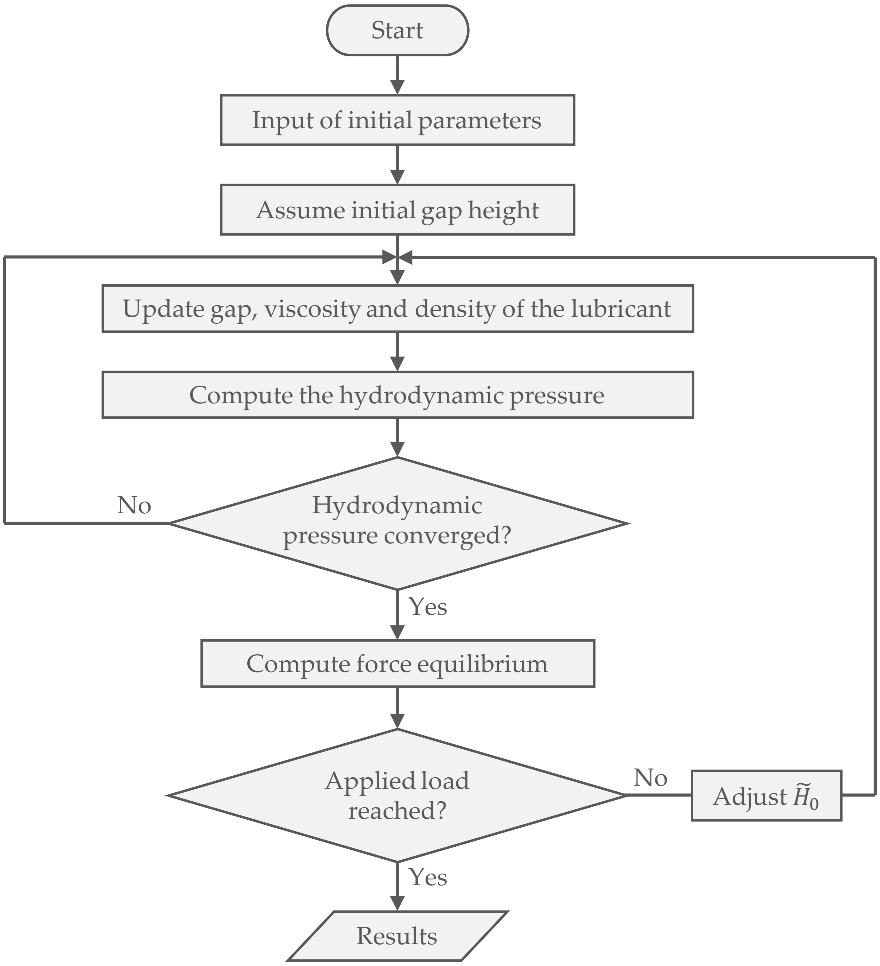

Figure 5.4: Flow chart of the iterative calculation method for the numerical solution of the EHL equation system (based on [SOS21])

A representative result provided by the numerical EHL simulation is shown in Figure 5.5. The conditions used in the simulation represent the contact conditions of a thrust ball bearing 51208 with an axial load of 1500 N (i.e., 100 N load per rolling element), a rotational speed of 1000 min^{-1}, and an oil temperature of 40 °C. In this example, the lubricant properties of test oil 1 were applied. The figure shows the results of the simulation that are used in the following section for the capacitance calculation of the rolling contact, namely the pressure-, gap height- and phase distributions. The pressure distribution in the central region shows a similar course as the hertzian pressure distribution. In this area, the film thickness can be well approximated by the calculation method of Hamrock and Dowson presented in Chapter 2.2.5. In the outlet direction, it is followed by a horseshoe-shaped narrowing of the gap height and the corresponding increase of the pressure values. With the help of the calculated phase distribution, the area and location of the inlet and outlet regions can be determined around the hertzian contact region. The modelling of the contact regions and their characteristic features (e.g., minimum gap height, cavitation) plays an important role in the present investigations, since their effects on the rolling bearing capacitance are usually simplified and integrated into the correction factors during the capacitance calculations.

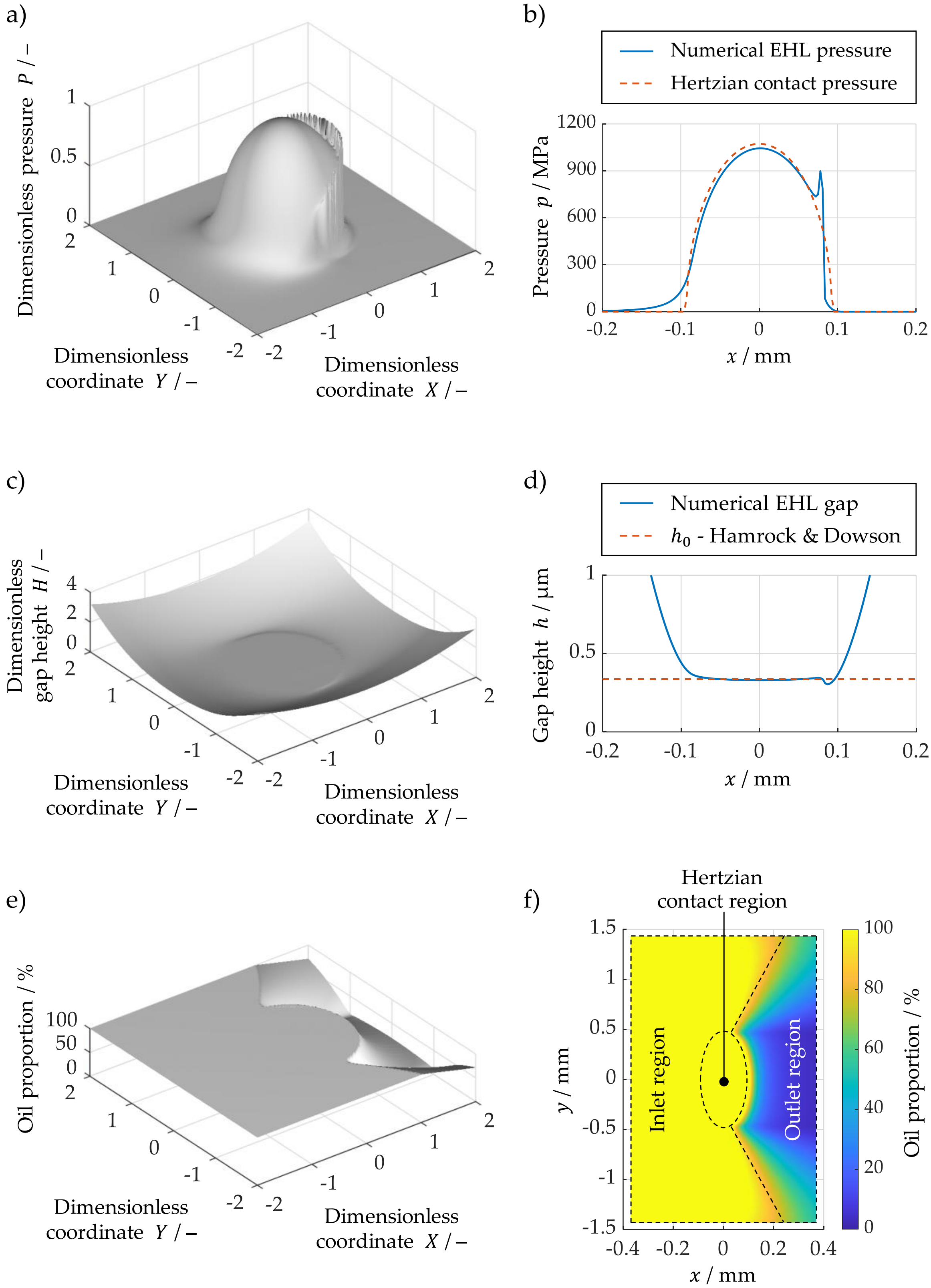

Figure 5.5: Representative results of the numerical EHL simulation: a) Dimensionless pressure distribution; b) Pressure distribution in the $y = 0$ plane; c) Dimensionless gap height; d) Gap height in the $y = 0$ plane; e) Oil proportion in the dimensionless domain; f) Oil proportion with the representation of the contact regions

5.1.2 Electrical extension of the EHL simulation

The capacitance calculation of the rolling contact is built on the previously presented results of the EHL simulation. During the electrical extension, each cell of the EHL simulation is considered as an elementary parallel plate capacitor, where the plate area is obtained by the area of the cells $dA = dx \cdot dy$ and the plate distance is defined by the calculated gap height h_{ij}, as shown in Figure 5.6. Accordingly, parallel electric field lines are assumed within the investigated domain. A similar modelling approach was used in [SLBF19] for the development of a correction function.

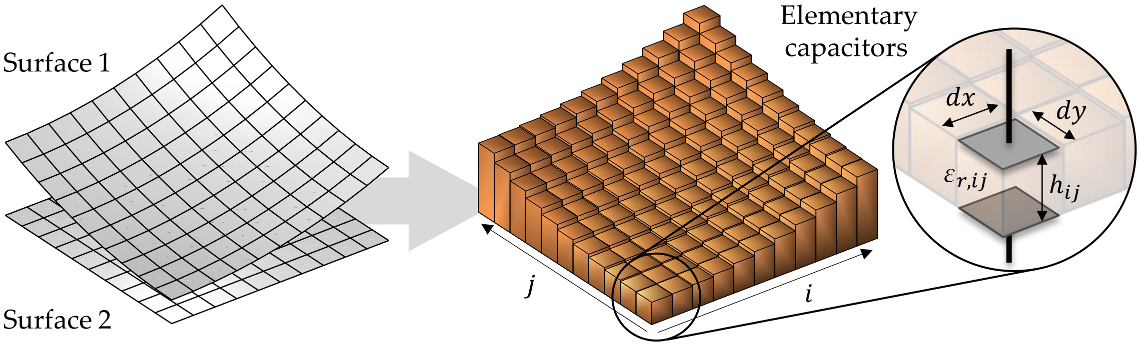

Figure 5.6: Modelling strategy for the electrical extension of the EHL simulation

With the help of this modelling technique, a capacitance value C_{ij} can be assigned to each cell, i.e., a capacitance distribution can be obtained over the investigated range of the contact applying the following equation:

$$C_{ij} = \varepsilon_0 \cdot \varepsilon_{r,ij}(p_{ij}, T_{ij}) \cdot \frac{dx \cdot dy}{h_{ij}} \tag{5.10}$$

The vacuum permittivity ε_0 is a constant, and the relative permittivity $\varepsilon_{r,ij}$ can be described as a function of pressure p_{ij} and temperature T_{ij} using the corresponding Bode equations (Eq. (2.34) - (2.36) in Chapter 2.2.4). Similar to the density and dynamic viscosity, the relative permittivity of the test oils was also measured as a function of temperature and pressure in an external laboratory. The gained lubricant-specific constants, which are necessary for the application of the Bode equations, are summarised in Table 5.1 in Chapter 5.1.1. The results of the high-pressure permittivity measurements are shown in Figure 5.7, where the results of the Bode equations are also presented. The curves provided by the Bode equations show good agreement with the measurements. The values obtained for the two test oils differ significantly both in terms of magnitude and their dependence on pressure and temperature. While the relative permittivity of test oil 1 varies less than 15 % comparing the end values of the measured pressure range (0 - 10000 bar) at all three temperatures (20 - 40 - 80 °C), these differences are more than 35 % in case of test oil 2. Since the pressure within the simulated contact domain can vary from atmospheric value up to the order of GPa (Figure 5.5 b)), the pressure dependence of the lubricant permittivity can be considered as a significant factor in case of certain lubricants.

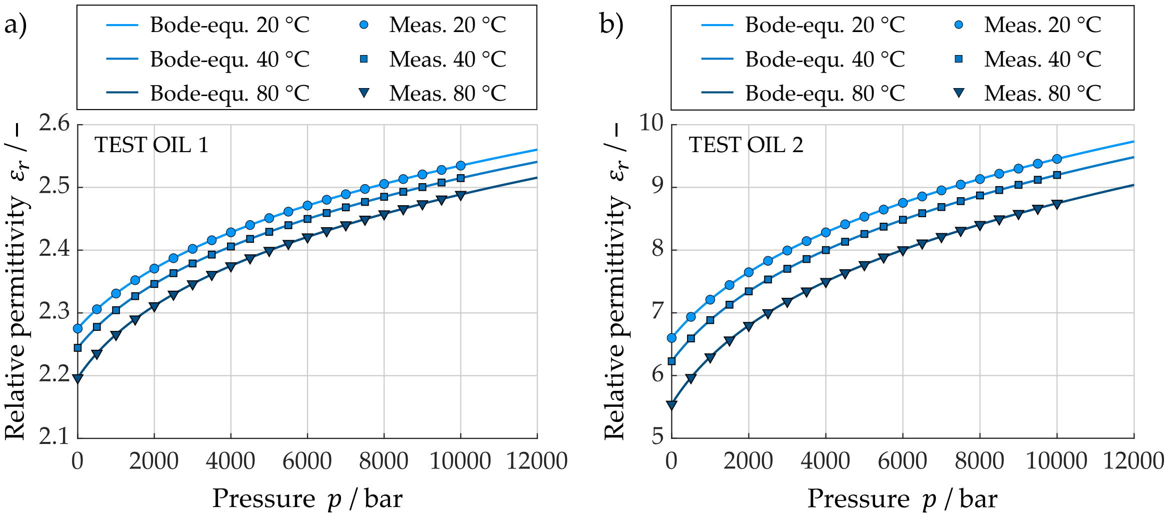

Figure 5.7: Pressure- and temperature dependence of the relative permittivity in case of the applied lubricants by comparing the measured values with the results of the Bode equations: a) Test oil 1; b) Test oil 2

The EHL simulation used in the present work assumes an isothermal temperature distribution in the rolling contact. It means that the temperature of the different operating conditions is taken into account in the electrical modelling, but the temperature distribution within the simulation domain is assumed to be constant. As described in Chapter 5.1.1, a mass-conserving cavitation model is implemented in the EHL simulation. Thus, with the help of the resulted cavity fraction θ_{ij}, the cavitation domain of the rolling contact and the oil-air ratio of this area can be approximated and used for the capacitance calculations. Since the cavitation is a complex phenomenon, where under different conditions, different degrees and types of gas-fluid mixtures can be distinguished (e.g., due to gas cavitation or vapor cavitation) [Bar10], certain simplifications are used for its electrical modelling. The capacitance modelling of the cavitation domain used in the present work is illustrated in Figure 5.8. The method assumes that if the cavity fraction is greater than zero, then the oil and air phases are completely separated in proportion to the value of the cavity fraction. Accordingly, in this domain, each numerical cell can be modelled by a parallel plate capacitor with three or, after mathematical simplification, two dielectric layers (oil and air) in series between its plates. The dimensions of the cell define the area of the capacitor plates, the phases define the permittivities of the dielectrics, and the gap height is distributed according to the cavity fraction. Similar modelling technique, where a complete separation of the phases in the cavitation domain is assumed, was applied in [SLBF19] for the analytical capacitance calculation of the rolling contact.

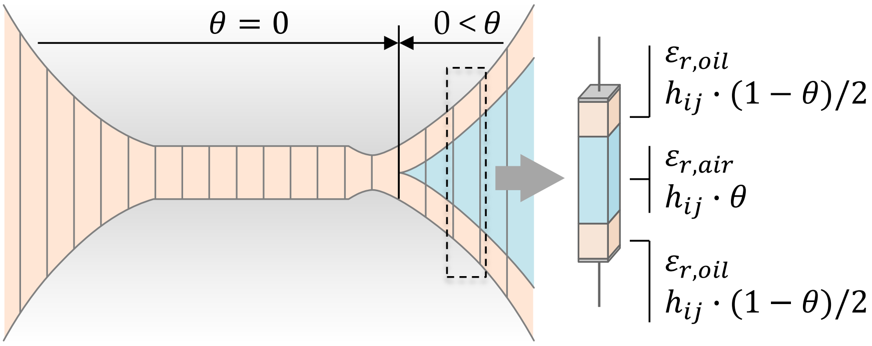

Figure 5.8: Modelling strategy for the calculation of the contact capacitances considering the cavitation domain

Using the presented modelling strategy, the equation for the calculation of the capacitance distribution in the investigated contact region can be written as:

$$C_{ij} = \left(\frac{h_{ij} \cdot (1-\theta_{ij})}{\varepsilon_0 \cdot \varepsilon_{r,oil}(p_{ij}, T_{ij}) \cdot dx \cdot dy} + \frac{h_{ij} \cdot \theta_{ij}}{\varepsilon_0 \cdot \varepsilon_{r,air} \cdot dx \cdot dy} \right)^{-1} \tag{5.11}$$

By the summation of the local capacitance values, the total capacitance of the rolling contact can be obtained. Representative capacitance distributions and their evaluations are shown in Figure 5.9. In the presented examples the axial load of the thrust ball bearing 51208 is 1500 N, the rotational speed is 1000 min^{-1}, the oil temperature is 40 °C, and the investigated lubricants are test oil 1 in Figure 5.9 a), c), e) and test oil 2 in Figure 5.9 b), d), f). The capacitance distribution shows specific characteristics of both the EHL pressure- and gap height distributions. In the central area of the hertzian contact region, a slight flattening of the capacitance course can be observed. This flattening course depends on the flattening in the deformation, the pressure distribution, and the pressure dependence of the lubricant permittivity. In addition, a horseshoe-shaped capacitance increase can be observed approaching the outlet region, which can be explained by the horseshoe-shaped narrowing of the gap height and a corresponding increase of the pressure values. A further characteristic of the capacitance distribution is a discontinuity in the outlet region, which is obtained by the first appearance of the air phase between the plates of the elementary capacitors in the cavitation domain.

Operating conditions
- Thrust ball bearing 51208
- Axial load: F_{ax} = 1500 N
- Rotational speed: n = 1000 min^{-1}
- Temperature: T = 40 °C

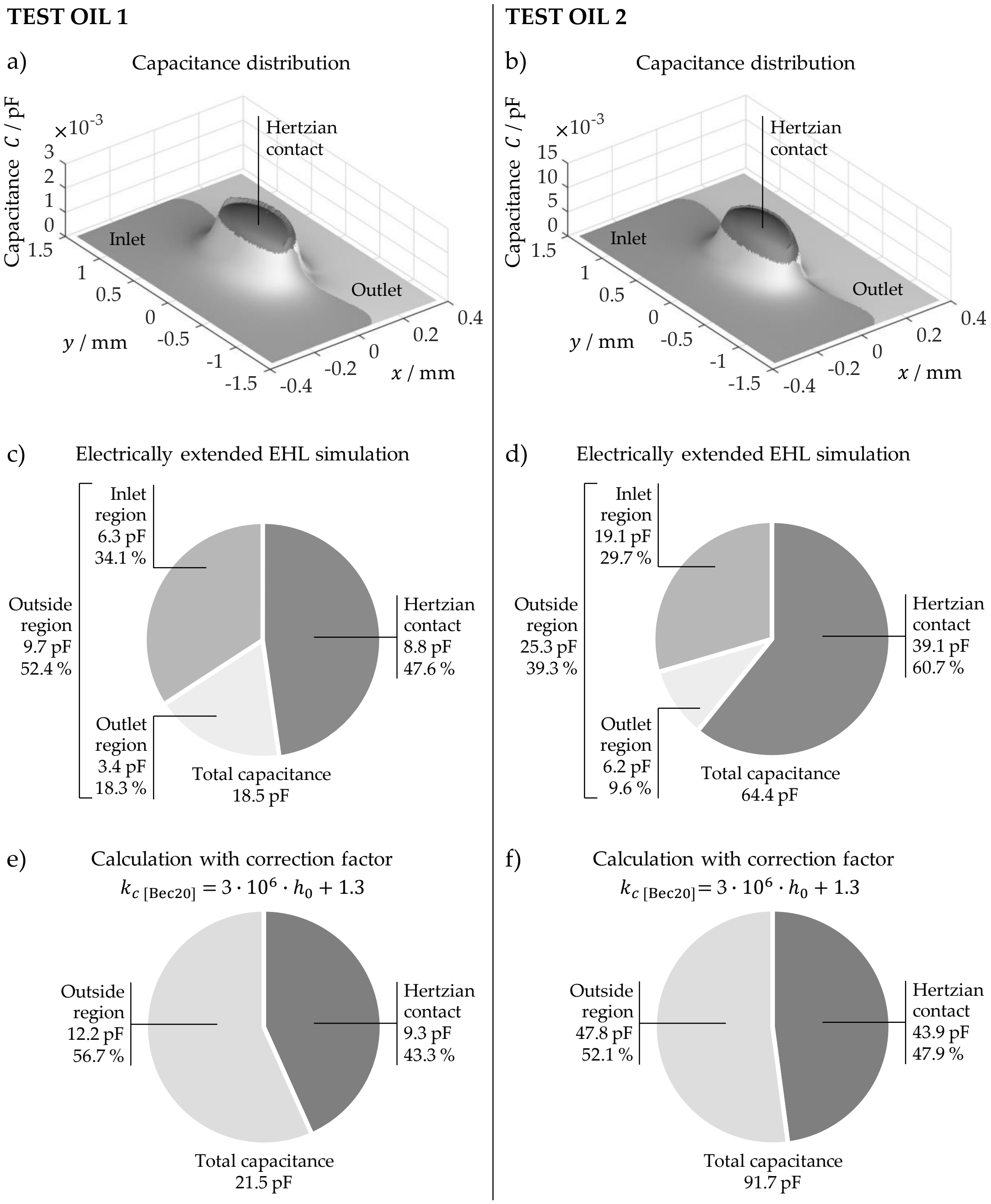

Figure 5.9: a) - b) Capacitance distribution over the simulation domain as the result of the electrically extended EHL simulation; c) - d) Capacitance of the contact regions in case of the numeric simulation; e) - f) Capacitance of the contact regions in case of the correction factor calculation method using the correction function from [Bec20]; (Test oil 1: a), c), e); Test oil 2: b), d), f))

Besides the possibility to consider the capacitance distribution in detail, further advantages of the modelling method are that no correction factor is needed for the determination of the contact capacitances, and that the capacitances of the different regions (inlet-, hertzian contact-, outlet region) can be determined separately, as shown in Figure 5.9 c), d). Although the operating conditions are the same in case of the two lubricants, the results of the EHL simulations (e.g., pressure-, gap height- and phase distributions) differ due to their different rheological properties. Because of them, and the different pressure dependence of the lubricant permittivities, the resulted capacitance distributions, the capacitance percentage of the contact regions, and the total contact capacitances differ significantly. The presented examples are also calculated using the correction factor calculation method with the correction function of Bechev [Bec20]. The resulted capacitances are shown in Figure 5.9 e), f). Comparing the results of the electrically extended EHL simulation and the correction factor calculation method, different degrees of agreement can be observed for the investigated cases. While the calculation results for test oil 1 show a relatively good agreement (16 % difference in total capacitance), for test oil 2, there are larger differences both in terms of magnitude (42 % in total capacitance) and capacitance percentage of the contact regions. It can be partly explained by the fact that the correction factor calculation method cannot consider certain characteristics of the rolling contact that can influence the capacitance distribution. As an example, Figure 5.10 shows the difference between the two calculation methods with respect to the capacitance distribution of the hertzian contact region.

Operating conditions	• Thrust ball bearing 51208	• Axial load: F_{ax} = 1500 N
	• Rotational speed: n = 1000 min^{-1}	• Temperature: T = 40 °C

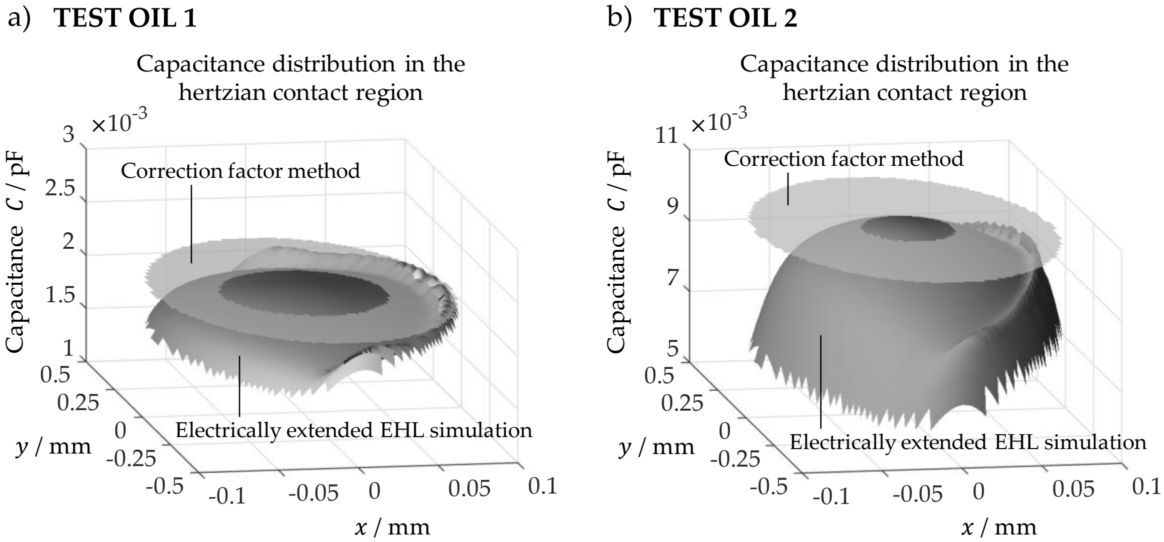
a) **TEST OIL 1**

b) **TEST OIL 2**

Figure 5.10: Capacitance distribution in the hertzian contact region with the comparison of the calculation methods: a) Test oil 1; b) Test oil 2

Since the hertzian contact area is defined for non-rotating, dry contact conditions, the described characteristics of the lubricated rolling contact (e.g., Petrusevitz pressure peak, horseshoe-shaped narrowing of the gap height) influence the capacitance of the hertzian contact area differently for different operating conditions or for the different oils. In contrast, in case of the capacitance calculations with correction factors, the hertzian contact region is assumed to have a constant gap height, a constant lubricant permittivity, and thus a theoretically uniform capacitance distribution. This theoretical capacitance distribution of the correction factor method is illustrated and compared with the results of the electrically extended EHL simulation in Figure 5.10. The capacitance distributions obtained by the two calculation methods show a better agreement for test oil 1 (with 5 % difference in the summed capacitances) than for test oil 2 (with 12 % difference in the summed capacitances). The capacitance differences in this region can explain only a part of the differences in total contact capacitances. Therefore, there are additional differences between the calculation methods, which are related to the different modelling techniques of the outside region of contact. The presented cases are representative examples to describe and compare the calculation methods and to show possible differences between their results. (The relatively larger difference between the results of the calculation methods for test oil 2 is not lubricant-specific. It can also be observed at certain operating conditions for test oil 1). Further results of the calculation methods are discussed in Chapter 6.2.

For the general application of the electrically extended EHL simulation, it is necessary to define the area of the simulation domain and its resolution. To define these parameters, the following aspects must be taken into account. By increasing the simulated area, the resulted total capacitance increases, because more and more elementary capacitances are summed. However, moving away from the hertzian contact region and from the deformed domain of the contact, these capacitance increments decrease, since the distance between the corresponding surfaces increases. In parallel, a larger simulation area requires more numerical elements to ensure the same resolution of the mesh, which affects the computation time. Consequently, the size of the simulation area should be dependent on the operating conditions, should be large enough to take into account the deformed areas of the contact (inside and outside the hertzian contact region), but should not be too large to increase the element number, i.e., the computation time excessively. Considering the described aspects, the defined size of the simulation area used in the investigations is $8a$ x $6b$, where a and b are the half-axes of the hertzian contact ellipse in rolling direction and perpendicular to it. The centre of the contact (defined by the centre of the rolling element) is located in the middle of the calculation area.

The required number of numerical elements can be defined by mesh refinement analysis, which is represented through an example in Figure 5.11.

Operating conditions
- Thrust ball bearing 51208
- Axial load: F_{ax} = 1500 N
- Test oil 1
- Rotational speed: n = 1000 min^{-1}
- Temperature: T = 40 °C

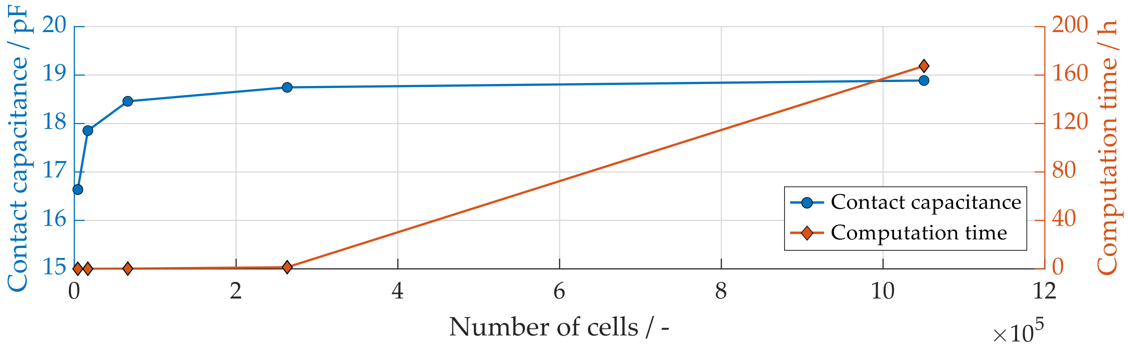

Number of cells / -	Capacitance / pF	Capacitance change / %	Computation time
4 225	16.64	-	1 min
16 641	17.85	7.3	2 min
66 049	18.46	3.4	9 min
263 169	18.75	1.6	1 h 21 min
1 050 625	18.88	0.7	167 h 32 min

Figure 5.11: Mesh refinement analysis of the electrically extended EHL simulation represented by an example

During the mesh refinement analysis, the calculated contact capacitance and the related computation time were examined as a function of the cell number in case of the previously defined simulation domain. (Since the computation time depends also on the performance of the computer, the ratios of the indicated time values are more relevant than their magnitude.) The number of elements were increased by close to a factor of four between the calculated cases. As the diagram shows, both the resulted capacitance and the computation time increase with increasing number of elements. However, while the computation time increases with increasing rate, the calculated capacitance tends to a certain value, and its change becomes smaller with the increasing number of elements. Based on the presented values, the case with approx. 66000 elements can be considered as an optimal resolution for the examined conditions. Further densification of the mesh does not lead to a significant change in capacitance, but considerably increases the computation time. Additional investigations, carried out in accordance with the presented example, confirm the described observations. After specifying the computational domain and its resolution, the presented electrically extended EHL simulation is suitable for the general investigation of the capacitance of the rolling contact.

5.2 Capacitance simulation with finite element method

For the electrical investigation of rolling bearing areas outside the EHL simulation domain, a finite element simulation model was developed in the *Ansys* simulation software, which is introduced in this chapter. The aim is to provide a computational technique, which can take into account various influencing factors, that are not considered by the state-of-the-art electrical rolling bearing models. Such factors are, among others, the quantity of oil (i.e., the different oil levels in the GESA cell) or the geometry and material (conductor or insulator) of the surrounding components. Since several conductive components (rings, rolling elements) can be found within the range under consideration, the task is to determine the capacitances of a multi-conductor system. A general three-conductor example (the third is ground) is represented in Figure 5.12.

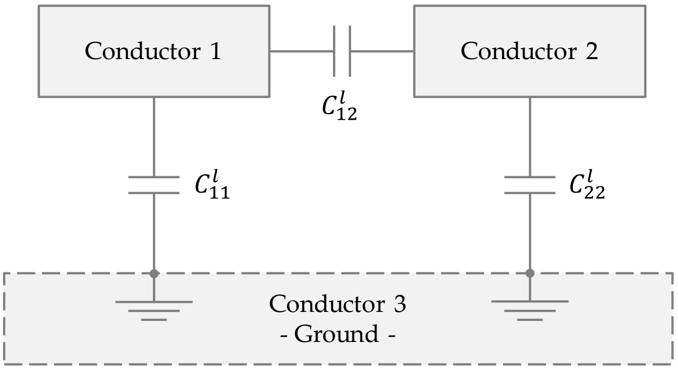

Figure 5.12: Capacitance network of a general multi-conductor system using lumped capacitances (based on [Ans19])

The charges on the conductors can be expressed in terms of the voltage differences between the conductors and the corresponding capacitances, using the $Q = C \cdot U$ relation:

$$Q_1 = C_{11}^l \cdot U_1 + C_{12}^l \cdot (U_1 - U_2) \tag{5.12}$$

$$Q_2 = C_{12}^l \cdot (U_2 - U_1) + C_{22}^l \cdot U_2 \tag{5.13}$$

where C_{ij}^l represents the lumped capacitances (also known as partial capacitance), which is generally used in circuit simulations, where a physical system is reduced to a network of discrete elements. They are usually summarised in matrix form as the lumped capacitance matrix:

$$C^l = \begin{bmatrix} C_{11}^l & C_{12}^l \\ C_{12}^l & C_{22}^l \end{bmatrix} \tag{5.14}$$

The equations (5.12)-(5.13) can be rearranged to the voltages:

$$Q_1 = \left(C_{11}^l + C_{12}^l\right) \cdot U_1 - C_{12}^l \cdot U_2 \tag{5.15}$$

$$Q_2 = -C_{12}^l \cdot U_1 + \left(C_{12}^l + C_{22}^l\right) \cdot U_2 \tag{5.16}$$

Thus, they can be written in the following matrix form:

$$\begin{bmatrix} Q_1 \\ Q_2 \end{bmatrix} = \begin{bmatrix} C_{11}^l + C_{12}^l & -C_{12}^l \\ -C_{12}^l & C_{12}^l + C_{22}^l \end{bmatrix} \begin{bmatrix} U_1 \\ U_2 \end{bmatrix} = \begin{bmatrix} C_{11}^g & C_{12}^g \\ C_{21}^g & C_{22}^g \end{bmatrix} \begin{bmatrix} U_1 \\ U_2 \end{bmatrix} \tag{5.17}$$

where C_{ij}^g represents the ground capacitances, which form the ground capacitance matrix (also known as Maxwell capacitance matrix). The ground capacitance matrix describes the relationship between the charges on the conductors and the conductor voltages with respect to the ground. The lumped and ground capacitance matrices can be calculated from each other using the following relations:

$$C_{ii}^l = \sum_j C_{ij}^g \tag{5.18}$$

$$C_{ij}^l = -C_{ij}^g \quad \forall \quad i \neq j \tag{5.19}$$

The presented capacitance matrices of the multi-conductor systems can be calculated by various simulation software (e.g., *Ansys*, *Comsol Multiphysics*). In the present work, the *Ansys* simulation software was applied, where the capacitance calculation is based on the energy principle [Ans19]. Since the focus of the investigations is on the reduced capacitance network of a physical system using discrete elements, the lumped capacitance values will be examined and evaluated as the result of FEM calculations in the following part of the work.

In case of the investigated thrust ball bearing 51208, the FEM simulations are performed according to the following strategy, which is illustrated in Figure 5.13. For the capacitance calculations, the dielectrics (lubricant, air, plastic cage) are modelled, and the conductive components are represented as boundary conditions on the corresponding boundary surfaces. To reduce the computational demand, a segment model is defined exploiting the geometrical periodicity of the rolling bearing. The 360° range of the bearing is divided into 15 identical segments according to the number of rolling elements, and a 24° segment is modelled with one rolling element. The conductive parts of this segment form a three-conductor system similar to the example in Figure 5.12. In case of the bearing segment, illustrated in Figure 5.13 b), C_{11}^l represents the capacitance between driven parts (the rotating ring with the connected shaft) and the stationary parts (stationary ring with the ring mount), C_{12}^l is the capacitance between the driven parts and the rolling element, and C_{22}^{l} is the capacitance between the stationary parts and the rolling element, where the stationary parts are grounded. Since the FEM simulation serves as a direct spatial extension of the electrically extended EHL simulation, the dielectrics and the conductive surfaces are not modelled within the domain of the EHL simulation. This approach avoids potential difficulties associated with the FEM meshing of the lubrication gap in the rolling contact. Using this modelling technique, the effect of the non-modelled region on the charge distribution of the components is neglected.

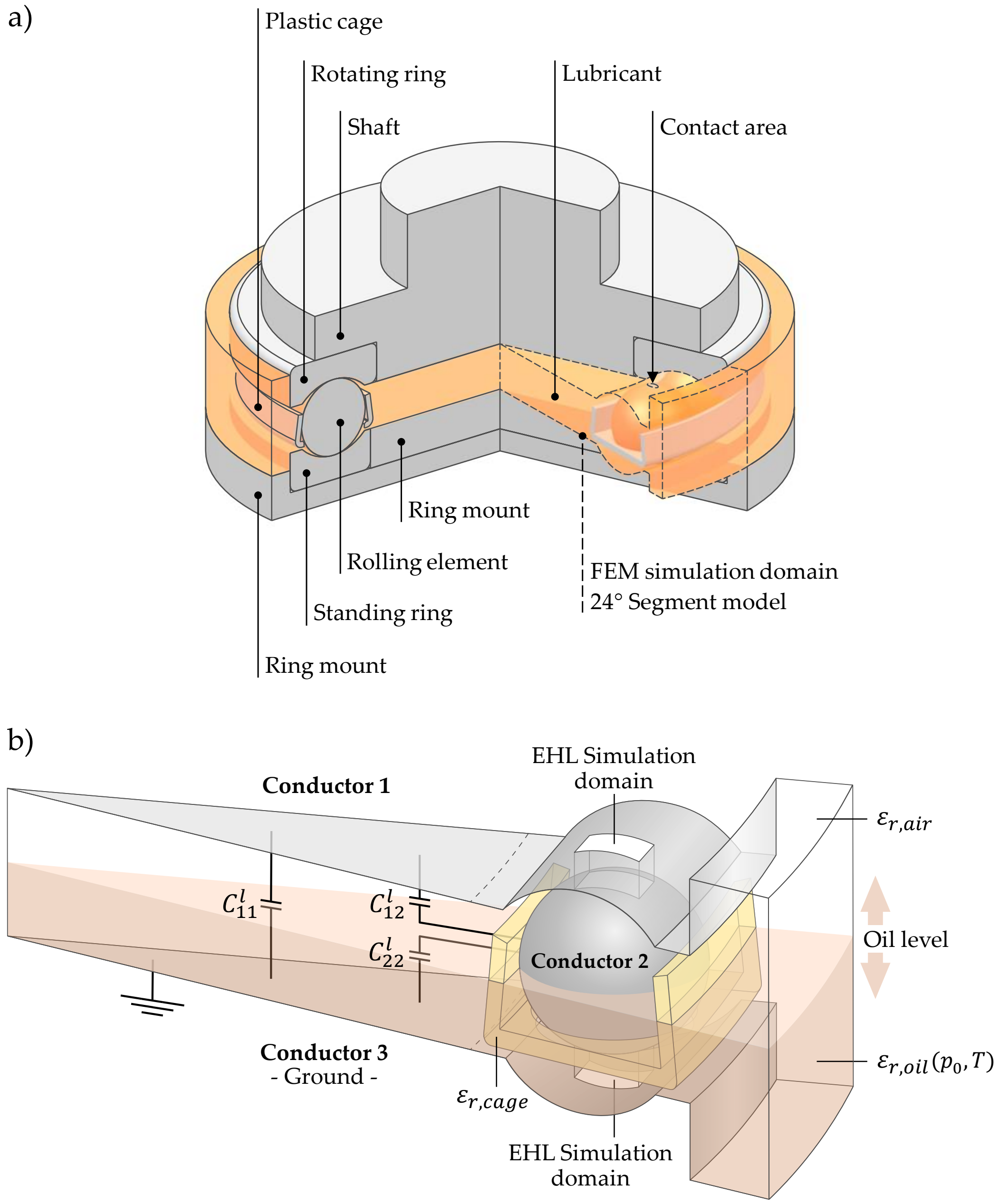

Figure 5.13: FEM modelling strategy: a) Definition of the periodic segment model of the rolling bearing; b) Representation of the lumped capacitances in the segment model with additional modelling details

The FEM modelling allows the definition of different dielectrics, which can be used to fill the volume between the conductors. Within the segment model, the plastic cage, the lubricating oil, and the air are modelled as dielectrics (Figure 5.13 b)). The plastic cage is always defined with the same position and constant relative permittivity ($\varepsilon_{r,cage}$ = 3.5). The quantity and relative permittivity of the oil can be varied according to the chosen operating conditions. If the cell is not completely flooded with oil, the remaining volume is filled with an air phase of constant permittivity ($\varepsilon_{r,air}$ = 1.00059). The amount of oil is defined by a horizontal oil level, i.e., the different vortex-shaped oil distributions resulting from the different rotational speeds of the rolling bearing are not considered. (If corresponding computational fluid dynamics (CFD) simulations are available, the resulting oil-air distributions can be implemented.) For the determination of the distance between the rolling bearing rings, the deformations of the bodies, i.e., their indentations, are also taken into account. Thus, after the EHL simulation is performed, the size of the simulation domain and the resulting indentations, which depend on the investigated operating conditions, are used as input parameters of the FEM simulation. The developed FEM segment model for a half flooded cell is shown in Figure 5.14 a), while the half of the segment (12° section of it) can be observed in Figure 5.14 b). The figures show the modelling technique, i.e., that the conductive components are only present with their boundary surfaces, and the FEM meshing is performed in accordance with the spatial distribution of the dielectrics. Figure 5.14 c) shows that the gaps between the conductive surfaces in the direct vicinity of the EHL simulation domains are significantly smaller than in the rest of the segment model. Accordingly, to obtain a well-conditioned computational mesh and high accuracy of the simulation results, mesh refinement is applied towards the EHL simulation domains. Although the distances between the surfaces in this region are larger compared to the lubricant film thickness resulted from the EHL simulation, the corresponding surfaces are also large compared to the EHL simulation domain. Therefore, these regions are of great importance for the modelling of rolling bearing capacitances. The presented FEM simulation model allows the determination of the rolling bearing capacitances outside the region of the rolling contact, which is not possible with the electrically extended EHL simulation. Thus, by combining the two calculation techniques, a more accurate total bearing capacitance can be obtained. The computational process of the combined calculation method is described in the next chapter.

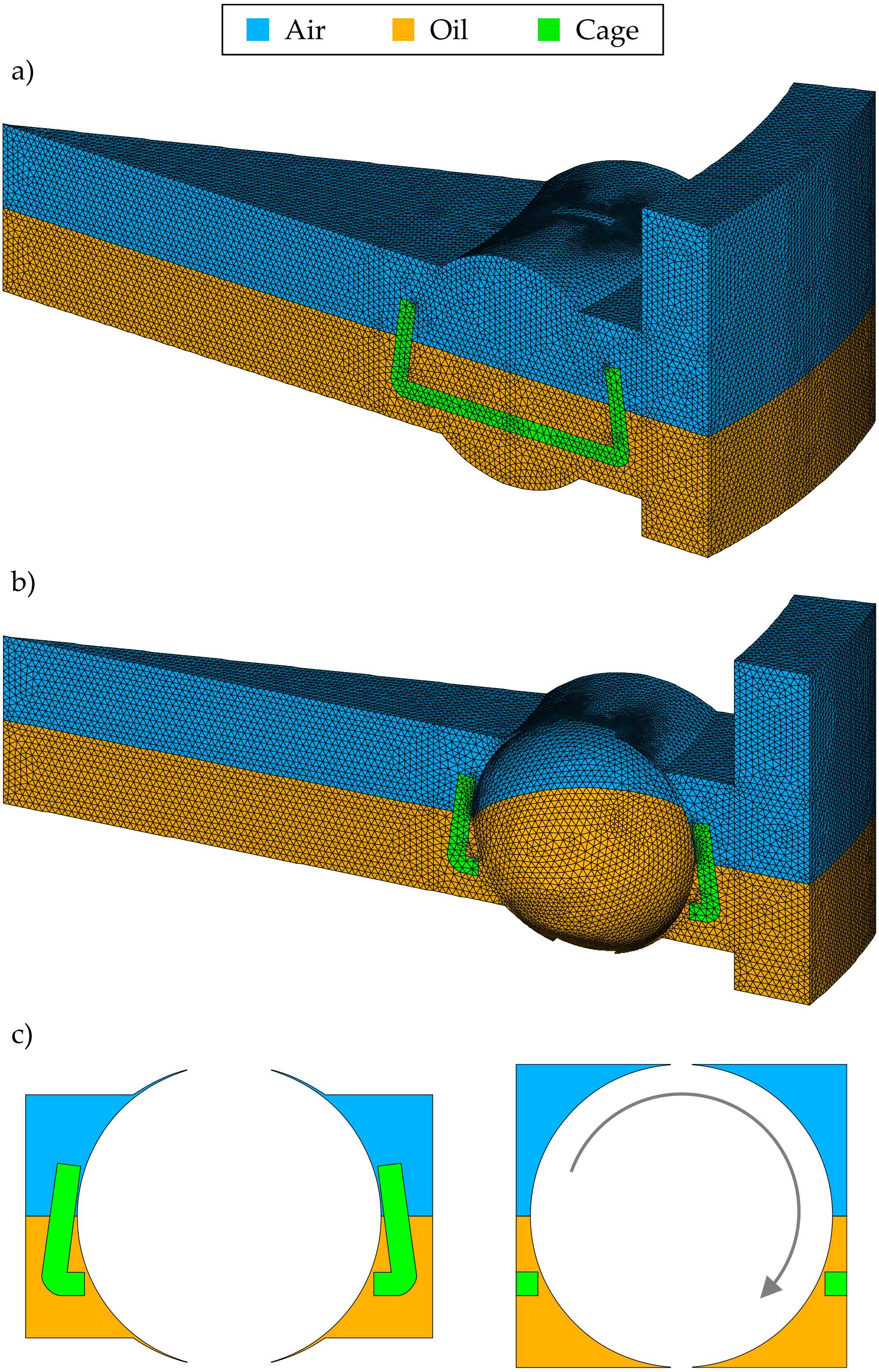

Figure 5.14: a) FEM segment model (24°) with mesh refinement towards the EHL simulation domain in case of a half flooded cell; b) Half of the FEM segment model (12°); c) Cross-section of the modelled dielectrics perpendicular to the rolling direction (left) and in rolling direction along the pitch diameter (right)

5.3 Combined simulation method

By combining the simulation methods presented in the previous chapters, the total rolling bearing capacitance can be determined taking into account various influencing factors that are not considered by the state-of-the-art electrical rolling bearing models. The calculation process and the connections between the simulation methods are represented in Figure 5.15 and described in the following. The geometric data, material- and lubricant properties, and the operating conditions are input parameters for both the EHL- and FEM simulations. After the contact conditions are defined (e.g., hydrodynamic velocity, contact load, hertzian contact parameters), the EHL simulation is performed. The resulting pressure distribution, gap height distribution and phase distribution are used in the electrical extension of the contact calculation, while the size of the EHL simulation domain and the indentation of the contacting bodies are added to the input parameters of the FEM simulation. The electrically extended EHL simulation results in a capacitance distribution, which is summed over the simulation domain to obtain the contact capacitance. Assuming identical contact conditions for the rolling contacts of the axial thrust ball bearing, the resulted contact capacitance can be used for both the inner ring (rotating ring) contact $C_{RE,Cont,ir}^{EEHL}$ and the outer ring (stationary ring) contact $C_{RE,Cont,or}^{EEHL}$ (where the EEHL index refers to the electrically extended EHL simulation method). In parallel, the additional non-contact capacitances between the conductive components are determined by the FEM simulation. These are the capacitance between the rolling element and its environment on the inner ring side $C_{RE,Env,ir}^{FEM}$ and on the outer ring side $C_{RE,Env,or}^{FEM}$, and the capacitance between the rings and further environmental components (e.g., shaft, ring mount) of the 24° segment $C_{Seg,Env}^{FEM}$. The capacitances, which are obtained by the electrically extended EHL simulation and the FEM simulation, are combined according to the circuit diagram of the rolling bearing segment presented in Figure 5.15. In this way, the total segment capacitance C_{Seg} can be calculated as:

$$C_{Seg} = C_{Seg,Env}^{FEM} + \frac{\left(C_{RE,Env,ir}^{FEM} + C_{RE,Cont,ir}^{EEHL}\right) \cdot \left(C_{RE,Env,or}^{FEM} + C_{RE,Cont,or}^{EEHL}\right)}{C_{RE,Env,ir}^{FEM} + C_{RE,Cont,ir}^{EEHL} + C_{RE,Env,or}^{FEM} + C_{RE,Cont,or}^{EEHL}} \tag{5.20}$$

The segments are considered to be connected in parallel. Therefore, the total bearing capacitance can be calculated by the sum of the segment capacitances. Since the capacitance of the segments are identical for the investigated bearing, the total rolling bearing capacitance C_{RB} can be obtained as:

$$C_{RB} = Z \cdot C_{Seg} \tag{5.21}$$

where Z is the number of rolling elements, i.e., the number of the segments.

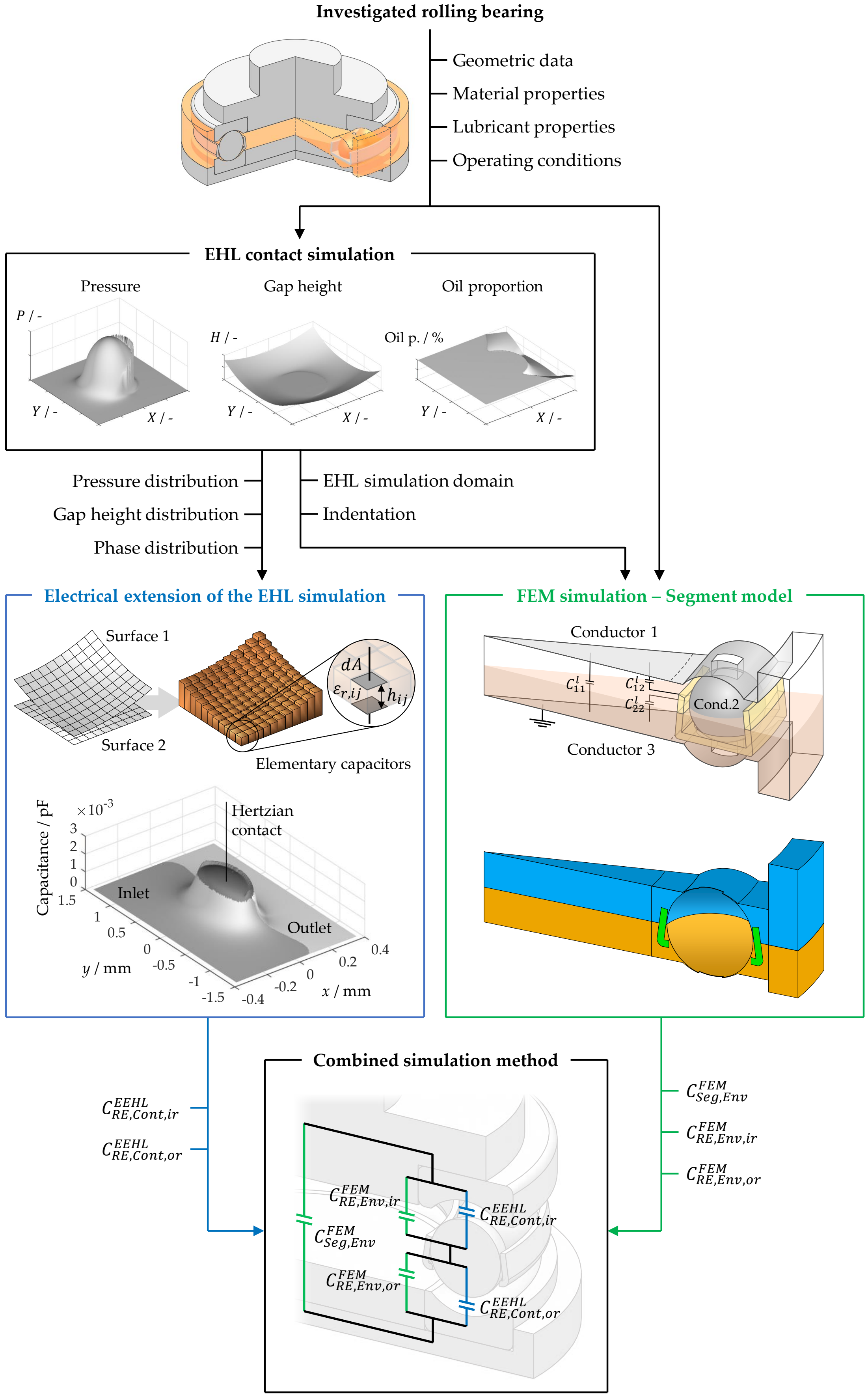

Figure 5.15: Strategy of the combined simulation method for the determination of the rolling bearing capacitance

The results provided by the combined simulation method are represented by an example in Figure 5.16. The simulation results are also compared with the result of the correction factor calculation method and with measured rolling bearing capacitances. In the investigated example, the rotational speed of the thrust ball bearing 51208 is 1000 min^{-1}, the axial load is 750 N, the operating temperature is 40 °C and the GESA cell is half flooded with the test oil 1.

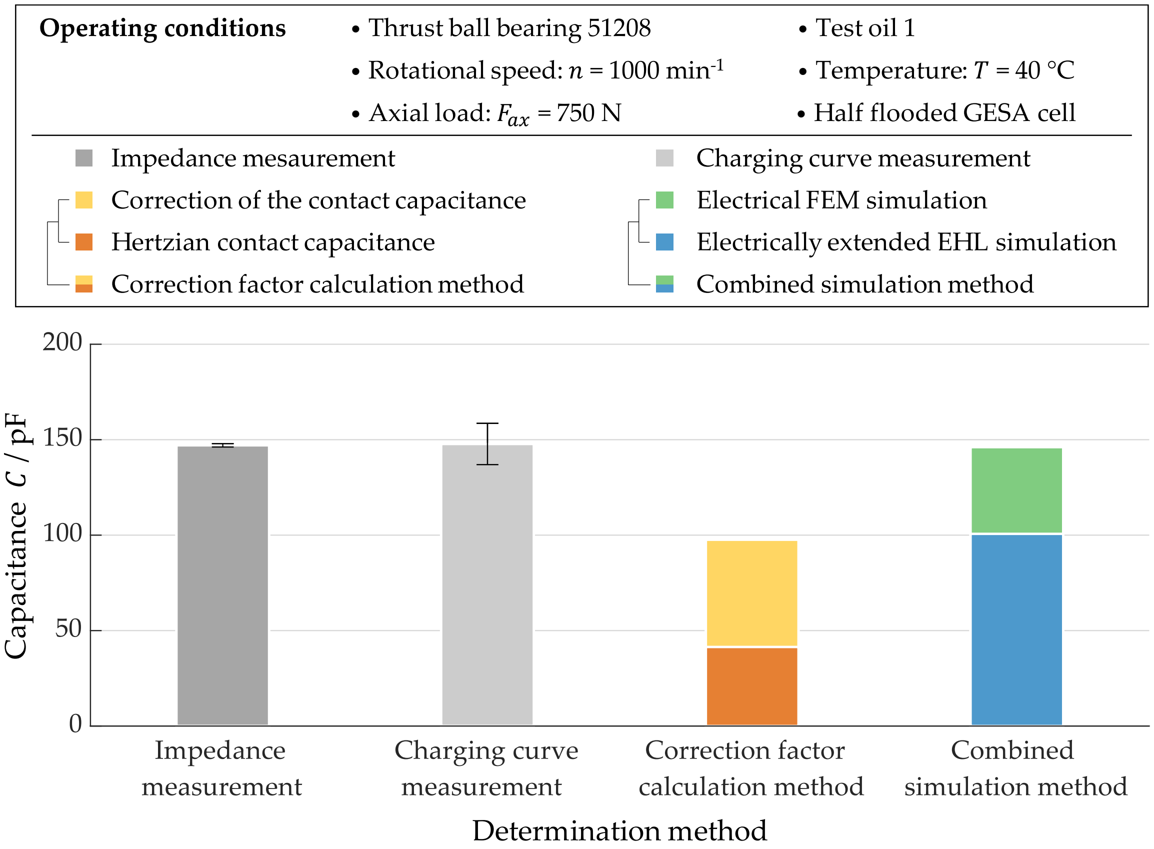

Figure 5.16: Example for the rolling bearing capacitances obtained by different determination methods

The impedance- and charging curve measurement methods are represented with the average result of five measurements and the corresponding standard deviation. In case of the correction factor calculation method, the correction function $k_{c,total}$ of Bechev (Figure 2.20) was applied. The total rolling bearing capacitance was determined based on the equivalent circuit diagram of the rolling bearing with insulating cage (Eq. (2.59)). The results were calculated both with and without the correction of the hertzian contact capacitance. The hertzian contact capacitance was determined analytically, using the central lubricant film thickness and the area of the hertzian contact ellipse based on the formulae of Hamrock and Dowson, and Hertz. To demonstrate the importance of the non-contact areas of the rolling bearing, the combined simulation method is represented both with and without the FEM simulation results. When the results of the FEM simulation are not considered, the FEM-indexed terms of the Eq. (5.20) are omitted, and the total rolling bearing capacitance is calculated only from the results of the electrically extended EHL simulation. (The capacitances of the FEM calculations are not added as a constant term to the total bearing capacitance calculated from the result of the electrically extended EHL simulation, but according to the circuit diagram of the segment.) While the result of the combined simulation method shows a good agreement with the results of the measurements, in case of the correction factor calculation method a larger difference can be observed. This difference can be explained by the capacitances of the non-contact areas of the rolling bearing, which cannot be considered by the correction factor calculation method. By definition, the purpose of the correction factor is to describe the ratio between the total capacitance of the contact and the capacitance of the hertzian contact region. Accordingly, the capacitance calculations using the correction factor method (without taking additional capacitances into account) are not intended to accurately calculate the total bearing capacitance, although they are frequently used as an approximation of it. In addition, the results of the correction factor calculation method should theoretically agree with the results of the electrically extended EHL simulation, since both methods describe the capacitance of the same area, i.e., the capacitances of the inlet-, hertzian contact- and outlet regions of the contact. Based on the results of the combined simulation method, the capacitance increase obtained by the inclusion of the capacitances of the non-contact areas (i.e., the capacitances determined by the FEM simulation) is approx. 30 % of the total bearing capacitance in the investigated example. This value can be influenced, for example, by changing the oil level in the GESA cell, or changing the geometry of the parts connected to the rolling bearing. Among others, these aspects can be also investigated by the developed combined simulation method. To determine the capacitance sources of the rolling bearings, and to validate the results of the combined simulation method, additional investigations were carried out, which are presented in Chapter 6.

6 Systematic investigation of rolling bearing capacitances

In this chapter, the systematic investigations of the rolling bearing capacitances are presented, which have been carried out using the experimental and simulation methods described in the previous chapters. First, the possible capacitance sources of rolling bearings are examined with the aim of identifying and categorising the factors affecting the total rolling bearing capacitance. Subsequently, the developed combined simulation method is validated, where the simulation results are compared with both the results of the two presented measurement methods, and the results of the correction factor calculation method. During these investigations, in addition to the variation of specific operating parameters, the influence of the oil quantity, i.e., the oil level is also considered. After the examinations on the thrust ball bearing 51208, the axially loaded angular contact ball bearing 7206 is also investigated using the presented experimental methods and the developed combined simulation method.

6.1 Capacitance sources in rolling bearings

As already shown in the description of the combined simulation method, the approximation of the total rolling bearing capacitance by considering only the contact capacitances can lead to significant deviations from the measured values. Accordingly, it is necessary to investigate the non-contact areas of the rolling bearing and their role in the total bearing capacitance. Therefore, different investigations were carried out in order to identify and categorise possible capacitance sources of rolling bearings. These experimental investigations were performed with the trust ball bearing 51208 and are presented in the following.

6.1.1 Rolling element dependent and independent capacitances

In the first experiment, the relationship between the number of rolling elements and the measured rolling bearing capacitance was investigated. For this purpose, impedance measurements were carried out under constant operating conditions with 3, 6, 9, 12 and 15 rolling elements. The rotational speed of the rolling bearing was 1000 min^{-1}, the operating temperature was adjusted to 40 °C and the GESA cell was fully flooded with the test oil. In order to perform the measurements under the same contact conditions, the axial load of the rolling bearing was increased according to the number of rolling elements. Thus, it can be assumed that the lubricant film thickness in the rolling contacts was identical during the measurements. The investigations were carried out with 100 N and 200 N axial load per rolling element, both with test oil 1 and 2. The results are shown in Figure 6.1.

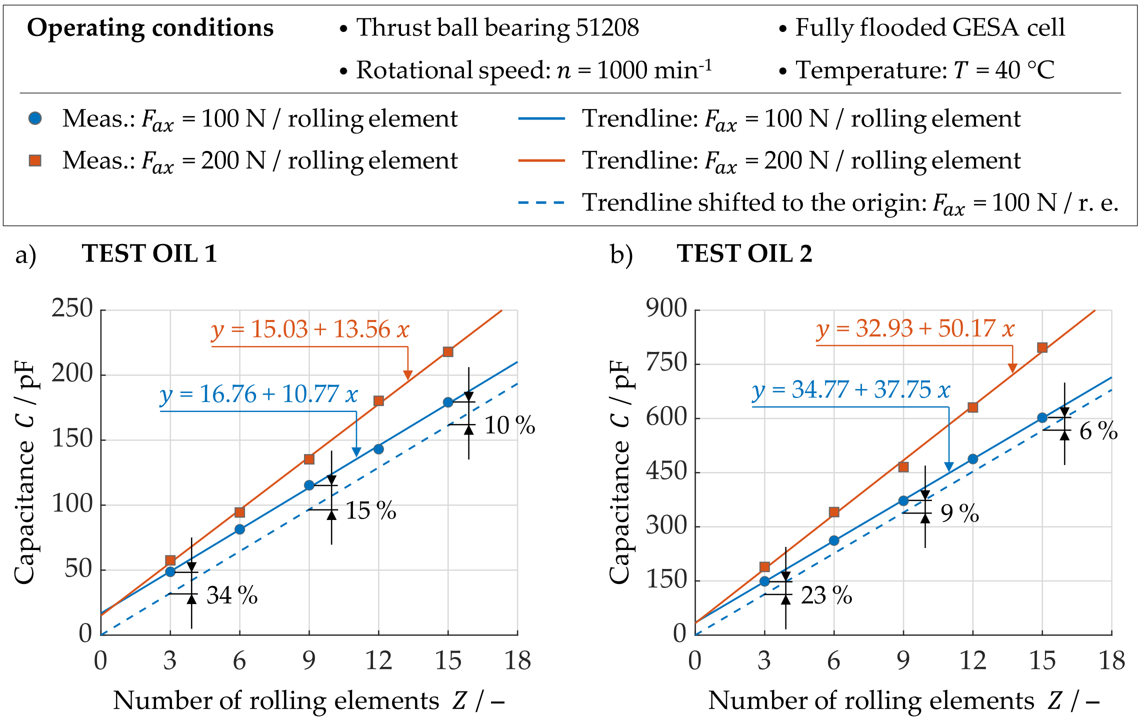

Figure 6.1: Investigation of the relationship between the number of rolling elements and the rolling bearing capacitance: a) Test oil 1; b) Test oil 2

The presented measurement results are obtained from the average of five impedance measurements under the investigated operating conditions. In addition, fitted linear trendlines and their equations are shown, which describe the course of the rolling bearing capacitance as a function of the rolling element number. Since the linear trendlines show a good agreement with the course of the measured values, the dependence of the rolling bearing capacitance on the rolling element number can be described in the following form:

$$y = A + B \cdot x \tag{6.1}$$

where y indicates the rolling bearing capacitance and x is the number of rolling elements. Based on this equation, the capacitances can be divided into two groups. There are rolling bearing capacitances, which are independent (denoted by "A") and dependent (denoted by "B") on the rolling elements. Thus, the value "B" can be interpreted as the capacitance increase per rolling element. The fitted trendlines are steeper for higher load, i.e., the capacitance increase per rolling element is also larger. It can be explained by the thickness of the lubricating film in the rolling contacts, which is smaller at higher loads, leading to higher contact capacitances. It is important to note that the trendlines (for a given lubricant) take nearly identical, non-zero values at their starting points, i.e., when the number of rolling elements is zero. It indicates that components besides the rolling elements are also involved in the generation of the rolling bearing capacitances. The presented trendline equations show that the rolling element independent capacitance "A" has a similar magnitude as the capacitance increase per rolling element "B". Therefore, considering only the contact capacitances in the calculations (especially for rolling bearings with lower number of rolling elements) can lead to significant deviations from the measured values. For the measurements with 100 N load per rolling element, the trendlines are also plotted starting from the origin, i.e., without the capacitance "A". In this way, the rolling element independent capacitance can be illustrated relative to the total rolling bearing capacitance for different numbers of rolling elements. This ratio decreases with increasing number of rolling elements. In contrast, as the lubricant film thickness increases (e.g., due to decreasing axial load), the importance of this constant capacitance term increases. In general, the rolling element independent capacitances become significant when the rolling element related capacitances are low (either by a high lubricant film thickness in the rolling contact or by the low number of rolling elements). The capacitance sources, identified by the presented investigations, are illustrated in Figure 6.2.

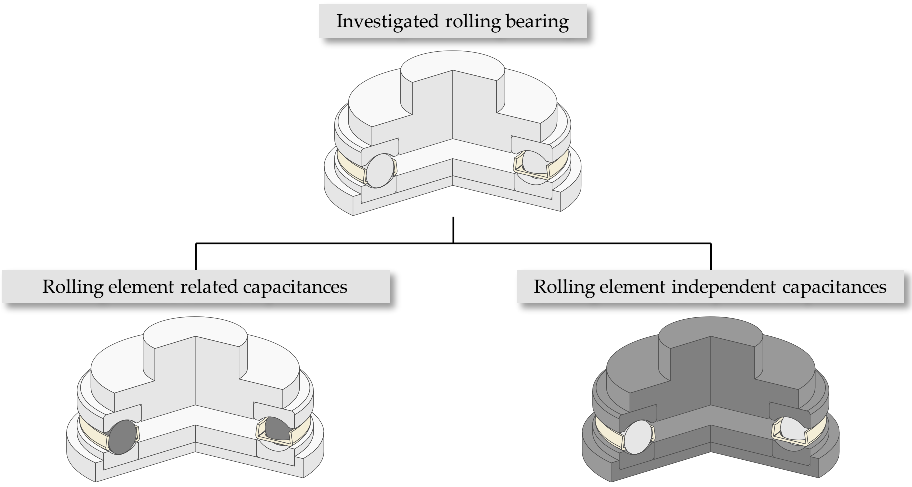

Figure 6.2: Categorisation of the rolling bearing capacitances: Rolling element related capacitances, and rolling element independent capacitances

6.1.2 Environmental influences

To investigate the rolling element independent capacitances of the rolling bearing, targeted experiments were carried out. Assuming that these capacitances can be influenced by the environmental parts, i.e., by the components mounted directly to the rolling bearing, different design variants of the GESA cell were constructed, which are shown in Figure 6.3 and presented below:

Variant 1: The rolling bearing is mounted to insulating PVC parts. It can be considered as the case, where the environmental parts have minimal influence on the rolling bearing capacitance.

Variant 2: The rolling bearing is mounted to steel parts. It is the reference variant of this work. This variant is also used in other investigations and for the validation of the combined calculation method.

Variant 3: The rolling bearing is mounted to modified steel parts. The shaft has been modified in order to provide additional electrical capacitance by its reduced distance from the stationary steel parts.

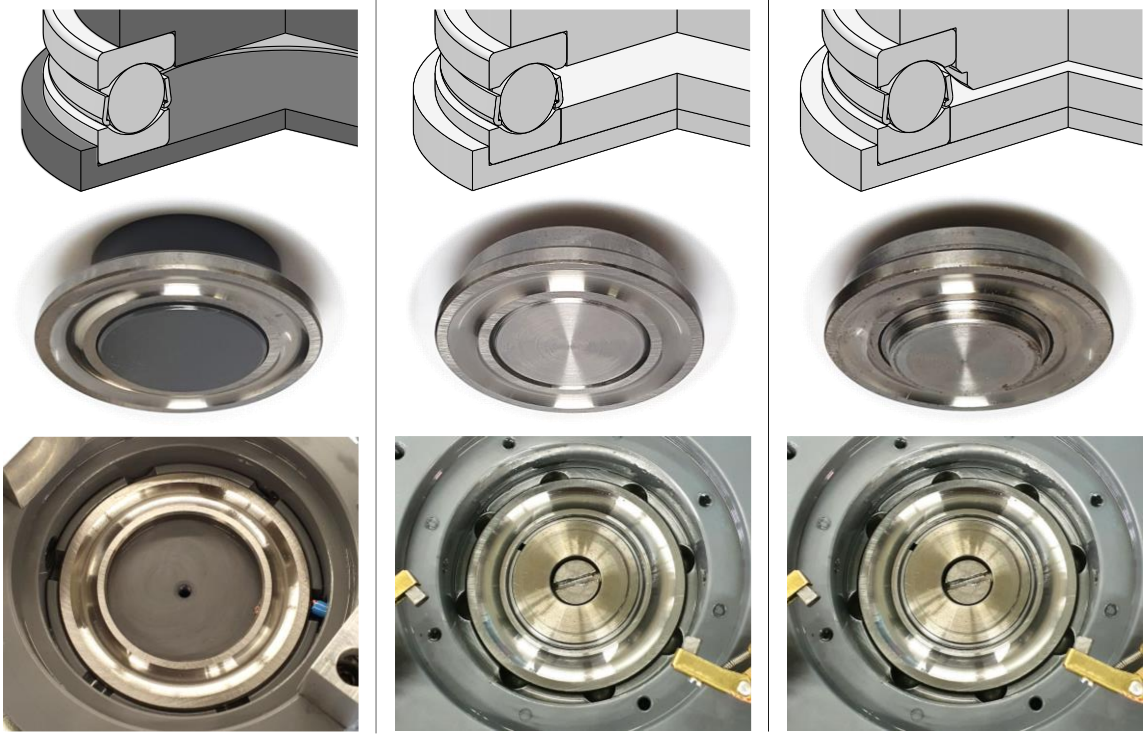

Variant 1: Rolling bearing with PVC connecting parts

Variant 2: Rolling bearing with steel connecting parts

Variant 3: Rolling bearing with modified steel connecting parts

Figure 6.3: Design variants of the GESA cell for the investigation of the rolling element independent capacitances

The relationship between the number of rolling elements and the measured rolling bearing capacitance was investigated for each variant of the GESA cell. During the measurements, the rotational speed of the rolling bearing was 1000 min^{-1}, the operating temperature was adjusted to 40 °C and the GESA cell was fully flooded with the test oil. The investigations were carried out with 100 N and 200 N axial load per rolling element, and with test oil 1 and 2. The average results of the impedance measurements, the fitted trendlines, and the trendline equations are summarised in Figure 6.4 and in Table 6.1.

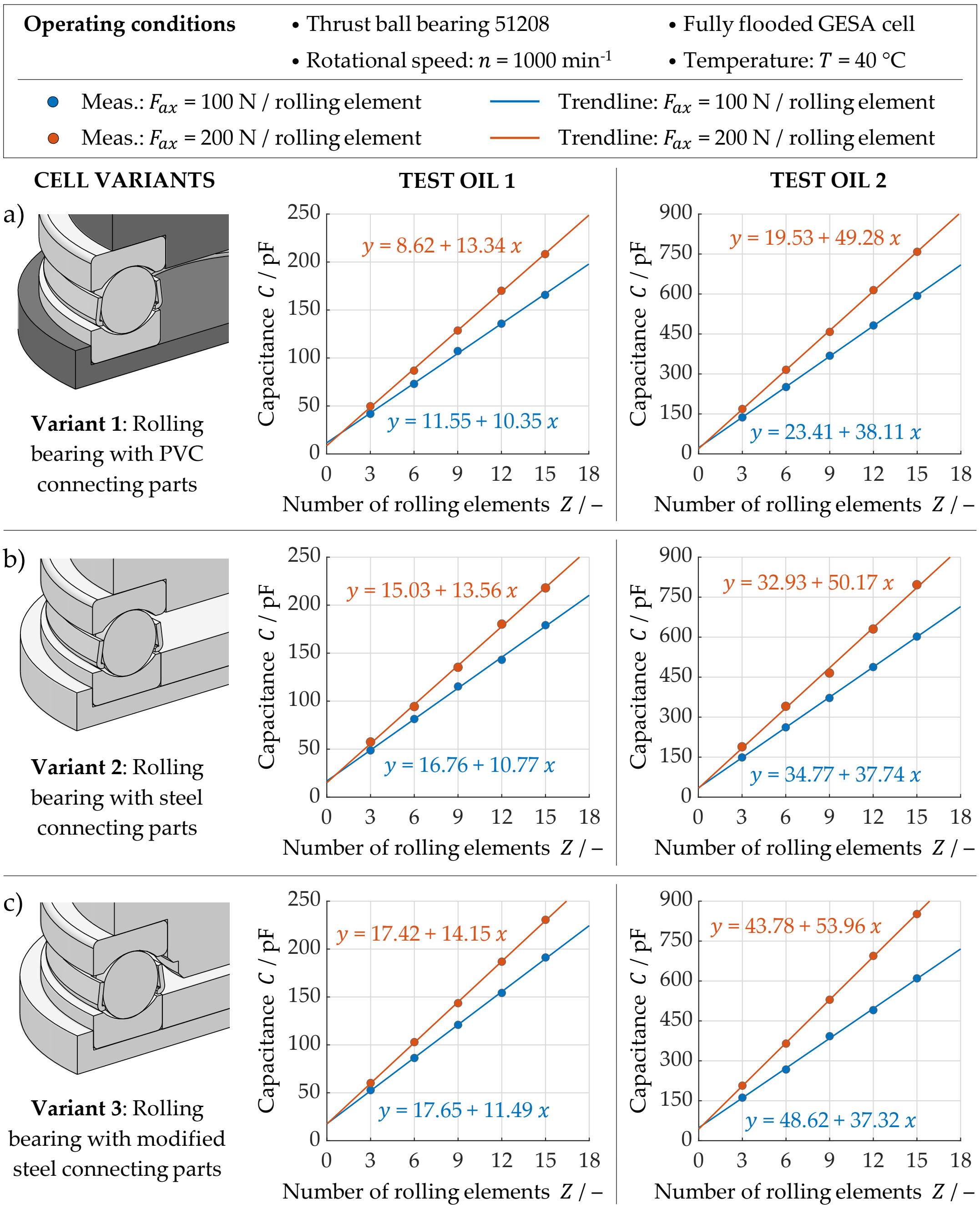

Figure 6.4: Rolling bearing capacitance as the function of the rolling element number for different design variants of the GESA cell: a) Variant 1; b) Variant 2; c) Variant 3

Table 6.1: Trend line equations for the description of the rolling bearing capacitances as the function of the rolling element number in case of different design variants of the GESA cell

CELL VARIANT	**TEST OIL 1**		**TEST OIL 2**	
	100 N / rolling element	200 N / rolling element	100 N / rolling element	200 N / rolling element
Variant 1	$y = 11.55 + 10.35\ x$	$y = 8.62 + 13.34\ x$	$y = 23.41 + 38.11\ x$	$y = 19.53 + 49.28\ x$
Variant 2	$y = 16.76 + 10.77\ x$	$y = 15.03 + 13.56\ x$	$y = 34.77 + 37.74\ x$	$y = 32.93 + 50.17\ x$
Variant 3	$y = 17.65 + 11.49\ x$	$y = 17.42 + 14.15\ x$	$y = 48.62 + 37.32\ x$	$y = 43.78 + 53.96\ x$

Rolling element independent capacitance

Capacitance increase per rolling element

The results show that for a given test oil and cell variant, the trendlines start from nearly the same capacitance value regardless of the applied axial load. This initial capacitance value, i.e., the predicted capacitance of the rolling bearing without rolling elements, can be influenced by the different design variants of the GESA cell. It is shown by the rolling element independent terms of the trendline equations for the different cell variants. In Variant 1, the rings were mounted to insulating PVC parts. Since the rolling bearing without rolling elements works as a capacitor, where the capacitor plates are defined by the rings and the connected conductive components, the effective area of the capacitor plates was the smallest for Variant 1. Accordingly, the rolling element independent capacitance was the lowest in this case. In Variant 2, the rings were mounted to steel parts, which led to larger conductive surfaces and thus to a significant increase of the rolling element independent capacitance. For Variant 3, not only the area of the conductive surfaces was increased by the steel parts, but also the distance between them was reduced due to the modified shaft. In this way, a further increase of the rolling element independent capacitance was obtained. In addition, the results show that, despite the variation of the cell design, the rolling element related capacitances remained nearly the same for a given oil and load, i.e., the different design variants did not considerably influence the capacitance increase per rolling element.

Since the measurements, presented above, cannot be performed with less than three rolling elements, the rolling bearing capacitances for zero rolling element were obtained by the extrapolation of the fitted trendlines. For the targeted investigation of these values, further determination methods were elaborated. First, the developed FEM simulation model was adjusted for this purpose. The investigated cell variants were modelled without rolling elements, and according to the geometry and material of the components. In addition, a supporting frame was constructed for the GESA cell, which can hold the rolling bearing rings and the connected components at a distance corresponding to the size of the rolling elements.

Thus, the rolling elements could be removed for the measurements. During this experiment, the impedance measurements were carried out with stationary rings, the oil temperature was adjusted to 40 °C, and the cell was fully flooded with the test oil. As a result, for the investigation of the rolling element independent capacitance of the rolling bearing, the following methods were applied: the modified FEM simulation method (without modelling the rolling elements); the impedance measurements with stationary rings and without rolling elements; and the trendline equation based on the impedance measurements with the variation of the rolling element number for 100 N and 200 N axial load per rolling element. The results obtained by these methods are presented in Figure 6.5 for the different cell variants, and with both investigated lubricants.

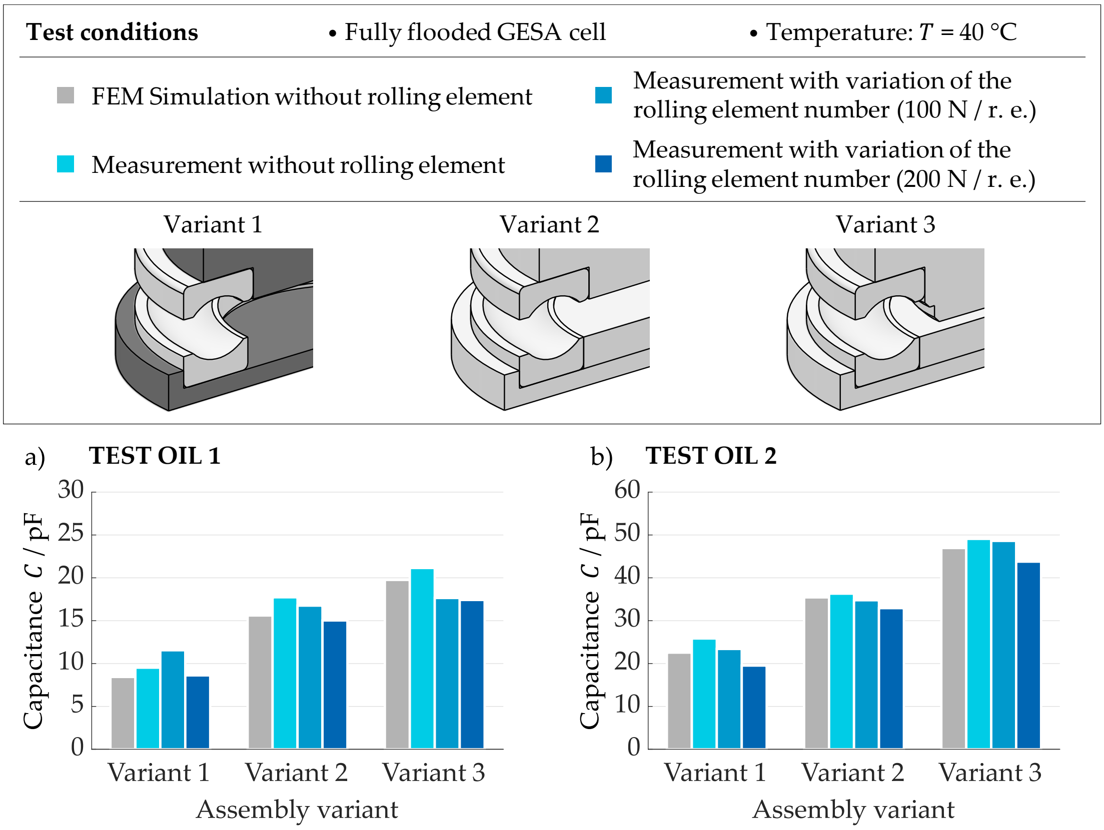

Figure 6.5: Investigation of rolling element independent capacitance of the rolling bearing in case of different cell variants: a) Test oil 1; b) Test oil 2

In case of Variant 1, where the rolling bearing rings were mounted to insulating parts, the lowest capacitance values were obtained. For Variant 2, due to the use of conductive components, higher capacitance values were achieved. By the modified shaft, i.e., by reducing the distance between the conductive elements, an additional increase of the capacitance can be observed in case of Variant 3. Comparing Variant 1 with Variant 3, the rolling element independent capacitances nearly doubled for both test oils based on the average results of the different investigation methods. In addition, the results provided by the different investigation methods show a good agreement.

Based on the results of the investigations presented in this chapter, the following observations can be made. The rolling element independent capacitances can be influenced by the components connected to the rolling bearing. Accordingly, the rolling element independent capacitances can be divided into two groups, the capacitance of the rings and the capacitance of the connected components, i.e., the capacitance of the environmental parts (Figure 6.6). For the correct modelling of the rolling bearing, the capacitances of the environmental parts must be identified and separated from the capacitances of the rolling bearing. In this interpretation, the investigations performed with Variant 1 of the GESA cell were used to estimate the capacitance of the rings, while the capacitance increase caused by the Variant 2 and 3 can be considered as the capacitances that were generated by the environmental parts.

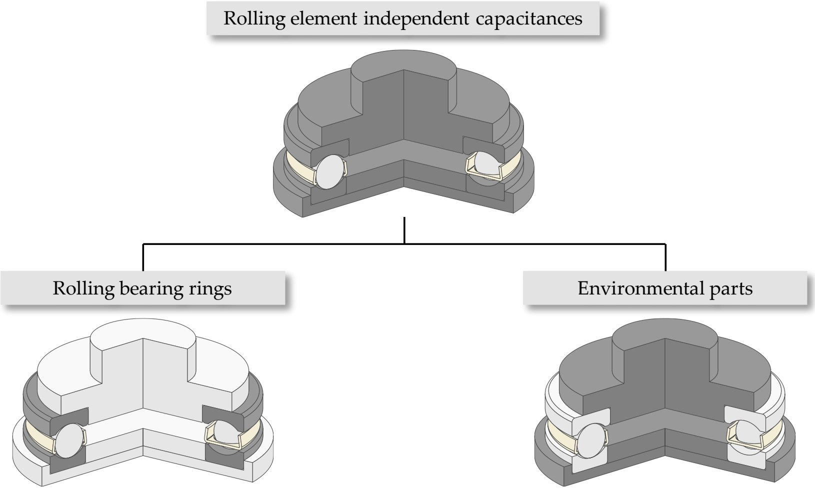

Figure 6.6: Categorisation of the rolling element independent capacitances of the rolling bearing

The results have also shown that the impedance measurements with stationary components can be a suitable method for the investigation of the rolling bearing capacitances in specific cases. Furthermore, based on the results of the FEM simulations (considering the modelling process with and without rolling elements), the definition of the rolling element independent capacitances needs to be specified. The presence of the rolling elements reduces the volume of the dielectric between the rings and the connected conductive parts, and thus influences their capacitance. Consequently, the term "rolling element independent capacitances" is limited to the capacitance values determined for zero rolling element.

6.1.3 Rolling element related capacitances

For the investigation of rolling element related capacitances, two different experiments were performed. In the first experiment, the capacitance of the rolling bearing was examined as the function of the rolling element number in case of three different oil quantities, i.e., three different oil levels in the GESA cell. The impedance measurements were carried out using the test oil 1 at 1000 min^{-1} rotational speed, at an operating temperature of 40 °C and with axial loads of 100 N and 200 N per rolling element. The investigated oil quantities were minimum oil quantity (which is necessary for the stable operation of the rolling bearing), half flooded cell (i.e., the cell was filled up until the half of the rolling elements with the test oil) and fully flooded cell. In Figure 6.7, the average results of the impedance measurements, the fitted trendlines describing the relationship between the number of rolling elements and the rolling bearing capacitance, and the trendline equations are presented.

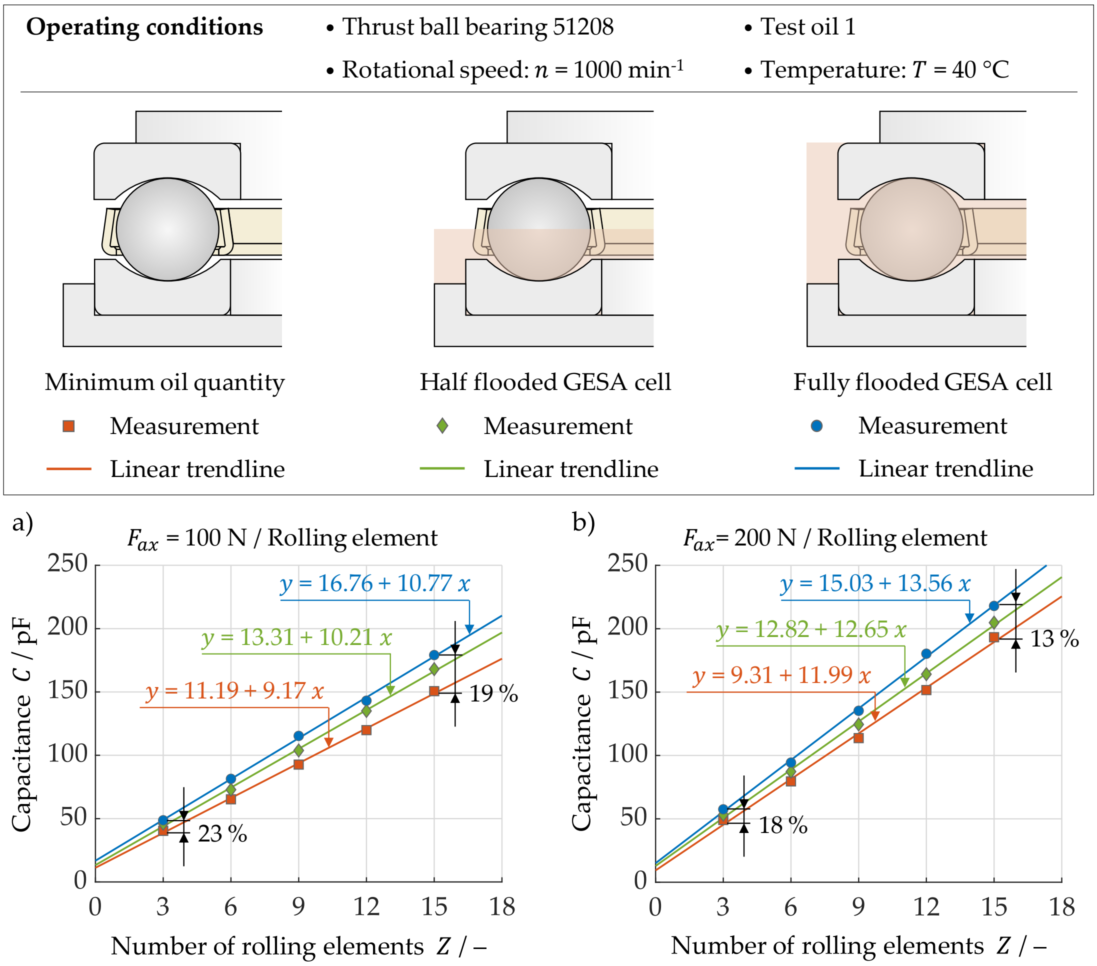

Figure 6.7: Investigation of the rolling bearing capacitance as the function of the rolling element number in case of different oil quantities

The trendlines and their equations show that the increase of the oil quantity leads to an increase in both the rolling element independent and dependent capacitances of the rolling bearing. The change in the rolling element independent capacitances can be explained by the change in the composition of the dielectric between the conductive components. As the relative permittivity of the lubricant is greater than the relative permittivity of the air, replacing the air with lubricant in the cell leads to an increase in the rolling element independent term of the trend line equations. In parallel, the rolling element dependent capacitance also increases with the increasing oil quantity. Since the calculated lubricant film thickness is the same for the different oil quantities (assuming that there is sufficient amount of oil in the rolling contact for all cases), the different steepness of the trendlines can only be obtained by additional capacitance sources related to the rolling element. These additional capacitances can be explained by the gaps in the surrounding of the rolling contacts, which are influenced by the oil quantity in the cell. Accordingly, the rolling element dependent capacitances can be divided into two groups, the contact capacitances, and the capacitances of the surrounding of the contact. The diagrams also show that the rolling bearing capacitances obtained by the measurements with fully flooded cell are significantly higher (up to 23 %) than the measurement results with a minimum amount of oil. This difference is meaningful, because it results from such capacitance sources of the rolling bearing that are not taken into account by the state-of-the-art calculation methods (such as the capacitance calculation with correction factor). To model the rolling bearing capacitances in case of different oil quantities, the combined simulation method, presented in Chapter 5, can be applied. The comparison of the simulation results with the measurement results for different oil quantities is described in Chapter 6.2.4.

To examine the rolling element related capacitances, a further experiment was also carried out. The rolling bearing capacitance was measured as the function of the rolling element number in case of stationary components, where the surfaces of the rolling bearing rings were covered with insulating foils. The impedance measurements were carried out at a temperature of 40 °C, with an axial load of 10 N per rolling element, and in case of air, test oil 1 and test oil 2 as dielectric between the conductive components. The results of the impedance measurements, the fitted trendlines and the trendline equations are presented in Figure 6.8. (Since the described experiment was performed in the presence of an insulating foil in the contact, the presented values are not comparable with the results of other investigations described in this work. They serve to demonstrate the existence and importance of different capacitance sources of the rolling bearing.)

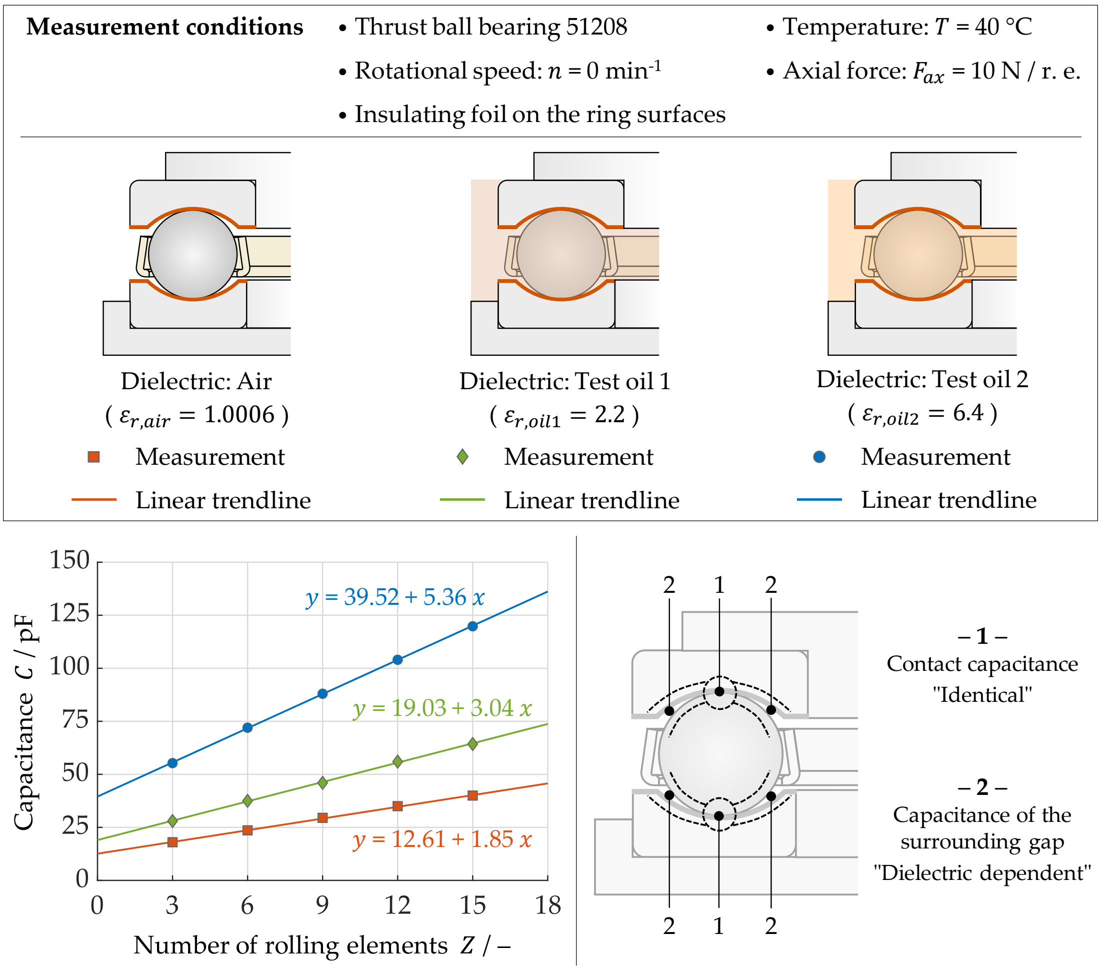

Figure 6.8: Investigation of the rolling bearing capacitance as the function of the rolling element number with different dielectrics between the stationary components covered with insulating foil

Since the stationary rolling elements are in direct contact with the insulating foil, and the axial load is adjusted in accordance with the number of the rolling elements, the same contact conditions (i.e., contact area, deformation, foil thickness) and therefore identical contact capacitances can be assumed for all impedance measurements regardless of the applied dielectric. Consequently, the differences in the slope of the fitted trendlines, i.e., the differences in the rolling element dependent capacitances, result solely from the surrounding of the contacts, which were filled with different dielectrics. The experiment thus confirmed that the rolling element related capacitances can be divided into two groups, the contact capacitances, and the capacitances of the surrounding of the contact, which are illustrated in Figure 6.9.

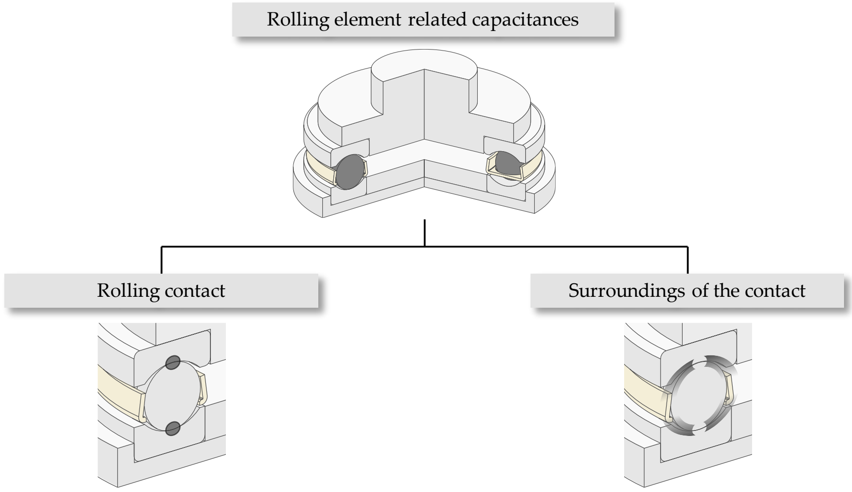

Figure 6.9: Categorisation of the rolling element related capacitances of the rolling bearing

6.1.4 Capacitance structure of rolling bearings

As the result of the investigations, presented in the previous chapters, the different capacitance sources of the rolling bearings have been identified. By considering the capacitance sources systematically, the capacitance structure of the rolling bearings is outlined, as presented in Figure 6.10. First, it is necessary to distinguish the capacitance of the rolling bearing and the capacitance of the connected environmental parts, whose design is independent of the rolling bearing. Although the capacitance of the environmental components is always present in the measured values, this capacitance source is often not considered in the modelling. The capacitance of the rolling bearing can be divided into the rolling element related capacitances and the capacitance of the rolling bearing rings. The capacitance of the rings is usually negligibly small, but for the completeness of the capacitance structure, it can be defined as a separate source. The rolling element related capacitances can be further divided into the contact capacitances and the capacitances of the surrounding of the contact. Although it is difficult to clearly distinguish these two regions, it is beneficial to consider them separately because of their different calculation methods. Figure 6.10 also shows the simulation methods used in this work for the modelling of the different capacitance sources. Accordingly, the capacitances of the environmental parts, the rolling bearing rings, and the surrounding of the contact are calculated by the electrical FEM simulation model, while the capacitance of the rolling contact is determined by the electrically extended EHL simulation. With the help of the electrically extended EHL simulation, the contact capacitances can be further divided into the capacitance of the inlet region, the hertzian contact region, and the outlet region. As a result, the capacitance structure of the investigated rolling bearing is complete. The significance of the presented capacitance sources compared to the total rolling bearing capacitance is investigated after the validation of the combined simulation method in Chapter 6.2.5.

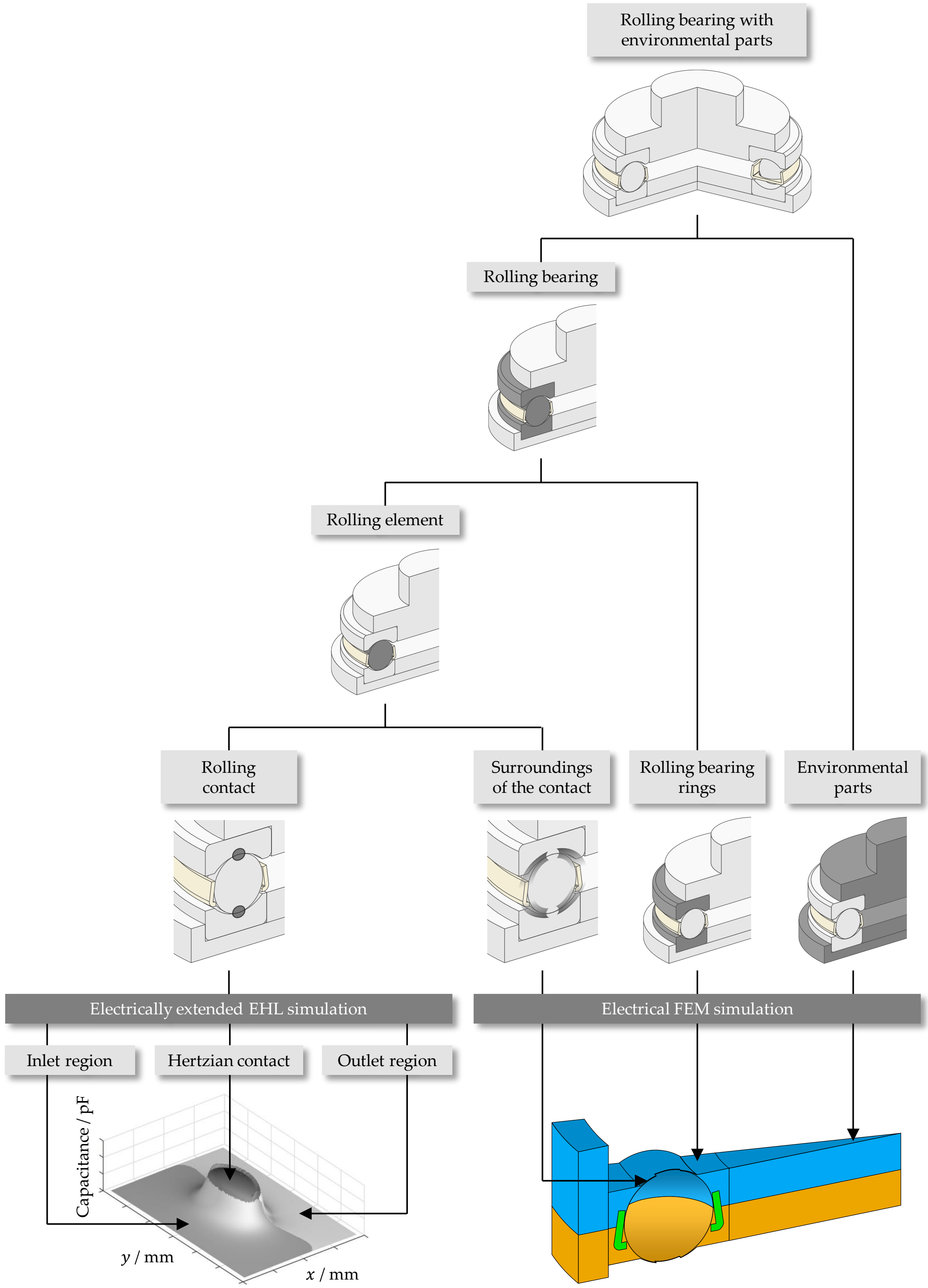

Figure 6.10: Capacitance sources of the investigated rolling bearing with their modelling possibilities

6.2 Validation of the combined simulation method

The validation of the combined simulation method and the evaluation of the experimental and simulation results are discussed in this chapter. For the investigations, the thrust ball bearing 51208 was used with plastic cage and with both test oils. The rolling bearing capacitances were determined by the presented measurement methods (impedance measurement and charging curve measurement), the correction factor calculation method, and the combined simulation method for every examined operating condition. Consequently, both the different measurement methods and the different calculation methods can be compared and evaluated. In case of the correction factor calculation method, the total rolling bearing capacitances were determined based on the equivalent circuit diagram of the rolling bearing with insulating cage (Eq. (2.59)) and applying the correction factor of Bechev [Bec20]:

$$k_{c\,[\mathrm{Bec20}]}(h_0) = 3 \cdot 10^6 \cdot h_0 + 1.3 \tag{6.2}$$

The hertzian contact capacitance was determined analytically, using the central lubricant film thickness and the area of the hertzian contact ellipse based on the formulae of Hamrock and Dowson, and Hertz. To show the importance of the non-contact regions of the rolling bearing, the results of the combined simulation method are represented in the following both with and without the capacitances obtained by the FEM simulations. The impedance- and charging curve measurement methods are represented with the average result of five measurements and the corresponding standard deviations. During the investigations, the influence of individual operating parameters was first examined, i.e., one selected operating parameter was varied while the other operating parameters were kept constant. With this strategy the influence of the axial load, the rotational speed, the temperature and the oil quantity on the rolling bearing capacitance was examined. Subsequently, further data were collected from the investigation of a full-factorial combination of the operating parameters to provide the basis for a general analysis of the calculation methods and their applicability. Finally, the capacitance sources of the rolling bearing were analysed based on the collected data, i.e., their significance compared to the total rolling bearing capacitance.

6.2.1 Influence of the axial load

In this chapter, the influence of the axial load on the rolling bearing capacitance, and the description of this influence by the different calculation methods are investigated. For this purpose, capacitance measurements were carried out with constant rotational speed, temperature, and oil quantity, while the axial load was varied between 250 and 4000 N. The measurement results and the corresponding results of the calculation methods are shown in Figure 6.11.

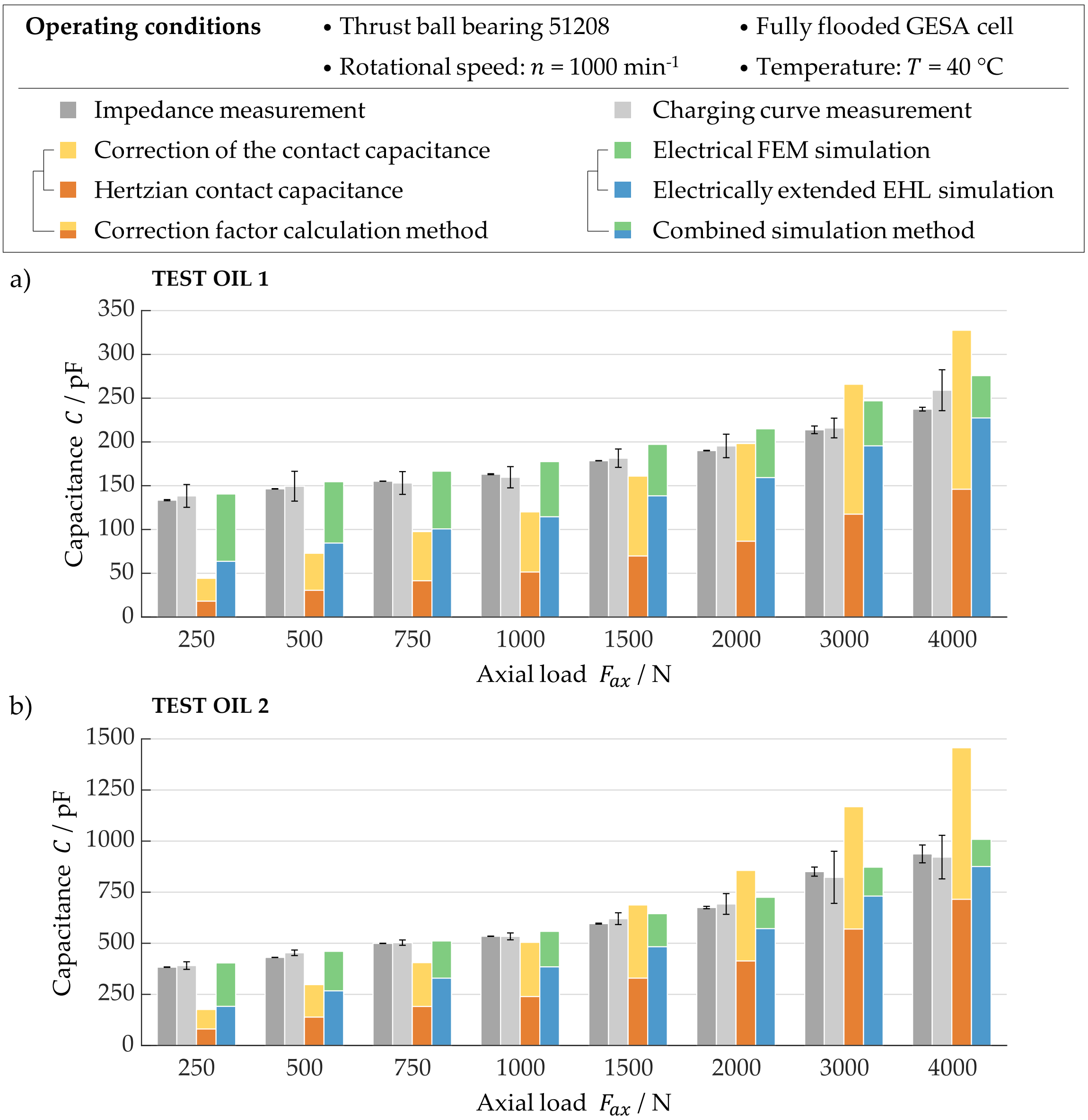

Figure 6.11: Comparison of the measurement and calculation results under the variation of the axial load: a) Test oil 1; b) Test oil 2

In general, the results of the impedance measurements and the charging curve measurements show a good agreement, although their standard deviations differ significantly. The charging curve measurements lead to larger standard deviations, which increase with decreasing lubricant film thickness, i.e., with increasing axial load. By the decreasing lubricating film thickness, the asperity peaks of the surfaces are more frequently in contact, or the insulating ability of the oil film is more frequently exceeded by the measurement voltage. It leads to disturbances during the measurements and thus to a higher standard deviation of the evaluated results. The charging curve measurement is more sensitive to the mentioned disturbances. Between the results of the calculation methods, significant differences can be observed. While the combined simulation method leads to a good approximation of the measurement results in both magnitude and course, the applicability range of the correction factor calculation method is limited. The measurement results are underestimated at low loads and overestimated at high loads by the correction factor calculation method within the range of the considered operating conditions. The results of the combined simulation method show that a significant part of the rolling bearing capacitances is provided by the non-contact regions of the rolling bearing, which are modelled by the FEM simulation. This part increases in both magnitude and percentage as the thickness of the lubricant film increases, i.e., as the axial load decreases. In addition, with decreasing lubricant film thickness the accuracy of the combined simulation method slightly decreases. The large difference between the capacitance values provided by the different test oils can be explained by their different rheological and electrical properties.

6.2.2 Influence of the rotational speed

To investigate the influence of the rotational speed on the rolling bearing capacitance, the calculations and the measurements were carried out with constant axial load, temperature, and oil quantity, while the rotational speed was varied between 500 and 3000 min^{-1}. The measurement results and the results of the calculation methods are presented in Figure 6.12. Both calculation methods provide a good approximation of the measured values over the considered range of the operating parameters, although they show slight differences in their trends. As in the previous section, the results of the measurement methods show a good agreement, and their standard deviations differ significantly. Especially in case of the charging curve measurements, the standard deviations are larger and more sensitive to changes in the lubricant film thickness. Based on the results of the combined simulation method, the non-contact regions still provide a considerable part of the total rolling bearing capacitance.

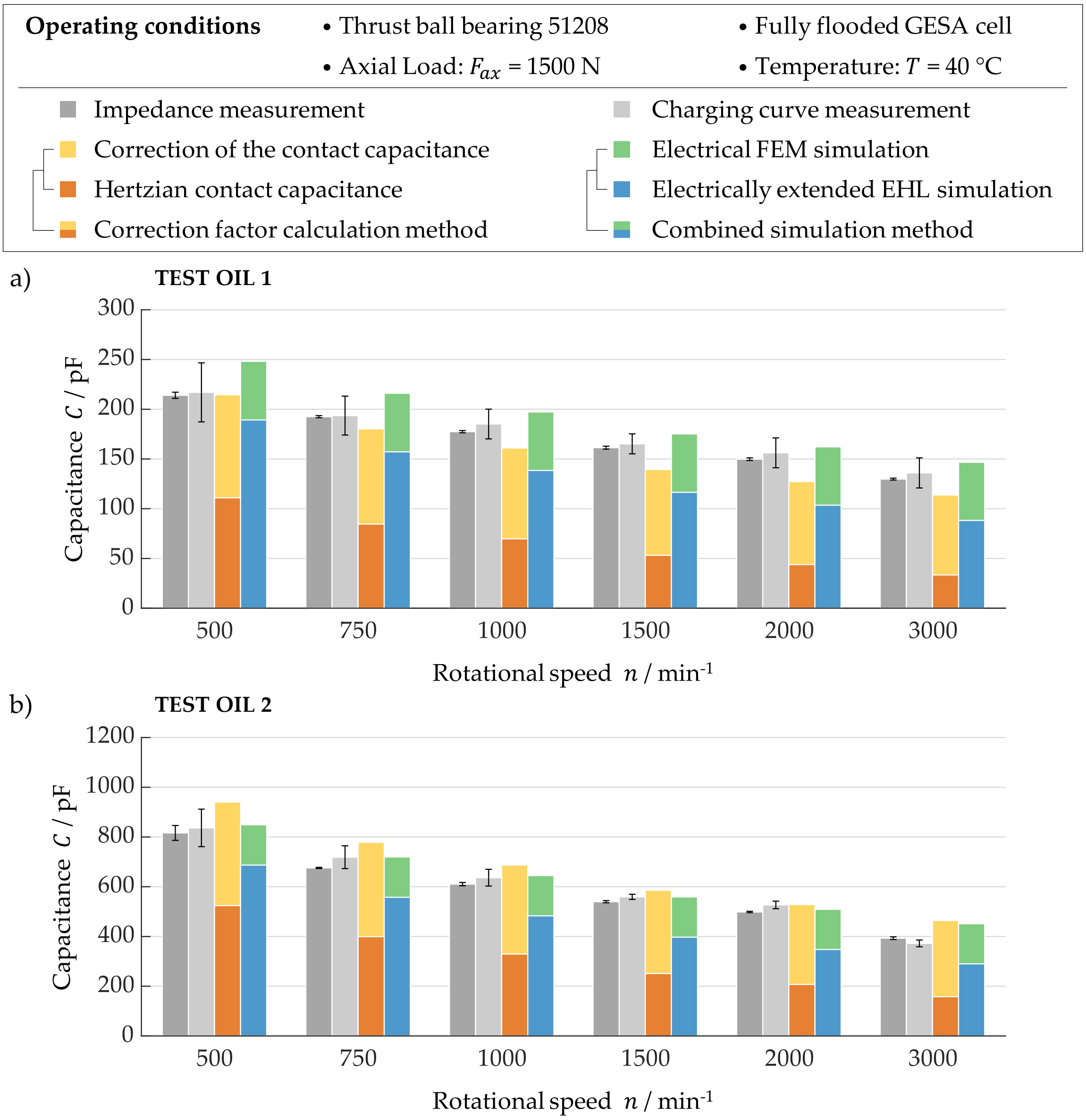

Figure 6.12: Comparison of the measurement and calculation results under the variation of the rotational speed: a) Test oil 1; b) Test oil 2

6.2.3 Influence of the temperature

The effect of temperature on the rolling bearing capacitance was examined by varying its value between 20 and 60 °C, while the other operating conditions were kept constant. The corresponding measurements and the calculations were carried out in case of two different axial loads (750 N and 1500 N) for both test oils. The results of the investigations are summarised in Figure 6.13.

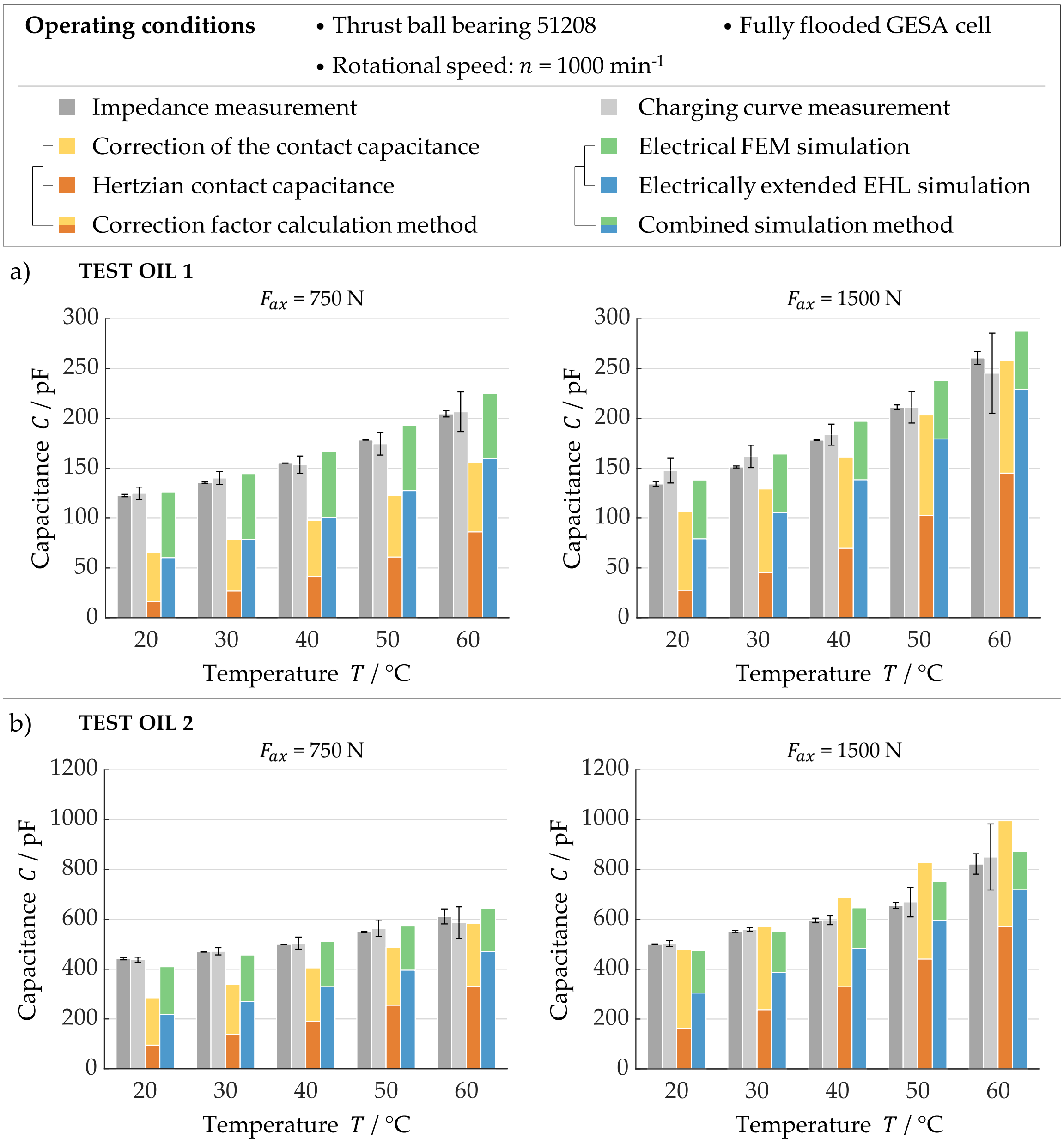

Figure 6.13: Comparison of the measurement and calculation results under the variation of the temperature: a) Test oil 1; b) Test oil 2

The results of the combined simulation method can describe and follow the course of the measured rolling bearing capacitances for the investigated cases. As observed earlier, with decreasing lubricant film thickness (in this case by increasing temperature), the results of the combined simulation method show a slightly increasing difference compared to the measured values. In parallel, the standard deviations of the measured results increase due to the increasing frequency of the asperity contacts. In contrast with the combined simulations method, the calculations with correction factor cannot approximate the measured values sufficiently in all investigated cases, and their results follow different trends. This suggests that the range of applicability of the applied correction factor calculation method is more limited compared to the combined simulation method.

6.2.4 Influence of the oil quantity

To investigate the influence of oil quantity on the rolling bearing capacitance, measurements and calculations were performed with three different oil quantities, while the other operating parameters were kept constant. The investigations were carried out with minimum oil quantity (which is necessary for the stable operation of the rolling bearing), with half flooded GESA cell (where the cell is filled up to the middle of the rolling element with the test oil) and with fully flooded GESA cell. The results of the investigations are summarised in Figure 6.14.

Since the purpose of the correction factor is to describe the ratio between the total capacitance of the contact and the capacitance of the hertzian contact region, this calculation method (without taking additional capacitances into account) cannot consider the influence of the oil quantity, i.e., it provides the same capacitance values independent of the oil level in the GESA cell. In contrast, the combined simulation method can take these influences into account. While the electrically extended EHL simulations estimate sufficient amount of oil in the rolling contact for the development of the lubricant film regardless of its environment, the FEM simulation can model the quantity and distribution of the oil in the GESA cell. It can be observed that for large rolling bearing capacitances, the influence of the oil quantity is smaller, and the capacitances of the non-contact regions are less significant. However, for higher lubricant film thicknesses (resulting from lower axial loads), the capacitance of the non-contact regions and thus the results of the FEM simulation become more important. Filling the GESA cell completely with the test oil leads to a capacitance increase of more than 25 % compared to the values measured with minimum oil quantity in case of the lowest axial load. The capacitances provided by the FEM simulation vary over a wide range, from a minimum of 7 % up to a maximum of 39 % of the total rolling bearing capacitance for the investigated cases. It shows that the non-contact capacitances of the rolling bearings can reach significant values that cannot be taken into account by the state-of-the-art correction factor calculation methods. Furthermore, the results of the applied correction factor calculation method can significantly under- or overestimate the total rolling bearing capacitances in certain cases, regardless of the oil level in the cell.

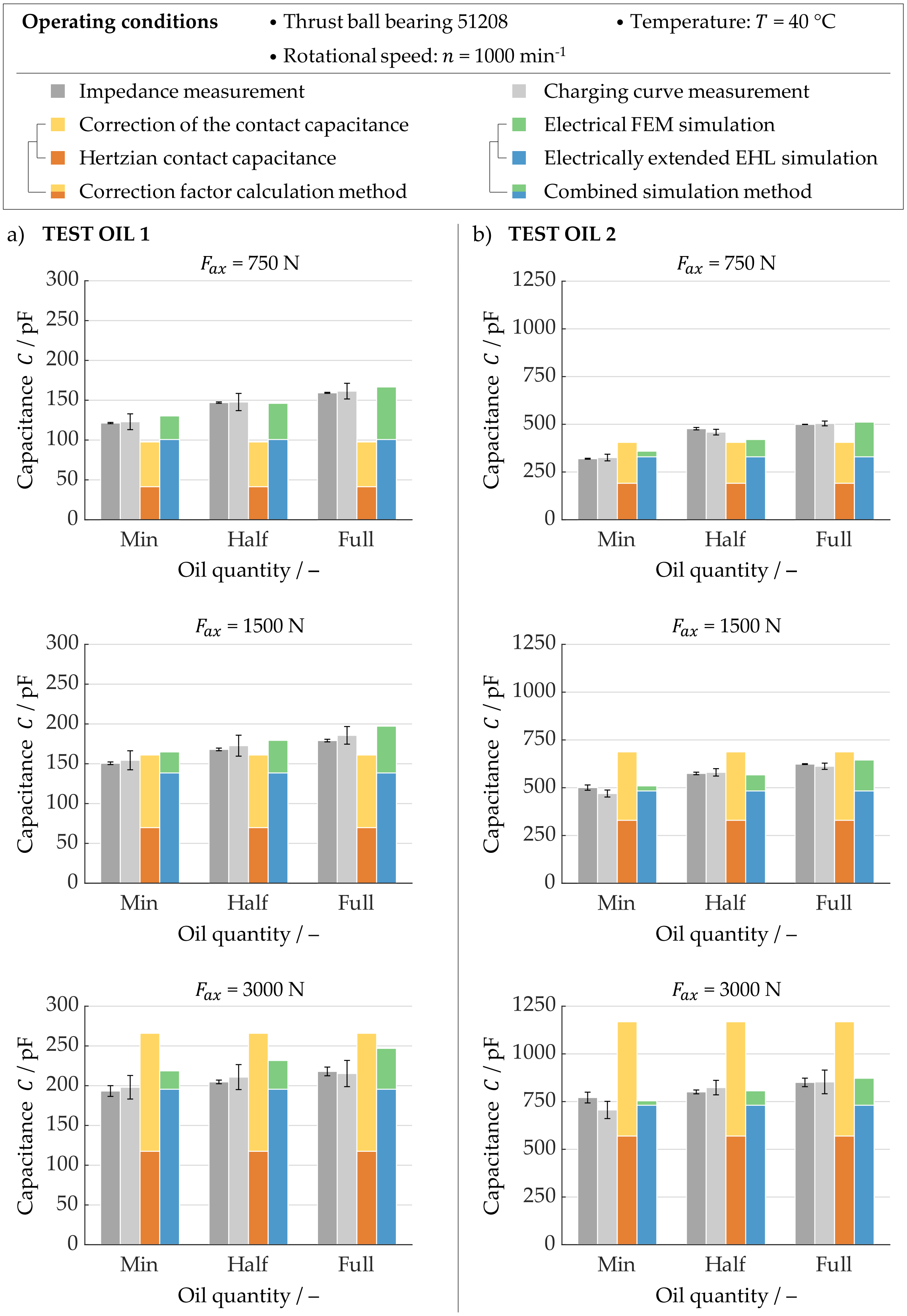

Figure 6.14: Comparison of the measurement and calculation results under the variation of the oil quantity: a) Test oil 1; b) Test oil 2

6.2.5 Validation and evaluation of the results

After examining the influence of the operating parameters, the measured and calculated rolling bearing capacitances are investigated in general. For this purpose, measurements and calculations were carried out at all operating points defined by the full-factorial combinations of the operating parameters summarised in Table 6.2. These investigations were performed with fully flooded GESA cell in case of both test oils. The increased number of the examined operating points helps in the generalised evaluation of the calculation methods, and in the analysis of the capacitance sources of the rolling bearing.

Table 6.2: Values of the operating parameters for their full-factorial investigation

Rotational speed / min^{-1}	**Temperature / °C**	**Axial load / N**
1000	30	500
2000	40	1000
	50	1500
		2000
		3000

The results of the full-factorial investigations are shown in Figure 6.15 for test oil 1 and in Figure 6.16 for test oil 2. Based on the diagrams, the observations made in the previous sections are still valid. The results of the combined simulation method show a good agreement with the measured results. The degree of this agreement slightly decreases with the decreasing lubricant film thickness. In contrast, the correction factor calculation method provides good agreement with the measured values only in a limited range of the operating conditions. Especially at low axial loads, the results of the correction factor calculation method underestimate the measurement results. The two calculation methods show significant differences in their trends. Similar to the results of the previous sections, the significance of the FEM simulation results, and hence the significance of the non-contact capacitances increases as the total rolling bearing capacitance decreases. The two measurement methods show good agreement. In general, the charging curve measurement method has a larger standard deviation and is more sensitive to the decrease in the lubricant film thickness. Accordingly, the impedance measurement is considered as the preferred measurement method for the evaluation of the rolling bearing capacitances.

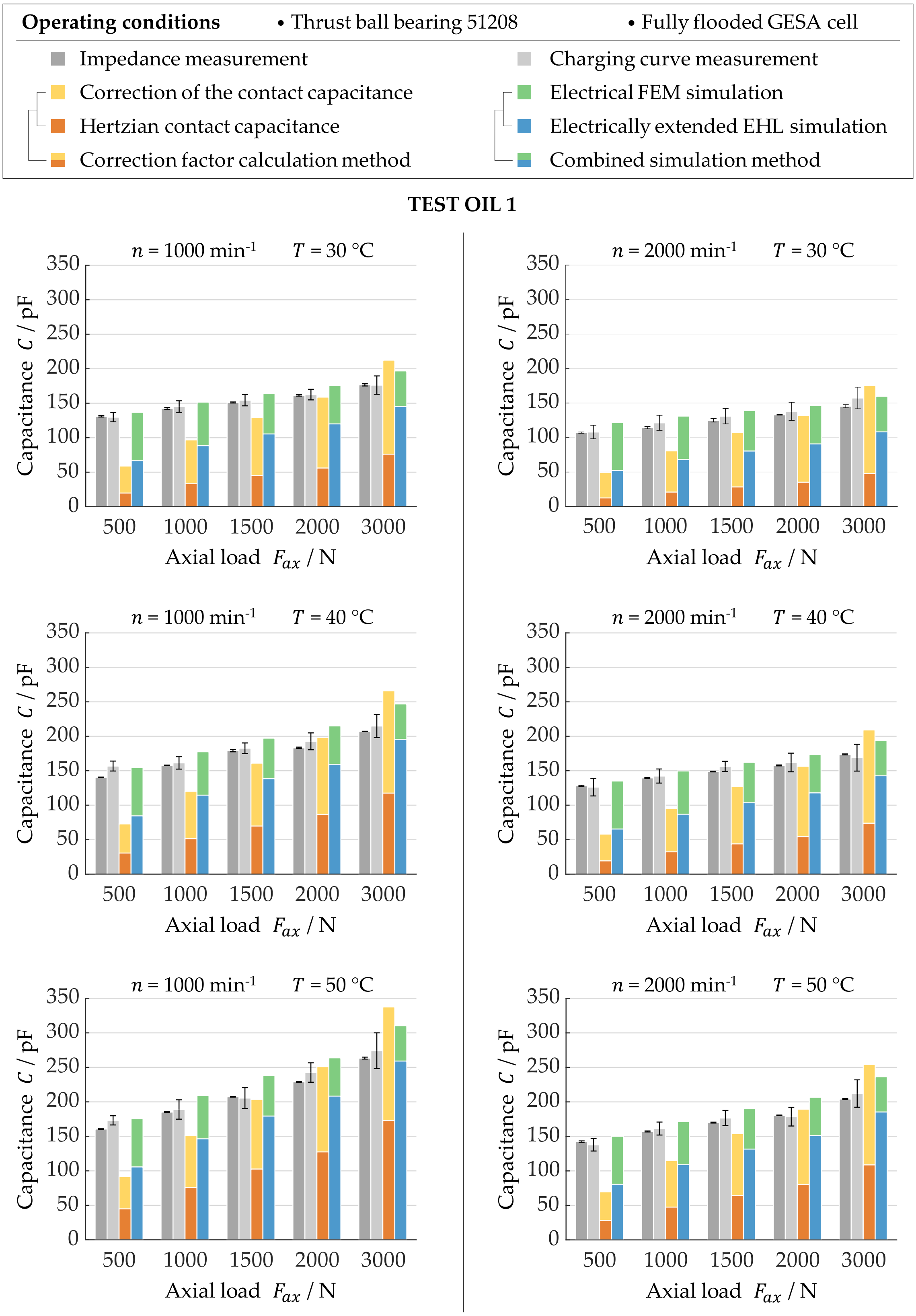

Figure 6.15: Comparison of the measurement and calculation results with a full-factorial combination of the operating parameters in case of the test oil 1

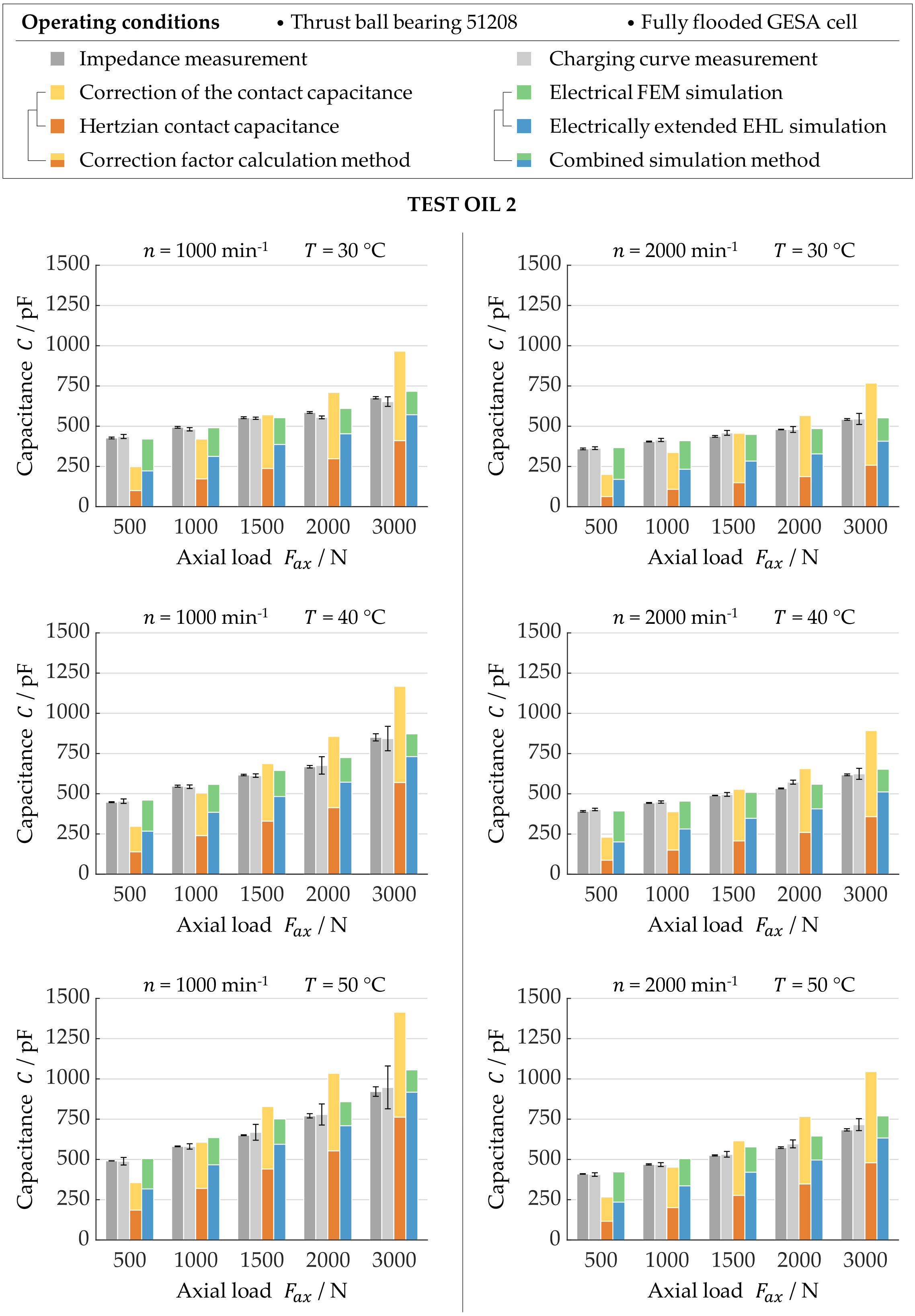

Figure 6.16: Comparison of the measurement and calculation results with a full-factorial combination of the operating parameters in case of the test oil 2

As a final step of the validation studies, all operating points examined in Chapter 6.2 (a total of 49 operating points per lubricant) are summarised and evaluated in the form of scatter plots in Figure 6.17. On the diagrams, the markers represent the examined operating points, where their value on the horizontal axis indicates the corresponding result of the impedance measurement, and their value on the vertical axis indicates the corresponding result of the calculation method. Consequently, the smaller the difference between the measured and calculated values for the considered operating point, the closer the marker is to the diagonal line of the diagram, which represents the perfect agreement of the results. The limits of the range, in which the maximum difference between the results is less than 20 %, are also illustrated. In addition, the markers are coloured in accordance with the corresponding value of the specific lubricant film thickness to support the analysis. The results of the correction factor calculation method (Figure 6.17 a)) and the combined simulation method (Figure 6.17 b)) are evaluated for both test oils.

The results obtained by the combined simulation method and the impedance measurements show a high degree of agreement for both test oils. In case of the examined operating points, the maximum difference between the measured and simulated results is 19 % and the average difference is 10 %, which indicates a high modelling accuracy. The distribution of the markers is similar for the different test oils. It shows that, despite the significantly different composition (mineral oil and synthetic oil) and relative permittivity of the test oils, the simulation method can model the influence of the operating parameters on their rheological and electrical properties. A better agreement can be observed for full film lubrication, and then the differences between the measured and simulated results slightly increase as the specific lubrication film thickness decreases. The results show that the combined simulation method can be applied also to a certain range of the mixed lubrication regime. In contrast, the applicability of the correction factor calculation method is limited to a smaller range of the operating conditions. Based on the examined operating points, the maximum difference between the calculations and the measurements is 67 % and the average difference is 25 %. Furthermore, no correlation can be observed between the degree of agreement of the results and the specific lubricant film thickness values. As mentioned before, the correction factor is intended to describe the ratio between the total capacitance of the contact and the capacitance of the hertzian contact region. Thus, this calculation method takes into account only the capacitances of the contact regions, which can lead to the described deviations from the measured values. In case of other correction functions, the degree of agreement with the measurement results may change, but considerable differences are still expected, since the non-contact capacitances are neglected by this calculation method.

As a result, the presented combined simulation technique serves as a validated calculation method for the determination of rolling bearing capacitances. The method has a wide range of applicability and can take numerous influencing factors into account.

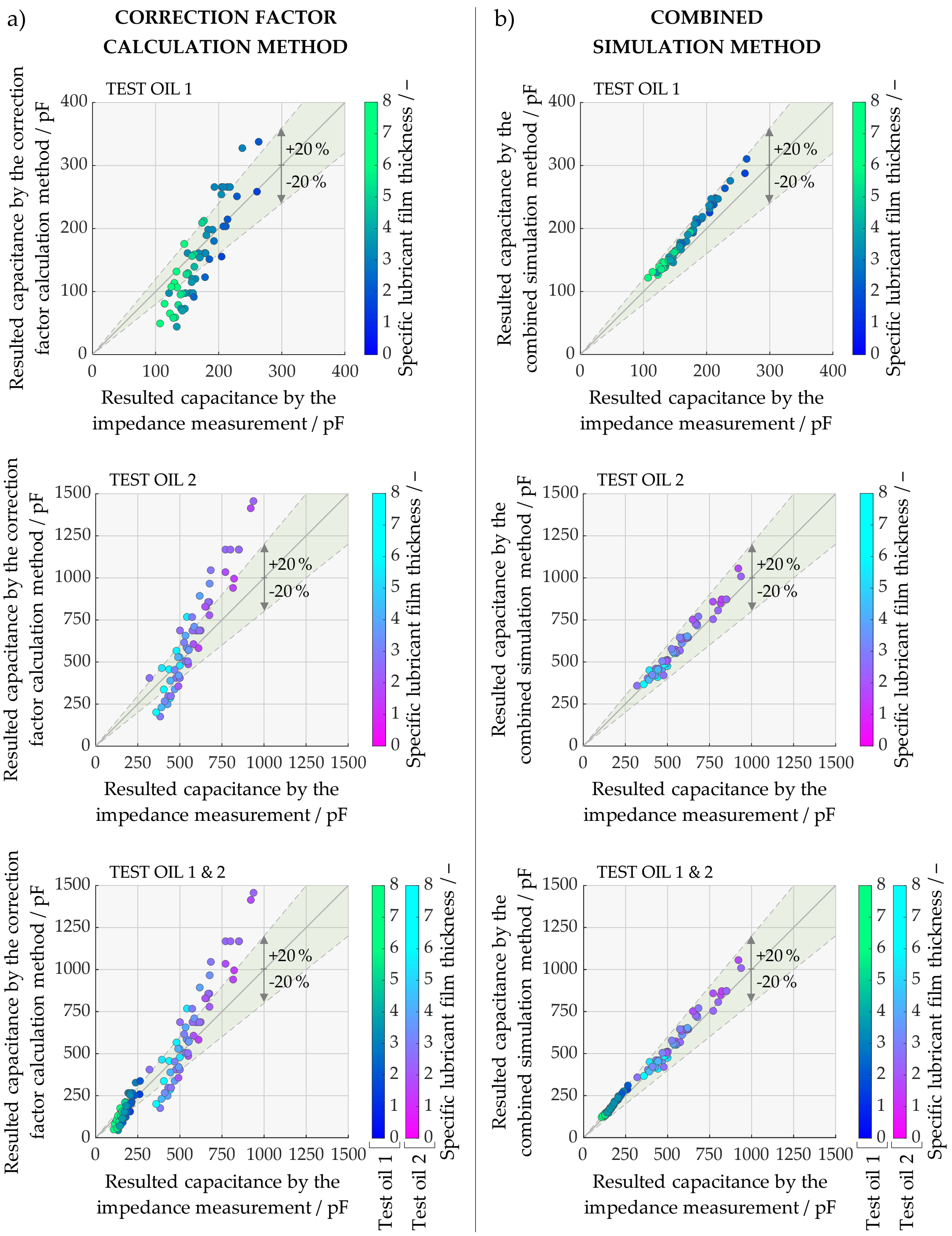

Figure 6.17: Comparison of the calculated results and the results of the impedance measurements for both test oils: a) Correction factor calculation method; b) Combined simulation method

In the following, the evaluation of the results focuses on the analysis of the capacitance sources of the rolling bearing, which were presented in Chapter 6.1.4. First, the significance of the FEM simulation results, i.e., the significance of the non-contact capacitances can be examined with the help of Figure 6.18. The figure represents the equivalent electrical circuit of the rolling bearing segment and the agreement between the simulated and measured values in the cases where the FEM simulation results are neglected (Figure 6.18 a)) and where the FEM simulation results are taken into account (Figure 6.18 b)). The results of the combined simulation method without considering the FEM simulation part significantly underestimate the measured values for high specific lubricant film thickness values. In this case, the average difference between the simulated and measured results is increased to 24 %. Therefore, the consideration of the non-contact capacitances of rolling bearings is particularly important in conditions where the lubricant film thickness is high.

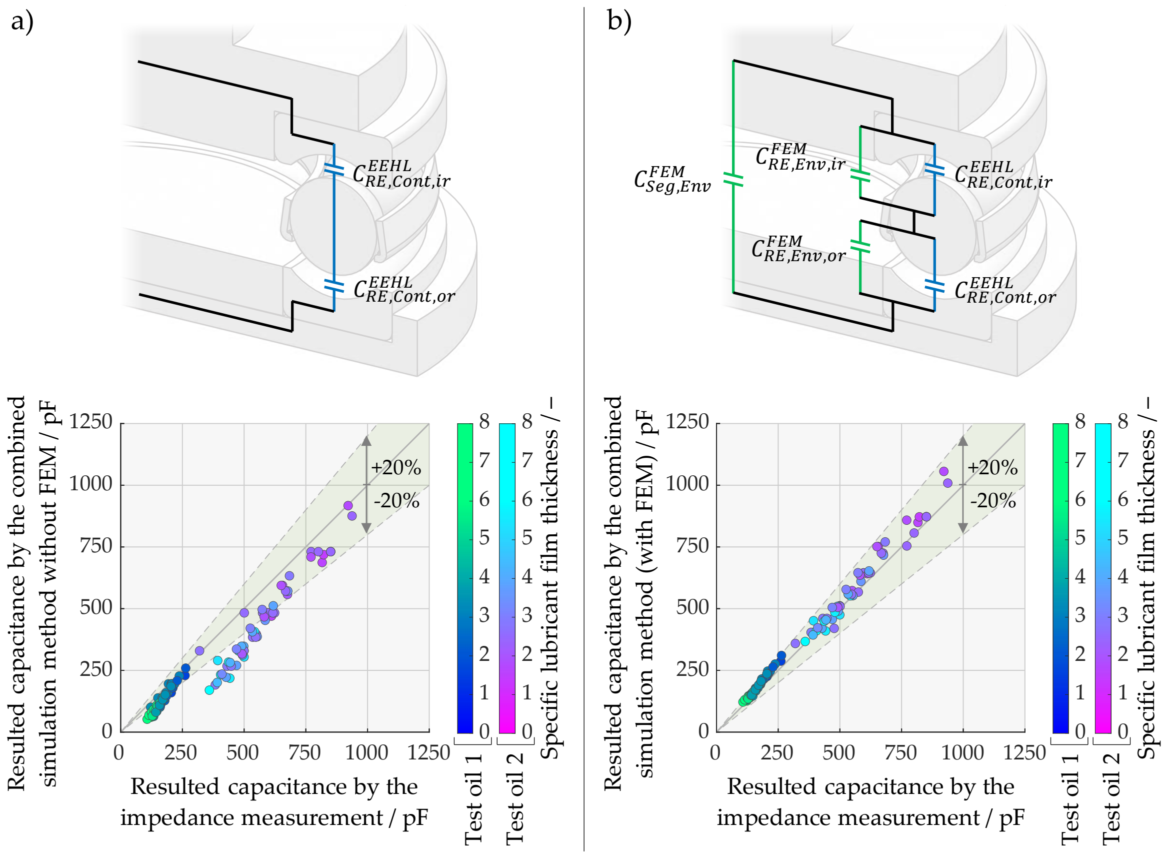

Figure 6.18: Investigation of the significance of the FEM simulation results: a) Calculations without FEM simulation results; b) Calculations with FEM simulation results

The different capacitance sources with their percentage value compared to the total rolling bearing capacitance are shown in Figure 6.19. They are represented by their minimum, maximum, and average values shown during the investigations.

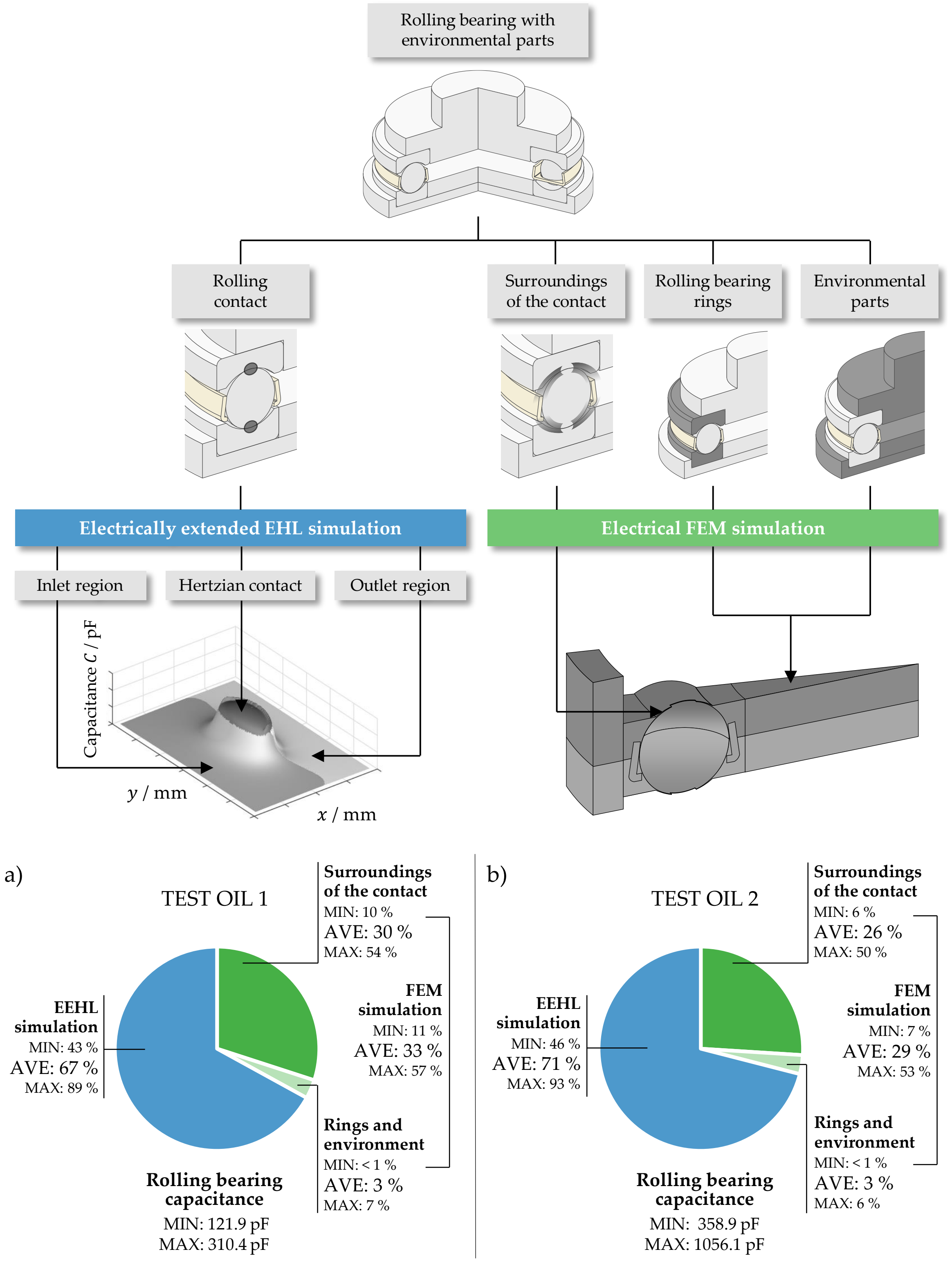

Figure 6.19: The significance of different capacitance sources of the rolling bearing based on the results of the combined simulation method summarised in Figure 6.17: a) Test oil 1; b) Test oil 2

While the magnitude of the results obtained by the two test oils differ significantly, they provide similar percentage values regarding the different capacitance sources. The results of the electrically extended EHL simulation, i.e., the capacitances of the rolling contacts, provide on average approx. 70 % of the total rolling bearing capacitance. In extreme cases, it reaches a minimum of 43 % and a maximum of 93 %. The remaining part of the total bearing capacitance is obtained by the FEM simulation results, i.e., by the capacitances of the non-contact regions. The FEM results are divided into two further parts during this analysis. The capacitance of the rolling bearing rings and the environmental components is on average only 3 % of the total rolling bearing capacitance and in some cases negligible. In contrast, the surroundings of the rolling contact (i.e., the interaction between the rolling element and the surrounding components, excluding the region of the EHL simulation) is responsible for a significant part of the total capacitance, which is on average approx. 30 %. In certain cases, it reaches a maximum of 54 % and a minimum of 6 % of the total rolling bearing capacitance.

The capacitance values of the single rolling contact are similarly evaluated based on the collected data of the performed electrically extended EHL simulations. The results are illustrated in Figure 6.20, where the capacitances provided by the inlet region, outlet region and the hertzian contact region are compared. The distribution of capacitances between these regions shows significant differences in case of the investigated oils. While for test oil 1 an average of 44 % of the total contact capacitance is provided by the hertzian contact region, this value is 57 % for test oil 2. The capacitance of the inlet region is responsible for an average of approx. 35 % of the total contact capacitance in case of both test oils. For test oil 2, the outlet region is less significant, with an average value of 11 %, compared to test oil 1, where this value is 20 %. The difference in the resulted capacitance distributions of the two oils can be explained by their different rheological properties and the different pressure dependence of their relative permittivities. In addition, the definition of the hertzian contact area must be mentioned at this point, since it is intended to describe dry contact between stationary bodies, i.e., it considers only the geometry, material properties and loads of the contacting bodies. Further parameters (e.g., rotational speed, lubricant properties) that influence the capacitance distribution of this region are not considered in the definition of this area.

Based on the evaluation of the results shown in Figure 6.19 and Figure 6.20, it can be observed that the combined simulation method allows a detailed analysis of the bearing capacitances taking into account a wide range of influencing factors. Besides providing results with high accuracy, this calculation method can help to evaluate or extend existing correction functions and allows the development of new capacitance models for different rolling bearings.

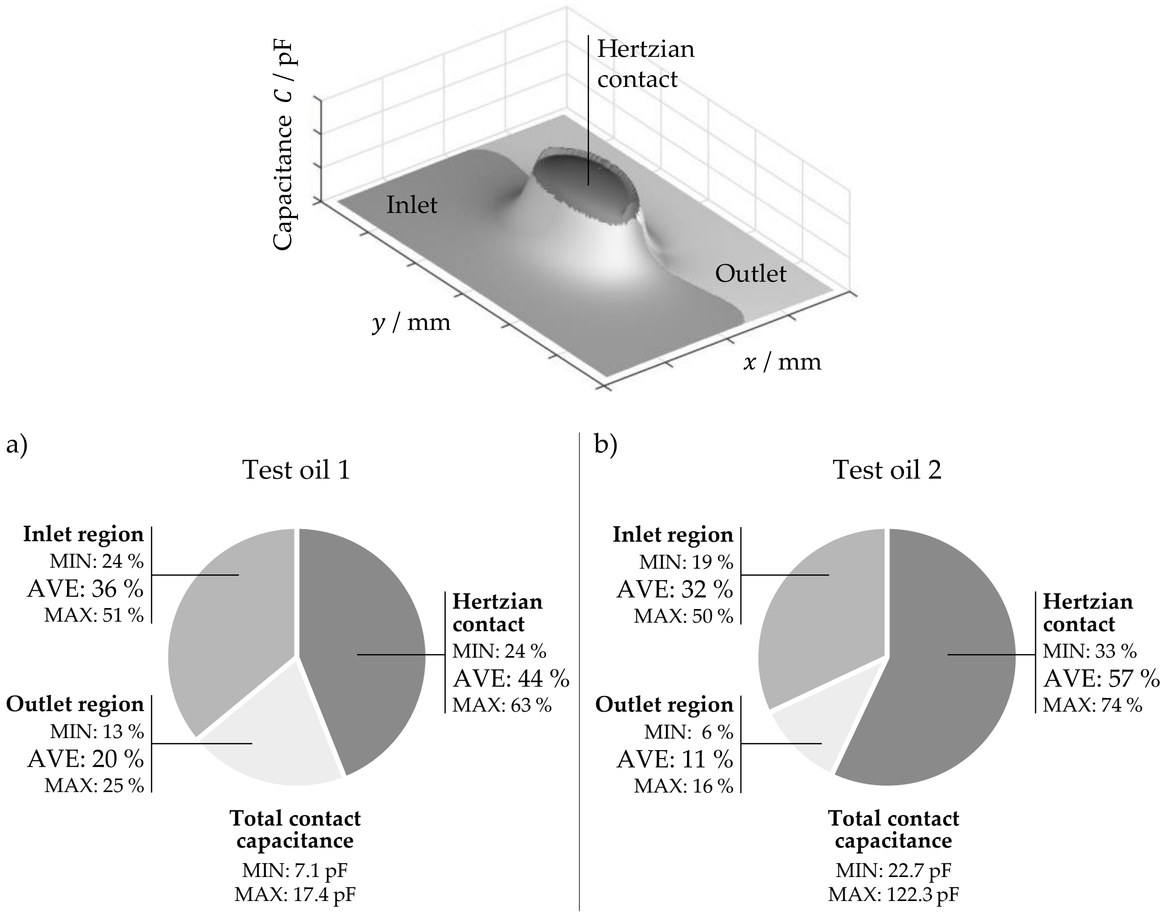

Figure 6.20: The capacitance percentage of the input-, output- and hertzian contact regions with respect to the total contact capacitance based on the results of the electrically extended EHL simulations: a) Test oil 1; b) Test oil 2

6.3 Investigations with axially loaded angular contact ball bearing

In the previous sections, it has been shown that the combined simulation method provides appropriate, validated results for the modelling of the thrust ball bearing 51208. Since in e-mobility applications, radial rolling bearings (e.g., deep groove ball bearings, angular contact ball bearings) are of greater practical importance, it is necessary to investigate the applicability of the simulation model for these bearings. Accordingly, with the help of the presented measurement and calculation methods and the gained experiences regarding the possible capacitance sources of the bearings, the angular contact ball bearing 7206 was investigated. The bearing was chosen because of its suitable dimensions for the installation into the GESA cell and its practical relevance in electric drive units. The data and properties of the rolling bearing are summarised in Appendix A.1. Since the bearings in the GESA cell cannot be loaded radially, the tests are performed under pure axial load, which is equally distributed on the rolling elements. Therefore, in the calculations with the combined simulation method, it was assumed that the rolling bearing segments are identical, similar to the modelling of the thrust ball bearing. However, in contrast to the previous calculations, the two rolling contacts of the segments have different geometries (radii in x- and y-direction), and thus two electrically extended EHL simulations are required to model them. The bearing was tested in vertical arrangement as it is illustrated in Figure 6.21. To determine the input parameters for both the electrically extended EHL simulation and the FEM simulation, the assumption of static equilibrium was applied and the effect of centrifugal forces was neglected. An exception is the contact angle considered in the FEM simulations, which was assumed to be its nominal value.

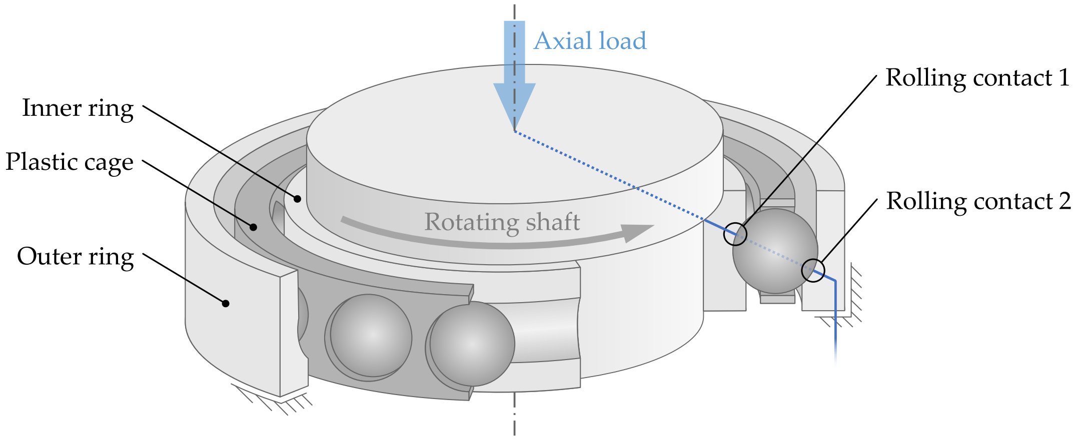

Figure 6.21: Illustration of the test conditions for the axially loaded angular contact ball bearing 7206 with plastic cage

For the calculations with the correction factor calculation method, the correction function of Furtmann was applied, which was developed for axially loaded rolling bearings [Fur17]:

$$k_{c\,[\mathrm{Fur17}]}(h_0) = 3.11 \cdot 10^6 \cdot h_0 + 1.16 \tag{6.3}$$

The investigations were performed with fully flooded GESA cell and with the full-factorial combinations of the operating conditions listed in Table 6.3. The measurement methods are represented by the average result of five measurements and the corresponding standard deviations. For the investigations, test oil 1 was used. The measurement and calculation results are summarised in Figure 6.22.

Table 6.3: Values of the operating parameters for their full-factorial investigation

Rotational speed / min^{-1}	**Temperature / °C**	**Axial load / N**
1000	30	300
2000	40	600
		900
		1200

The results obtained by the angular contact ball bearing show similar trends to the results obtained by the thrust ball bearing. The combined simulation method can still describe the course of the measured rolling bearing capacitances with high accuracy. The applied correction factor calculation method has a limited range of validity, and it underestimates the rolling bearing capacitances in case of low axial loads, i.e., in case of high lubricant film thickness. For the examined operating points, the maximum difference between the results of the impedance measurement and the results of the combined simulation method is 14 % and the average difference is 8 %. For the correction factor calculation method, the maximum difference is 49 % and the average difference is 20 %. Based on the results of the combined simulation method, the ratio of the capacitances provided by the electrically extended EHL simulation and the electrical FEM simulation is comparable to the previously investigated cases with thrust ball bearing. For operating conditions that lead to higher lubricant film thickness in the rolling contact, the FEM simulations provide a higher percentage of the total capacitance. The FEM simulation results, i.e., the capacitances of the non-contact regions, are responsible on average for 36 % of the total rolling bearing capacitance in case of the investigated fully flooded angular contact ball bearing. The presented results show that the combined simulation method was properly extended for the capacitance calculation of axially loaded angular contact ball bearings and suggest that it can be extended analogously to other axially loaded ball bearings.

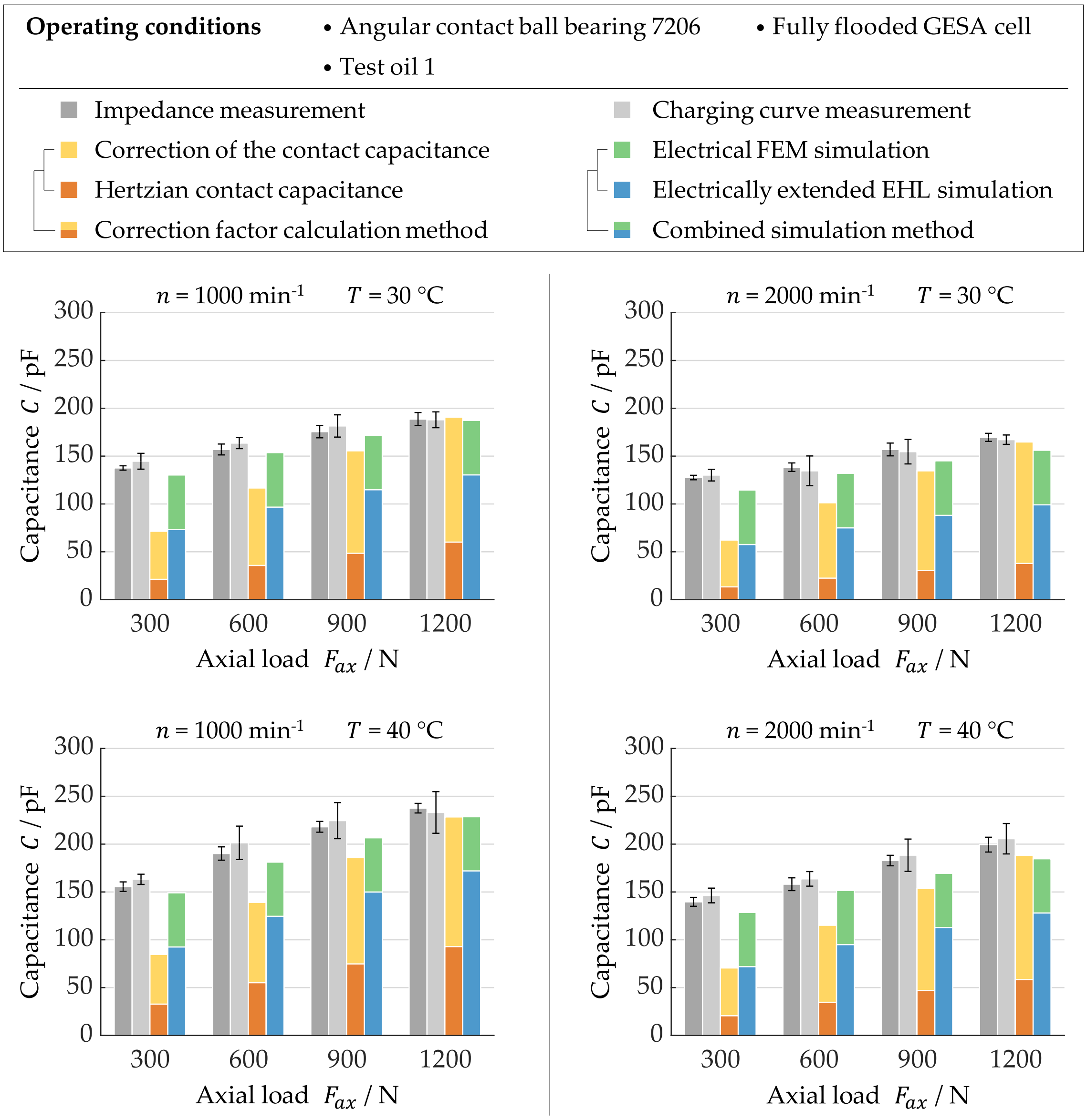

Figure 6.22: Comparison of the measurement and calculation results for the angular contact ball bearing 7206 with test oil 1

7 Summary and outlook

With the increasing number of frequency inverter-controlled electric motors and generators, the number of bearing failures caused by frequency inverter-induced parasitic currents has also increased in the recent years. The type and magnitude of the parasitic currents, and thus the caused damages depend on the operating condition-related electrical properties of the rolling bearings and further mechanical components. In order to predict the harmful electrical conditions, and to elaborate preventive measures against the parasitic current-induced damages, the electrical modelling of the rolling bearing is necessary. This modelling is based on the electrical insulating ability of the lubricant film, which develops in the rolling contacts. Since the accurate mechanical and fluid dynamical modelling of this area is already a complex task, simpler calculation methods in combination with various correction factors are usually used for the determination of the related electrical values. The state-of-the-art correction factors vary widely, and their validity range also differ significantly, which leads to uncertainty in their general application and to the demand for further investigations of this field. Accordingly, the aim of the present work was to develop a validated computational method for determining the capacitance of axially loaded rolling bearings without the application of correction factors, focusing on the full film lubrication condition.

For the experimental investigation of the rolling bearing capacitances, two measurement methods were applied, namely the charging curve measurement method and the impedance measurement method. Based on the performed investigations, the results of the impedance measurements show better reproducibility, lower sensitivity to disturbances associated with unfavourable lubrication conditions and thus a wider range of applicability in terms of the investigation of rolling bearing capacitances. Although the two methods can lead to comparable results in cases, where the conditions are favourable for the development of a separating lubricant film in the rolling contact, the impedance measurement is considered the preferred measurement method for determining the rolling bearing capacitance, based on its mentioned advantages.

For the determination of the rolling bearing capacitances, a combined simulation method was developed. In the first step of the calculations, a numerical EHL simulation is performed, which is responsible for the tribological modelling of the rolling contact. The resulting pressure distribution, gap height distribution and phase distribution (obtained by the applied cavitation algorithm) are used in the electrical extension of the contact simulation. During the electrical extension, each cell of the EHL simulation is considered as an elementary parallel plate capacitor with the corresponding plate area, distance, and dielectric (oil and air) between the plates. Thus, a capacitance distribution can be obtained over the simulation domain, which can be used for the determination of the capacitance of the rolling contact, and the capacitance of the contact regions (inlet-, outlet- and hertzian contact region). In parallel, an electrical FEM simulation is carried out, which was developed to model additional capacitance sources of the rolling bearing. The FEM simulation serves as a direct spatial extension of the electrically extended EHL simulation. To reduce the computational demand, the FEM model is defined as a segment of the rolling bearing exploiting its geometrical periodicity. In the segment, the different dielectrics (lubricant, air, plastic cage) are modelled, and the conductive components are represented as boundary conditions on the corresponding boundary surfaces. With this modelling technique, different oil quantities can be considered in the simulation domain. The provided capacitances of the electrically extended EHL simulation and the FEM simulation are combined based on the electrical equivalent circuit of the rolling bearing segment. By summing the segment capacitances, the total rolling bearing capacitance can be obtained without the application of corrector factors.

In order to identify the different capacitance sources of the rolling bearings, targeted experimental investigations were carried out. Based on the measurements of the rolling bearing capacitance as the function of the rolling element number, the rolling bearing capacitances can be divided into two groups. There are capacitances that can be considered as rolling element independent capacitances, and there are capacitances that show a linear trend as the function of the rolling element number. Further investigations showed that the rolling element independent capacitances can be influenced by the different design variants of the environment. Thus, the rolling element independent capacitance can be further divided into the capacitance of the rolling bearing rings and the capacitance of the environmental components. Subsequently, measurements were carried out with different oil levels in the measurement cell and with the same operating conditions, i.e., with theoretically identical lubricant film thicknesses. The results showed that the capacitance increase per rolling element was significantly influenced by the oil quantity. Consequently, the rolling element-related capacitances can be divided into the contact capacitances (related to the lubricant film in the contact), and the capacitances of the surrounding gap of the rolling contact. Finally, due to the electrically extended EHL simulation, the capacitances of the contact regions (inlet-, outlet- and hertzian contact region) can be considered separately. As a result, the detailed capacitance structure of the investigated rolling bearing was determined.

The developed combined simulation method was validated using the presented measurement methods in case of a thrust ball bearing 51208 with two different test oils. In parallel, the results were also compared with the results of the correction factor calculation method. In general, the results of the combined simulation method show a good agreement with the measurement results in both magnitude and course. With decreasing lubricant film thickness, the results of the combined simulation method show a slightly increasing difference compared to the measured values. Although the investigations partly covered also the mixed lubrication condition, the maximum difference between the measured and simulated results was 19 % and the average difference was 10 %, which indicates a high modelling accuracy. In contrast, the applied correction factor calculation method had a limited validity range. It generally underestimated the measurement results at low capacitance values and overestimated at high capacitance values within the range of the considered operating conditions. In addition, while the combined calculation method can describe the influence of the oil quantity on the rolling bearing capacitance, the correction factor calculation method cannot model this influence. Since the purpose of the correction factor is to describe the ratio between the total capacitance of the contact and the capacitance of the hertzian contact region, this calculation method cannot consider the influence of the oil quantity and further influences related to the non-contact areas of the rolling bearing. Thus, the correction factor calculation methods (without taking additional capacitances into account) can only be applied for the calculation of the total rolling bearing capacitance if the non-contact capacitances are negligibly small.

Based on the results of the combined simulation method, the different capacitance sources of the investigated rolling bearing were analysed. The results showed that the contact capacitances (i.e., the total capacitance of the inlet-, outlet-, and hertzian contact regions) are responsible on average for approx. 70 % of the total rolling bearing capacitances in case of a fully flooded measurement cell, while the remaining approx. 30 % is obtained by the non-contact regions. In addition, the capacitance of the non-contact regions is mainly determined by the surrounding gap around the rolling contacts, while the environmental influences are responsible for only approx. 5 % of the total bearing capacitance.

After the investigations with the thrust ball bearing 51208, the combined simulation method was successfully adjusted for the capacitance calculation of the axially loaded angular contact ball bearing 7206. The results of the combined simulation method still showed good agreement with the measured values. It suggests that the simulation method can be extended analogously to other axially loaded ball bearings. Furthermore, the presented modelling strategy can be potentially extended to ball and roller bearings with combined loads. In the case of combined loads, by knowing the load distribution within the rolling bearing, the segment capacitances can be calculated separately and subsequently summed. While the electrically extended EHL simulation can calculate the contact capacitance of the loaded rolling contacts, the FEM simulation can be used for the capacitance calculation of the surroundings of the rolling contacts and the unloaded rolling elements. Furthermore, the combined simulation method can be potentially applied to the capacitance calculation of gear contacts, where the capacitances can be similarly divided into the contact capacitances and the capacitance of the non-contact regions.

The accurate calculation of the rolling bearing capacitances is of great practical importance since it is essential for the correct estimation and prediction of the parasitic currents in the electric motors and in the driven unit. The rolling bearing capacitances are used for the determination of the bearing voltage ratio (BVR), which describes the ratio of the voltage acting on the rolling bearing to the common-mode voltage of the electric motor. Thereby, knowing the stary capacitances of the motor, the effective bearing voltage can be calculated. In addition, if the parasitic currents also appear in the driven unit, further bearings and gear contacts can be subjected to electrical loads. In such complex systems, the accurate electrical modelling of the individual components is necessary. In this way, the electrical interactions between components can be taken into account and parasitic currents can be predicted. As a result, the developed simulation method of the rolling bearing can support the system-level electrical calculations of the frequency inverter-controlled motors and generators, thus improving the prediction of harmful parasitic currents on the mechanical components and the development of preventive measures against them.

A Appendix

A.1 Rolling bearing data

Table A1.1: Data of the thrust ball bearing 51208

Parameter	Symbol	Unit	Value
Outer diameter	D_o	mm	68
Bore diameter	D_i	mm	40
Width	W	mm	19
Pitch diameter	d_p	mm	54
Rolling element diameter	d_{re}	mm	10.3
Raceway radius outer ring	$r_{rw,or}$	mm	5.6
Raceway radius inner ring	$r_{rw,ir}$	mm	5.6
Number of rolling elements	Z	–	15
Nominal contact angle	α_0	°	90
Poisson's ration	ν	–	0.3
Modulus of elasticity	E	GPa	210
Cage material	–	–	Plastic
Sealing	–	–	No

Table A1.2: Data of the angular contact ball bearing 7206

Parameter	Symbol	Unit	Value
Outer diameter	D_o	mm	62
Bore diameter	D_i	mm	30
Width	W	mm	16
Pitch diameter	d_p	mm	46
Rolling element diameter	d_{re}	mm	9.53
Raceway radius outer ring	$r_{rw,or}$	mm	4.95
Raceway radius inner ring	$r_{rw,ir}$	mm	4.95
Number of rolling elements	Z	–	13
Nominal contact angle	α_0	°	25
Poisson's ration	ν	–	0.3
Modulus of elasticity	E	GPa	210
Cage material	–	–	Plastic
Sealing	–	–	No

Bibliography

[Ans19] ANSYS, Inc.: *ANSYS Mechanical APDL Theory Reference*. Published in the U.S.A.; ANSYS, Inc. and ANSYS Europe; Release 18.2, 2017.

[Aul14] Aul, V.: *Kontaktmodelle zur dynamischen Simulation vollrolliger Zylinderrollenlager.* Dissertation, Technische Universität Kaiserslautern, 2014.

[Bal05] Baly, H.: *Reibung fettgeschmierter Wälzlager.* Dissertation, Universität Hannover, 2005.

[Bar10] Bartel, D.: *Simulation von Tribosystemen – Grundlagen und Anwendungen.* Habilitationsschrift, Universität Magdeburg, Vieweg + Teubner Research, 2010.

[Bar93] Barus, C.: Isothermals, isopiestics and isometrics relative to viscosity. *American journal of science* 3(266), (1893), p. 87-96.

[Bar96] Barz, M.: *Die Schmierfilmbildung in fettgeschmierten schnelllaufenden Spindellagern*. Dissertation, Universität Hannover, 1996.

[BCGS19] Bechev, D.; Capan, R.; Gonda, A.; Sauer, B.: Method for the investigation of the EDM breakdown voltage of grease and oil on rolling bearings. *Bearing World Journal* 4, (2019), p. 83-91.

[Bec20] Bechev, D.: *Prüfmethodik zur Charakterisierung der elektrischen Eigenschaften von Wälzlagerschmierstoffen*. Dissertation, Technische Universität Kaiserslautern, 2020.

[BFT17] Bader, N.; Furtmann, A.; Tischmacher, H.; Poll, G.: Capacitances and lubricant film thicknesses of grease and oil lubricated bearings. *STLE Annual Meeting & Exhibition*, Atlanta, Georgia, USA, 21-25 May, 2017.

[BH77] Brewe, D. E.; Hamrock, B. J.: Simplified solution for elliptical-contact deformation between two elastic solids. *Journal of Lubrication Technology* 99(4), (1977), p. 485-487.

[BKRS18] Bechev, D.; Kiekbusch, T.; Radnai, B.; Sauer, B.: Untersuchung der Auswirkungen von leitenden und nichtleitenden Schmierfetten auf die Oberflächeneigenschaften bei spannungsbeaufschlagten Wälzlagern. *Tribologie und Schmierungstechnik* 65(3), (2018), p. 5-11.

[Bod84] Bode, B.: *Entwicklung eines Quarzviskosimeters für Messungen bei hohen Drücken*. Dissertation, Technische Universität Clausthal, 1984.

[Bod89] Bode, B.: Modell zur Beschreibung des Fließverhaltens von Flüssigkeiten unter hohem Druck. *Tribologie und Schmierungstechnik* 35(5), (1989), p. 256-261.

[Bon51] Bondi, A. A.: *Physical chemistry of lubricating oils*. Book Division, Reinhold Publishing Corp.: New York, USA, 1951.

[Bou85] Boussinesq, J.: *Application des potentiels à l'étude de l'équilibre et du mouvement des solides élastiques: principalement au calcul des déformations et des pressions que produisent, dans ces solides, des efforts quelconques exercés sur une petite partie de leur surface ou de leur intérieur: mémoire suivi de notes étendues sur divers points de physique mathématique et d'analyse*. Paris: Gauthier-Villars, 1885.

[Brü72] Brüser, P.: *Über die elastohydrodynamische Schmierfilmdicke bei elliptischen Hertzschen Kontaktflächen*. Dissertation, Technische Universität Braunschweig, 1972.

[CDDT85a] Chittenden, R. J.; Dowson, D.; Dunn, J. F.; Taylor, C. M.: A theoretical analysis of the isothermal elastohydrodynamic lubrication of concentrated contacts. I. Direction of lubricant entrainment coincident with the major axis of the hertzian contact ellipse. *Proceedings of the Royal Society of London. A. Mathematical and Physical Sciences* 397(1813), (1985), p. 245-269.

[CDDT85b] Chittenden, R. J.; Dowson, D.; Dunn, J. F.; Taylor, C. M.: A theoretical analysis of the isothermal elastohydrodynamic lubrication of concentrated contacts. II. General case, with lubricant entrainment along either principal axis of the hertzian contact ellipse or at some intermediate angle. *Proceedings of the Royal Society of*

London. A: Mathematical and Physical Sciences 397(1813), (1985), p. 271-294.

[CDV07] Chaomleffel, J.-P.; Dalmaz, G.; Vergne, P.: Experimental results and analytical film thickness predictions in EHD rolling point contacts. *Tribology International* 40(10-12), (2007), p. 1543-1552.

[CH10] Czichos, H.; Habig, K. H.: *Tribologie-Handbuch: Tribometrie, Tribomaterialien, Tribotechnik*. Springer-Verlag, 2010.

[CLN98] Chen, S.; Lipo, T. A.: Circulating type motor bearing current in inverter drives. *IEEE Industry Applications Magazine*, *4*(1), (1998), p. 32-38.

[CVL10] Canzi, A.; Venner, C. H.; Lubrecht, A. A.: Film thickness prediction in elastohydrodynamically lubricated elliptical contacts. *Proceedings of the Institution of Mechanical Engineers, Part J: Journal of Engineering Tribology* 224(9), (2010), p. 917-923.

[Dam03] Damiens, B.: *Modélisation de la lubrification sous-alimentée dans les contacts élastohydrodynamiques élliptiques*. Dissertation, Institut National des Sciences Appliquées de Lyon, 2003.

[DIN 26281] DIN 26281: *Rolling bearings - Methods for calculating the modified reference rating life for universally loaded bearings.* Deutsches Institut für Normung (DIN), 2010.

[DIN 51412] DIN 51412-1: *Testing of petroleum products - Determination of the electrical conductivity - Part 1: Laboratory method*. Deutsches Institut für Normung (DIN), 2005.

[DIN 51757] DIN 51757: *Testing of mineral oils and related materials - Determination of density*. Deutsches Institut für Normung (DIN), 2011.

[DIN EN 60247] DIN EN 60247: *Insulating liquids - Measurement of relative permittivity, dielectric dissipation factor (tan δ) and d.c. resistivity.* Deutsches Institut für Normung (DIN), 2004.

[DIN EN 60156] DIN EN 60156: *Insulating liquids - Determination of the breakdown voltage at power frequency - Test method.* Deutsches Institut für Normung (DIN), 1966.

[DIN ISO 281] DIN ISO 281: *Rolling bearings - Dynamic load ratings and rating life.* Deutsches Institut für Normung (DIN), 2010.

[Elr91] Elrod, H.: A cavitation algorithm. *Journal of Lubrication Technology* 103(3), (1981), p. 350-354.

[Eng02] Engel, S.: *Reibungs- und Ermüdungsverhalten des Rad-Schiene-Systems mit und ohne Schmierung*. Dissertation, Universität Magdeburg, 2002.

[Fur17] Furtmann, A.: *Elektrisches Verhalten von Maschinenelementen im Antriebsstrang.* Dissertation, Universität Hannover, 2017.

[GCBS19] Gonda, A.; Capan, R.; Bechev, D.; Sauer, B.: The influence of lubricant conductivity on bearing currents in the case of rolling bearing greases. *Lubricants* 7(12), (2019), p. 108-110.

[Gem16] Gemeinder, Y.: *Lagerimpedanz und Lagerschädigung bei umrichtergespeisten Antrieben.* Dissertation, Technische Universität Darmstadt, 2016.

[GSRS14] Gemeinder, Y.; Schuster, M.; Radnai, B.; Sauer, B.; Binder, A.: Calculation and validation of a bearing impedance model for ball bearings and the influence on EDM-currents. *2014 International Conference on Electrical Machines (ICEM)*, 2014, p. 1804-1810.

[Gun91] Gundrum, J.: *Entwicklung eines Quarzviskosimeters für Messungen bei hohen Temperaturen und Drücken*. Dissertation, Technische Universität Clausthal, 1991.

[HD77] Hamrock, B. J.; Dowson, D.: Isothermal elastohydrodynamic lubrication of point contacts: III-Fully flooded results. *Journal of Lubrication Technology* 99(2), (1977), p. 264-275.

[Her81] Hertz, H.: Über die Berührung fester elastischer Körper. *Journal für die reine und angewandte Mathematik* 92, (1881), p. 156-171.

[HK06] Harris, T. A.; Kotzalas, M. N.: *Rolling bearing analysis - 2 volume set*. 5th edition, CRC Press, 2006.

[HP19] Hansa Press- und Maschinenbau GmbH: *The Four-ball-Tester (FBT-110).* Product description document, 2019. URL: https://hansapress.de/four-ball-tester.html

[HSJ04] Hamrock, B. J.; Schmid, S. R.; Jacobson, B. O.: *Fundamentals of fluid film lubrication*. CRC Press, 2004. ISBN 0-8247-5371-2.

[HXL20] He, F.; Xie, G.; Luo, J.: Electrical bearing failures in electric vehicles. *Friction* 8, (2020), p. 4-28.

[Jab15] Jablonka, K.: *Study of film thickness in elastohydrodynamic contacts by electrical capacitance*. Dissertation, University of Sussex, 2015.

[Jag05] Jagenbrein, A.: *Investigations of bearing failures due to electric current passage*. Dissertation, Technische Universität Wien, 2005.

[JDY06] Jin, Z. M.; Dowson, D.; Yang, P.: Discussion - Transient elastohydrodynamic point contact analysis using a new coupled differential deflection method. *Proceedings of the Institution of Mechanical Engineers, Part J.: Journal of Engineering Tribology* 220(4), (2006), p. 413-414.

[JF57] Jakobsson, B.; Floberg, L.: The finite journal bearing considering vaporization. *Transactions of Chalmers University of Technology* 190, (1957), p. 1-116.

[JGB12] Jablonka, K.; Glovnea, R.; Bongaerts, J.: Evaluation of EHD films by electrical capacitance. *Journal of Physics D: Applied Physics* 45(38), (2012), p. 385301.

[JKB08] Jang, J. Y.; Khonsari, M. M.; Bair, S.: Correction factor formula to predict the central and minimum film thickness for shear-thinning fluids in EHL. *Journal of Tribology* 130(2), (2008), 024501.

[Joh70] Johnson, K. L.: Regimes of elastohydrodynamic lubrication. *Journal of Mechanical Engineering Science* 12(1), (1970), p. 9-16.

[Joh85] Johnson, K. L.: *Contact Mechanics*. Cambridge: Cambridge University Press, 1985.

[Kie17] Kiekbusch, T.: *Strategien zur dynamischen Simulation von Wälzlagern*. Dissertation, Technische Universität Kaiserslautern, 2017.

[Kre13] Kreil, O.: *Einfluss der Oberflächenstruktur auf Druckverteilung und Schmierfilmdicke im EHD-Kontakt*. Dissertation, Technische Universität München, 2013.

[Küc09] Küchler, A.: *Hochspannungstechnik: Grundlagen-Technologie-Anwendungen*. 3. Auflage. Springer, 2009.

[LBG16] Loos, J.; Bergmann, I.; Goss, M.: Influence of currents from electrostatic charges on WEC formation in rolling bearings. *Tribology Transactions* 59(5), (2016), p. 865-875.

[LBG21] Loos, J.; Bergmann, I.; Goss, M.: Influence of high electrical currents on WEC formation in rolling bearings. *Tribology Transactions* 64(4), (2021), p. 1-12.

[Lev44] Levenberg, K.: A method for the solution of certain non-linear problems in least squares. *Quarterly of Applied Mathematics* 2(2), (1944), p. 164-168.

[Mag12] Magyar, B.: *Tribo-dynamische Untersuchungen von Zylinderschneckengetrieben*. Dissertation, Technische Universität Kaiserslautern, 2012.

[Mar63] Marquardt, D. W.: An algorithm for least-squares estimation of nonlinear parameters. *Journal of the Society for Industrial and Applied Mathematics* 11(2), (1963), p. 431-441.

[MBWR20] Marian, M.; Bartz, M.; Wartzack, S.; Rosenkranz, A.: Non-dimensional groups, film thickness equations and correction factors for elastohydrodynamic lubrication: A review. *Lubricants* 8(10), (2020), p. 95.

[MSMK19] Manieri, F.; Stadler, K.; Morales-Espejel, G. E.; Kadiric, A.: The origins of white etching cracks and their significance to rolling bearing failures. *International Journal of Fatigue* 120, (2019), p. 107-133.

[MTLB18] Magyar, B.; Thielen, S.; Löwenstein, M.; Becker, A.; Sauer, B.: EHD Simulation eines Kettengelenkes. *Tribologie und Schmierungstechnik* 65(1), (2018), p. 40-47.

[Müt04] Mütze, A.: *Bearing currents in inverter-fed AC-motors*. Dissertation, TU Darmstadt, Shaker-Verlag GmbH, 2004.

[MW75] Murch, L. E.; Wilson, W. R. D.: A thermal elastohydrodynamic inlet zone analysis. *Journal of Lubrication Technology* 97(2), (1975), p. 212–216.

[Ols65] Olsson, K. O.: Cavitation in dynamically loaded bearings. *Transactions of Chalmers University of Technology.* Guthenberg, Sweden, (1965), p. 308.

[PBCN18] Plazenet, T.; Boileau, T.; Caironi C.; Nahid-Mobarakeh B.: A comprehensive study on shaft voltages and bearing currents in rotating machines. *IEEE Transactions on Industry Applications* 54(4), (2018), p. 3749-3759.

[Pra06] Prashad, H.: *Tribology in electrical environments*. 1st Edition, Elsevier, 2006.

[Pre02] Preisinger, G.: *Cause and effect of bearing currents in frequency converter driven electrical motors: Investigations of electrical properties of rolling bearings*. Dissertation, Technische Universität Wien, 2002.

[Rad16] Radnai, B.: *Wirkmechanismen bei spannungsbeaufschlagten Wälzlagern*. Dissertation, Technische Universität Kaiserslautern, Kaiserslautern, 2016.

[RG15] Radnai, B.; Gemeinder, Y.: Untersuchung des Schädigungsmechanismus und der zulässigen Lagerstrombelastung von Wälzlagern in E-Motoren und Generatoren, verursacht durch parasitäre hochfrequente Lagerströme. *Forschungsvereinigung Antriebstechnik (FVA)*. Frankfurt, Deutschland, FVA Heft 1127, 2015.

[Rod80] Rodermund, H.: Extrapolierende Berechnung des Viskositätsverlaufes unter hohen Drücken. *Schmiertechnik und Tribologie* 27(1), (1980), p. 3-5.

[Sch10] Schlecht, B.: *Maschinenelemente 2 - Getriebe, Verzahnungen und Lagerungen*. 1. Auflage, Pearson, 2009.

[Sch20] Schaeffler Technologies AG & Co. KG: *Stromisolierende Lager: Wälzlager zur Vermeidung von Stromdurchgangsschäden*. Technische Produktinformation (TPI 206), MATNR 036889601-0000, 2020.

[Sch18] Schaeffler Technologies AG & Co. KG: *Rolling bearings. Technical principles and product data for the design of rolling bearing arrangements*; Catalogue (HR 1); Printed in Germany by mohn, 2018. (Online: https://www.schaeffler.de/std/1D65)

[Sch19] Schaeffler Technologies AG & Co. KG: *Wälzlagerpraxis. Handbuch zur Gestaltung und Berechnung von Wälzlagerungen*. 5. Edition, Vereinigte Fachverlage, 2019.

[Sch88] Schrader, R.: *Zur Schmierfilmbildung von Schmierölen und Schmierfetten in elastohydrodynamischen Wälzkontakten*. Dissertation, Universität Hannover, 1988.

[Skf18] SKF Group: *Rolling bearings*; Catalogue with publication number PUB BU/P1 17000/1 EN, 2018.

[SLBF19] Schneider, V.; Liu, H.-C.; Bader, N.; Furtmann, A.; Poll, G.: Empirical formulae for the influence of real film thickness distribution on the capacitance of an EHL point contact and application to rolling bearings. *Tribology International* 154, (2021), p. 106714.

[SM19] Schröder, D.; Marquardt, R.: *Leistungselektronische Schaltungen: Funktion, Auslegung und Anwendung*. 4. Auflage, Springer Verlag, 2019.

[SOMS18] Simo Kamga, L., Oehler, M., Magyar, B.; Sauer, B.: Charakterisierung des strukturviskosen Verhaltens von Schmierstoffen durch Kombination von Experiment und EHD-Simulation mithilfe des Carreau-Modells. *Forschung im Ingenieurwesen* 82, (2018), p. 301-309.

[SOS21] Simo Kamga, L; Oehler, M; Sauer, B.: Characterization of the viscoelastic behaviour of gears oils by EHL Simulation. *14th WCCM-ECCOMAS Congress* (Vol. 1500), 2021.

[SS12] Steinhilper, W.; Sauer, B.: *Konstruktionselemente des Maschinenbaus 2: Grundlagen von Maschinenelementen für Antriebsaufgaben*. Springer, 2012.

[Str02] Stribeck, R.: Die wesentlichen Eigenschaften der Gleit- und rollenlager. *Zeitschrift des Vereines Deutscher Ingenieure* 46(37 (Part I), 38 (Part II), 39 (Part III)), (1902), 1341-1348 (Part I), 1432-1438 (Part II), 1463-1470 (Part III).

[Tal68] Tallian, T. E.: Rolling contact failure control through lubrication. *Proceedings of the Institution of Mechanical Engineers, Conference Proceedings* 182(1), (1968), p. 205–236.

[Tis17] Tischmacher, H.: *Systemanalysen zur elektrischen Belastung von Wälzlagern bei umrichtergespeisten Elektromotoren*. Dissertation, Universität Hannover, 2017.

[Tis17b] Tischmacher, H.: Bearing wear in electric motors and rotating equipment under the aspect of VSD converter operation. *Proceedings of the 33rd International Pump Users Symposium.* Turbomachinery Laboratory, Texas A&M Engineering Experiment Station, 2017.

[TMS20] Thielen, S.; Magyar, B.; Sauer, B.: Thermoelastohydrodynamic lubrication simulation of radial shaft sealing rings. *Journal of Tribology* 142(5), (2020), 052301.

[VB14] Vergne, P.; Bair, S.: Classical EHL versus quantitative EHL: a perspective part I – real viscosity-pressure dependence and the viscosity-pressure coefficient for predicting film thickness. *Tribology Letters* 54(1), (2014), p. 1–12.

[VB94] Venner, C. H.; Bos, J.: Effects of lubricant compressibility on the film thickness in EHL line and circular contacts. *Wear* 173(1-2), (1994), p. 151–165.

[Wan15] Wang, D.: *Berechnung der Wälzlagerreibung aufgrund weiterentwickelter Rheologischer Fluidmodelle*. Dissertation, Universität Hannover, 2015.

[Wit17] Wittek, E. C.: *Charakterisierung des Schmierungszustandes im Rillenkugellager mit dem kapazitiven Messverfahren*. Dissertation, Universität Hannover, 2017.

[WKT10] Wittek, E. C.; Kriese, M.; Tischmacher, H.; Gattermann, S.; Ponick, B.; Poll, G.: Capacitances and lubricant film thicknesses of motor bearings under different operating conditions. *The XIX International Conference on Electrical Machines (ICEM)*. Rome, Italy, 2010, p. 1-6.

[WPS15] Woloszynski, T.; Podsiadlo, P.; Stachowiak, G. W.: Efficient solution to the cavitation problem in hydrodynamic lubrication. *Tribology Letters* 58(1), (2015), p. 839.

[Zik10] Zika, T.: *Electric discharge damaging in lubricated rolling contacts*. Dissertation, Technische Universität Wien, 2010.

[ZW12] Zhu, D.; Wang, Q. J.: On the λ ratio range of mixed lubrication. *Proceedings of the Institution of Mechanical Engineers, Part J: Journal of Engineering Tribology* 226(12), (2012), p. 1010-1022.

List of own publications

Schwarz, M.; Liebrecht, J.; **Gonda, A.**; Sauer, B.: A study on the frictional torque and temperature behavior in tapered roller bearings. *Bearing World Journal* 3, (2018), p. 31-39. ISSN 2513-1753

Gonda, A.; Großberndt, D.; Sauer, B.; Schwarze, H.: Experimentelle und numerische Untersuchungen der hydraulischen Verluste in Wälzlagern unter praxisrelevanten Bedingungen. *Tribologie und Schmierungstechnik* 65(6), (2018), p. 7-13. ISSN 0724-3472

Gonda, A.; Großberndt, D.; Sauer, B.; Schwarze, H.: Experimentelle und numerische Untersuchungen der hydraulischen Verluste in Wälzlagern unter praxisrelevanten Bedingungen. *Tagungsband - 59 Tribologie-Fachtagung, Gesellschaft für Tribologie e.V. (GfT)*. Göttingen, 2018, 35/1-10.

Gonda, A.; Großberndt, D.; Sauer, B.; Schwarze, H.: Experimental and numerical investigations of hydraulic losses in rolling bearings. *Proceedings of the 2019 STLE Annual Meeting and Exhibition*, Nashville, Tennessee, USA, 2019.

Gonda, A.; Großberndt, D.; Sauer, B.; Schwarze, H.: Experimentelle und numerische Untersuchungen der hydraulischen Verluste in voll- und teilgefluteten Kegelrollenlagern. *13. VDI-Fachtagung Gleit- und Wälzlagerungen*. VDI Verlag GmbH, Düsseldorf, 2019. ISBN: 978-3-18-092348-2

Bechev, D.; **Gonda, A.**; Capan, R.; Sauer, B.: Untersuchung der Oberflächenmutationen und der Riffelbildung bei spannungsbeaufschlagten Wälzlagern. *13. VDI-Fachtagung Gleit und Wälzlagerungen*. VDI Verlag GmbH, Düsseldorf, 2019. ISBN: 978-3-18-092348-2

Bechev, D.; Capan, R.; **Gonda, A.**; Sauer, B.: Method for the investigation of the EDM breakdown voltage of grease and oil on rolling bearings. *Bearing World Journal* 4, (2019), p. 83-91. ISSN 2513-1753

Gonda, A.; Capan, R.; Bechev, D., Sauer, B.: The influence of lubricant conductivity on bearing currents in the case of rolling bearing greases. L*ubricants* 7(12), (2019), 108. https://doi.org/10.3390/lubricants7120108

Curriculum vitae

Personal details

Name	Attila Gonda
Nationality	Hungarian

Education

02/2014 - 07/2016	Budapest University of Technology and Economics Mechanical Engineering Modelling MSc Modules: Solid Mechanics and Fluid Mechanics
09/2010 - 01/2014	Budapest University of Technology and Economics Mechanical Engineering BSc Specialisation: Development engineer
09/2002 - 06/2010	Belvárosi Primary and Grammar School Békéscsaba, Hungary

Professional experience

10/2021 – present	ZF Friedrichshafen AG – Friedrichshafen Development engineer - Research and Development Rolling bearings
10/2016 - 09/2021	Institute of Machine Elements, Gears and Transmissions (MEGT), Technische Universität Kaiserslautern Research assistant
10/2014 - 08/2016	Robert Bosch GmbH – Budapest, Hungary Intern - Simulation and test engineer
06/2013 - 08/2013	eCon Engineering Ltd – Budapest, Hungary Intern - Simulation engineer
06/2011 - 07/2011	Csaba Metál AG – Szeghalom, Hungary Trainee - Technologist

Dissertations at the Chair of Machine Elements, Gears and Tribology (MEGT) of the TU Kaiserslautern

1. Gäthje, Heino: Bewertung der Naßbagger und der sich anschließenden Transportkette im Schelfbereich unter Anwendung eines EDV-Modells. Dissertation, Universität Kaiserslautern, 1981
2. Kahle, Ulrich: Das Micro-CAD-System ein Beitrag zur Einführung einer rechnerunterstützen Konstruktionsweise in kleinen und mittleren Unternehmen. Dissertation, Universität Kaiserslautern, 1983
3. Kreutz, Sax: Simulation von Vergleichmässigungsprozessen auf stirnseitig abgebauten Massenschüttgutkreislagerplätzen mit Hilfe eines elektrischen Analogiemodells und eines gleichwertigen digitalen Modells. Dissertation, Universität Kaiserslautern, 1983
4. Rende, Hikmet: Ein Beitrag zur Untersuchung der elastischen Nachgiebigkeiten der verspannten Teile von Schraubenverbindungen. Dissertation, Universität Kaiserslautern, 1984
5. Sponagel, Stefan: Gummi-Metall-Bauteile. Dissertation, Universität Kaiserslautern, 1987
6. Spaltofski, Ralf: Ein Beitrag zur Beurteilung der Trageigenschaften und des Reibungsverhaltens von nicht-newtonschen Flüssigkeiten in stationär und dynamisch bewegten Gleitlagerungen. Dissertation, Universität Kaiserslautern, 1988
7. Britz, Stefan: Ein Beitrag zur Erfassung der Funktionsprinzipien dynamischer Wellendichtungen unter besonderer Berücksichtigung des Radialwellendichtrings. Dissertation, Universität Kaiserslautern, 1988
8. Hennerici, Horst: Ein Beitrag zur Berechnung der Beanspruchungen und der nichtlinearen Rückstellkräfte und -momente von dünnen Kreisringblechen als Wirkglieder von Membrankupplungen. Dissertation, Universität Kaiserslautern, 1988

9. Jiang, Fuqing: Ratterschwingungen bei selbsthemmenden Schneckengetrieben. Dissertation, Universität Kaiserslautern, 1989

10. Endemann, Ulrich: Ein Beitrag zur theoretischen und experimentelle Untersuchung hydrodynamisch arbeitender Spiralrillen-Radialgleitlager. Dissertation, Universität Kaiserslautern, 1989

11. Schlossarczyk, Jörg: Ein Beitrag zur Berechnung, Modellbildung und experimentellen Untersuchung drehelastischer Scheibenkupplungen unter Berücksichtigung des im Betrieb auftretenden Wellenversatzes. Dissertation, Universität Kaiserslautern, 1990

12. Lutz, Thomas: Ein Beitrag zur Berechnung druckbelasteter Elastomerlager. Dissertation, Universität Kaiserslautern, 1990

13. Lehnertz, Hermann: Ein Beitrag zur Berechnung hydrodynamisch arbeitender Radialgleitlager bei stationärem Betrieb mit Hilfe von Kleinrechnern. Dissertation, Universität Kaiserslautern, 1990

14. Maier, Martin: Experimentelle Untersuchung und numerische Simulation des Crashverhaltens von Faserverbundwerkstoffen. Dissertation, Universität Kaiserslautern, 1990

15. Steiner, Matthias: Ein Beitrag zur theoretischen und experimentellen Erfassung der Funktionsmechanismen von axialen Gleitringdichtungen. Dissertation, Universität Kaiserslautern, 1992

16. Stopp, Ralf: Elastomere Werkstoffe für Formdichtungen. Ein Beitrag zur Dimensionierung von Dichtsystemen. Dissertation, Universität Kaiserslautern, 1993

17. Joo, Kwang-Taek: Beitrag zum Einfluß mechanischer Parameter auf das Spurverhalten von dreirädrigen fahrerlosen Transportfahrzeugen. Dissertation, Universität Kaiserslautern, 1993

18. Fritzsche, Ralf: Ein Beitrag zur Untersuchung des Verhaltens von Radialwellendichtringen aus Elastomer- und Polytetrafluoräthylen-Material bei speziellen Betriebsbedingungen. Dissertation, Universität Kaiserslautern, 1994

19. Becker, Matthias: Ein Beitrag zur Untersuchung der Temperaturentwicklung in einer drehelastischen Scheibenkupplung bei dynamischer Beanspruchung unter besonderer Berücksichtigung des im Betrieb auftretenden Winkelversatzes. Dissertation, Universität Kaiserslautern, 1994

20. Helfrich, Axel: Bestimmung der Kenngrößen von nicht-newtonschen Schmierstoffen für die Dimensionierung hydrodynamisch arbeitender Gleitlager. Dissertation, Universität Kaiserslautern, 1995

21. Mattheis, Fritz: Ein Beitrag zur theoretischen und experimentellen Untersuchung von Flachdichtungen am Beispiel von polymerbeschichteten Metallblechen. Dissertation, Universität Kaiserslautern, 1995

22. Koch, Jürgen: Das Gleitlager endlicher Breite eine Lösung der Reynoldsschen Differentialgleichung. Dissertation, Universität Kaiserslautern, 1995

23. Spieth, Gottfried: Mechanische und werkstofftechnische Untersuchung von Verbindungen mit Schrauben aus thermoplastischem Kunststoff. Dissertation, Universität Kaiserslautern, 1995

24. Kramm, Georg: Ein Beitrag zur Modellierung von nicht-newtonschen Schmierstoffen und deren Verwendung für hydrodynamisch arbeitende Gleitlager. Dissertation, Universität Kaiserslautern, 1996

25. Berg, Michael: Untersuchungen zum Schmierstoffdurchsatz und zur Reibungsleistung dynamisch belasteter Radialgleitlager. Dissertation, Universität Kaiserslautern, 1996

26. Mán, László: Ein Beitrag zur Vorhersage von Freßschäden an tribologischen Wirkstellen. Dissertation, Universität Kaiserslautern, 1997

27. Gast, Stefan: Zielfunktionen zur Optimierung der Laufeigenschaften räumlicher Mechanismen auf der Grundlage ebener Kontaktverlustkriterien. Dissertation, Universität Kaiserslautern, 2000, Fortschritt-Berichte VDI, Reihe 1, Nr. 331

28. Ruhl, Christian: Ein Beitrag zur Wirkungsweise von Radialwellendichtungen unter Berücksichtigung von rauheitsinduzierter Hydrodynamik und radialen Verlagerungen der Gegenlauffläche. Dissertation, Universität Kaiserslautern, 2000, Fortschritt-Berichte VDI, Reihe 1, Nr. 339

29. Huber, Matthias: Ein Beitrag zur Untersuchung hydrodynamisch arbeitender Radialgleitlager unter Berücksichtigung der Schmierölverdünnung mit Rapsölmethylester. Dissertation, Universität Kaiserslautern, 2000, Fortschritt-Berichte VDI, Reihe 12, Nr. 453

30. Fuerst, Axel: Analytische Simulation von hydrodynamischen Gleitlagern in Wasserkraftanlagen. Dissertation, Universität Kaiserslautern, 2000, Fortschritt-Berichte VDI, Reihe 1, Nr. 343

31. Reif, Andreas: Entwicklung eines integrierten automatisiert schaltenden Getriebes zum Einsatz in Elektrostraßenfahrzeugen. Dissertation, Universität Kaiserslautern, 2000, Fortschritt-Bericht VDI, Reihe 1, Nr. 477

32. Lorreng, Dirk: Ein Beitrag zur Ermittlung und Beschreibung der Fließeigenschaften biologisch schnell abbaubarer Schmierstoffe. Dissertation, Universität Kaiserslautern, 2001, Fortschritt-Berichte VDI, Reihe 3, Nr. 741

33. Péteri, Szabolcs: Untersuchungen von Radialwellendichtringen unter Wellenschwingungen bei unterschiedlichen Temperaturen. Dissertation, Technische Universität Kaiserslautern, 2004, Fortschritt-Berichte VDI, Reihe 1, Nr. 379

34. Hahn, Kersten: Dynamik-Simulation von Wälzlagerkäfigen. Dissertation, Technische Universität Kaiserslautern, 2005, Skaker Verlag, Reihe Konstruktionstechnik, ISBN 3-83223-760-7

35. Teutsch, Roman: Kontaktmodelle und Strategien zur Simulation von Wälzlagern und Wälzführungen. Dissertation, Technische Universität Kaiserslautern, 2005, Maschinenelemente und Getriebetechnik Berichte Bd. 01/2005, ISBN 3-93689-073-0

36. Groß, Torsten: Ein Beitrag zur Entwicklung und Analyse serieller und paralleler Strukturen. Dissertation, Technische Universität Kaiserslautern, 2007, Maschinenelemente und Getriebetechnik Berichte Bd. 02/2007, ISBN 978-3-93943-246-3

37. Thullen, Carlo: Entwicklung und Validierung einer Universalprüfeinrichtung zur Untersuchung von dynamisch belasteten Radialwellendichtungen. Dissertation, Technische Universität Kaiserslautern, 2008, Maschinenelemente und Getriebetechnik Berichte Bd. 03/2008, ISBN 978-3- 93943-289-0

38. Nicola, Andreas: Versuchsgestützte Dynamiksimulation hydraulisch gespannter Kettentriebe und Drehungleichförmigkeiten. Dissertation, Technische Universität Kaiserslautern, 2008, Maschinenelemente und Getriebetechnik Berichte Bd. 04/2008, ISBN 978-3-93943-290-6

39. Aul, Eduard: Analyse von Relativbewegungen in Wälzlagersitzen. Dissertation, Technische Universität Kaiserslautern, 2008, Maschinenelemente und Getriebetechnik Berichte Bd. 05/2008, ISBN 978-3-93943-296-8

40. Bach, Peter: Umsturzsicherheit von Doppeldeckeromnibussen. Dissertation, Technische Universität Kaiserslautern, 2008, Maschinenelemente und Getriebetechnik Berichte Bd. 06/2008, ISBN 978-3-93943-297-5

41. Scheuermann, Miguel: Dynamiksimulation zur virtuellen Produktentwicklung von Rollenschienenführungen. Dissertation, Technische Universität Kaiserslautern, 2010, Maschinenelemente und Getriebetechnik Berichte Bd. 07/2010, ISBN 978-3-94143-849-1

42. Wohlgemuth, Martin: Ein Beitrag zur Lebensdauerverlängerung von feststoffgeschmierten Rillenkugellagern. Dissertation, Technische Universität Kaiserslautern, 2010, Maschinenelemente und Getriebetechnik Berichte Bd. 08/2010, ISBN 978-3-94143-864-4

43. Leichner, Tim: Prognose der Dichtlippenfolgefähigkeit von RWDR bei dynamisch verlagerter Welle. Dissertation, Technische Universität Kaiserslautern, 2012, Maschinenelemente und Getriebetechnik Berichte Bd. 09/2012, ISBN 978-3-94143-891-0

44. Magyar, Balázs: Tribo-dynamische Untersuchungen von Zylinderschneckengetrieben. Dissertation, Technische Universität Kaiserslautern, 2012, Maschinenelemente und Getriebetechnik Berichte Bd. 10/2012, ISBN 978-3-94399-503-9

45. Babbick, Till: Wandern von Wälzlagerringen unter Punktlast. Dissertation, Technische Universität Kaiserslautern, 2012, Maschinenelemente und Getriebetechnik Berichte Bd. 11/2012, ISBN 978-3-94399-505-3

46. Gastauer, Tobias: Reibungs und Verschleißuntersuchungen von Elastomerwerkstoffen für Dichtungsanwendungen. Dissertation, Technische Universität Kaiserslautern, 2012, Maschinenelemente und Getriebetechnik Berichte Bd. 12/2013, ISBN 978-3-94399-516-9

47. Gummer, Alexander: Analytische Untersuchung des Geometrieeinflusses auf das Verschleißverhalten von Antriebsketten. Dissertation, Technische Universität Kaiserslautern, 2013, Maschinenelemente und Getriebetechnik Berichte Bd. 13/2013, ISBN 978-3-94399-523-7

48. Aul, Viktor: Kontaktmodelle zur dynamischen Simulation vollrolliger Zylinderrollenlager. Dissertation, Technische Universität Kaiserslautern, 2014, Maschinenelemente und Getriebetechnik Berichte Bd. 14/2014, ISBN 978-3-94399-555-8

49. Marquart, Matthias: Ein Beitrag zur Nutzung feststoffgeschmierter Wälzlager. Dissertation, Technische Universität Kaiserslautern, 2014, Maschinenelemente und Getriebetechnik Berichte Bd. 15/2014, ISBN 978-3-94399-552-7

50. Buchmiller, Viktor: Wälzgelagerter Kurbeltrieb - Potenzial von Wälzlagern im Verbrennungsmotor. Dissertation, Technische Universität Kaiserslautern, 2015, Maschinenelemente und Getriebetechnik Berichte Bd. 16/2015, ISBN 978-3-94399-579-4

51. Kaiser, Fabian: Ein Simulationsmodell zur Analyse des Schmierfilms von Stangendichtungen. Dissertation, Technische Universität Kaiserslautern, 2015, Maschinenelemente und Getriebetechnik Berichte Bd. 17/2015, ISBN 978-3-95974-010-4

52. Bajer, Peter: Einflussgrößen auf das Schlupfverhalten von Wälzlagern in Generatorgetrieben. Dissertation, Technische Universität Kaiserslautern, 2016, Maschinenelemente und Getriebetechnik Berichte Bd. 18/2016, ISBN 978-3-95974-016-6

53. Jennewein, Barbara: Integrierter Berechnungsansatz zur Prognose des dynamischen Betriebsverhaltens von Radialwellendichtringen. Dissertation, Technische Universität Kaiserslautern, 2016, Maschinenelemente und Getriebetechnik Berichte Bd. 19/2016, ISBN 978-3-95974-015-9

54. Radnai, Benjamin: Wirkmechanismen bei spannungsbeaufschlagten Wälzlagern. Dissertation, Technische Universität Kaiserslautern, 2016, Maschinenelemente und Getriebetechnik Berichte Bd. 20/2016, ISBN 978-3-95974-029-6

55. Frölich, Daniel: Strategien und Modelle zur Simulation des Betriebsverhaltens von Radial-Wellendichtringen. Dissertation, Technische Universität Kaiserslautern, 2016, Maschinenelemente und Getriebetechnik Berichte Bd. 21/2016, ISBN 978-3-95974-030-2

56. Sappok, Daniel: Experimentelle und simulative Methoden zur Untersuchung der Verschleißvorgänge im Kettengelenk von Antriebs- und Steuerketten. Dissertation, Technische Universität Kaiserslautern, 2016, Maschinenelemente und Getriebetechnik Berichte Bd. 22/2016, ISBN 978- 3-95974-033-3

57. Kiekbusch, Timo: Strategien zur dynamischen Simulation von Wälzlagern. Dissertation, Technische Universität Kaiserslautern, 2017, Maschinenelemente und Getriebetechnik Berichte Bd. 23/2017, ISBN 978-3-95974-043-2

58. Kaiser, Christian: Entwicklung einer Prüfmethodik für Modelluntersuchungen an schmutzbeaufschlagten Radial-Wellendichtringen. Dissertation, Technische Universität Kaiserslautern, 2017, Maschinenelemente und Getriebetechnik Berichte Bd. 24/2017, ISBN 978-3-95974-052-459

59. Fingerle, Thorsten: Experimentelle und simulative Untersuchung des Schlupfverhaltens von Kegelrollenlagern, Dissertation, Technische Universität Kaiserslautern, 2017, Maschinenelemente und Getriebetechnik Berichte Bd. 25/2017, ISBN 978-3-95974-054-8

60. Eckstein, Christian: Ermittlung repräsentativer Lastkollektive zur Betriebsfestigkeit von Ackerschleppern. Dissertation, Technische Universität Kaiserslautern, 2017, Maschinenelemente und Getriebetechnik Berichte Bd. 26/2017, ISBN 978-3-95974-064-7

61. Fruth, Torben: Vom tribologischen Modellversuch zum Maschinenelement: Berücksichtigung des rheologischen Verhaltens von Schmierstoffen in der Wälzlagersimulation. Dissertation, Technische Universität Kaiserslautern, 2018, Maschinenelemente und Getriebetechnik Berichte Bd. 27/2018, ISBN 978-3-95974-084-5

62. Fábián, Csaba: Verbesserung des Wirkungsgrades von Steuerkettentrieben durch bedarfsgerechte Kettenspannung. Dissertation, Technische Universität Kaiserslautern, 2018, Maschinenelemente und Getriebetechnik Berichte Bd. 28/2018, ISBN 978-3-95974-091-3

63. Oehler, Manuel: Methodische Ansätze zur Optimierung des Wirkungsgrades von Schneckengetrieben. Dissertation, Technische Universität Kaiserslautern, 2018, Maschinenelemente und Getriebetechnik Berichte Bd. 29/2018, ISBN 978-3-95974-097-5

64. Jürgen, Liebrecht: Technisch-mathematischer Ansatz zur Berechnung der hydraulischen Verluste in Wälzlagern. Dissertation, Technische Universität Kaiserslautern, 2018, Maschinenelemente und Getriebetechnik Berichte Bd. 30/2018, ISBN 978-3-95974-103-3

65. Krupp, Frederik: Reibleistungsreduzierung in Steuerkettentrieben. Dissertation, Technische Universität Kaiserslautern, 2018, Maschinenelemente und Getriebetechnik Berichte Bd. 31/2018, ISBN 978-3-95974-107-1

66. Herweg, Sören: Entwicklung und Validierung einer Methodik für erweiterte Ventiltriebssimulationen. Dissertation, Technische Universität Kaiserslautern, 2019, Maschinenelemente und Getriebetechnik Berichte Bd. 32/2019, ISBN 978-3-95974-106-4

67. Pörsch, Sascha: Ansätze zur erweiterten Lebensdauerberechnung feststoffgeschmierter Wälzlager. Dissertation, Technische Universität Kaiserslautern, 2019, Maschinenelemente und Getriebetechnik Berichte Bd. 33/2019, ISBN 978-3-95974-113-2

68. Thielen, Stefan: Entwicklung eines TEHD-Tribosimulationsmodells für Radialwellendichtringe. Dissertation, Technische Universität Kaiserslautern, 2019, Maschinenelemente und Getriebetechnik Berichte Bd. 34/2019, ISBN 978-3-95974-120-0

69. Weyrich, Dominik: Tribologisches Prüfsystem für Dichtungsanwendungen. Dissertation, Technische Universität Kaiserslautern, 2020, Maschinenelemente und Getriebetechnik Berichte Bd. 35/2020, ISBN 978-3-95974-131-6

70. Wiesker, Sebastian: Axialschub an nadelgelagerten Stützrollen. Dissertation, Technische Universität Kaiserslautern, 2020, Maschinenelemente und Getriebetechnik Berichte Bd. 36/2020, ISBN 978-3-95974-136-1

71. Bechev, Dani: Prüfmethodik zur Charakterisierung der elektrischen Eigenschaften von Wälzlagerschmierstoffen. Dissertation, Technische Universität Kaiserslautern, 2020, Maschinenelemente und Getriebetechnik Berichte Bd. 37/2020, ISBN 978-3-95974-135-4

72. Zimmermann, Florian: Optimierung der Energieeffizienz von Kettenspannsystemen. Dissertation, Technische Universität Kaiserslautern, 2020, Maschinenelemente und Getriebetechnik Berichte Bd. 38/2020, ISBN 978-3-95974-138-5

73. Becker, Andre: Entwicklung einer Prüfmethodik für Verschleißuntersuchungen an Kettengelenken von Antriebs- und Steuerketten. Dissertation, Technische Universität Kaiserslautern, 2021, Maschinenelemente und Getriebetechnik Berichte Bd. 39/2020, ISBN 978-3-95974-143-9

74. Dahiwal, Rahul: Contribution to the Influence of Cage Wear on the Bearing Life of Solid-Lubricated Rolling Bearings. Dissertation, Technische Universität Kaiserslautern, 2021, Maschinenelemente und Getriebetechnik Berichte Bd. 40/2021, ISBN 978-3-95974-151-4

75. Hofmann, Markus: Auslegung von Berechnungsverfahren am Beispiel der Simulation von Mischreibung. Dissertation, Technische Universität Kaiserslautern, 2022, Maschinenelemente und Getriebetechnik Berichte Bd. 41/2022, ISBN 978-3-95974-174-3

76. Burkhart, Christoph: Ein Beitrag zum Verständnis des Verschleißverhaltens im System Radialwellendichtring. Dissertation, Technische Universität Kaiserslautern, 2022, Maschinenelemente und Getriebetechnik Berichte Bd. 42/2022, ISBN 978-3-95974-184-2

77. Mármol, Margarita: Development of a new bearing geometry to reduce friction losses. Dissertation, Technische Universität Kaiserslautern, 2022, Maschinenelemente und Getriebetechnik Berichte Bd. 43/2022, ISBN 978-3-95974-189-7

78. Sebteini, Seiedardeshir: Kritische Schlupfzustände von Wälzlagern im Mindestlastbereich. Dissertation, Rheinland-Pfälzische Technische Universität Kaiserslautern-Landau, 2023, Maschinenelemente und Getriebetechnik Berichte Bd. 44/2023, ISSN 1860-803

79. Meffert, Dominik: Einfluss der Bauteilkontur auf das Verschleiß- und Reibungsverhalten von Gelenkketten. Dissertation, Rheinland-Pfälzische Technische Universität Kaiserslautern-Landau, 2023, Maschinenelemente und Getriebetechnik Berichte Bd. 45/2023, ISBN 978-3- 95974- 195-8

80. Foko Foko, Flavien: Semi-analytische Kontaktmodellierung in Maschinenelementen. Dissertation, Rheinland-Pfälzische Technische Universität Kaiserslautern-Landau, 2023, Maschinenelemente und Getriebetechnik Berichte Bd. 46/2023

81. Graf, Simon: Charakterisierung und Auswirkungen von parasitären Lagerströmen in Mischreibung. Dissertation, Rheinland-Pfälzische Technische Universität Kaiserslautern-Landau, 2023, Maschinenelemente und Getriebetechnik Berichte Bd. 47/2023, ISBN 978-3-95974-201-6

82. Gonda, Attila: Determination of rolling bearing electrical capacitances with experimental and numerical investigation methods. Dissertation, Rheinland-Pfälzische Technische Universität Kaiserslautern-Landau, 2024, Maschinenelemente und Getriebetechnik Berichte Bd. 48/2023, ISBN 978-3-95974-216-0

ISSN 1860-8035
ISBN 978-3-95974-216-0